POLITECNICO DI MILANO
Bioengineering Department
PhD program in Bioengineering

FUNCTIONAL ANATOMY OF SENSORIMOTOR INTEGRATION IN THE HUMAN BRAIN AND PERSPECTIVES IN NEUROREHABILITATION

PhD thesis of

Marta Gandolla

Tutor: Prof. Giancarlo Ferrigno

Supervisors: Prof. Alessandra Pedrocchi; Dr Nick Ward; Dr. Simona Ferrante

Coordinator: Prof. Maria Gabriella Signorini

XXV Edition

2010-2012

LE RADICI PROFONDE NON GELANO MAI

DEEP ROOTS NEVER GET FROST

Alla mia famiglia, don Fabio e Luca

To my family, don Fabio, and Luca

Acknowledgments

This work comes at the end of three wonderful years full of research, but also full of many other things, and it is the result of the help of many hands.

Thanks to my tutor, Prof. Giancarlo Ferrigno who wanted me doing the PhD at Nearlab during those years. A huge thanks to Prof. Alessandra Pedrocchi who started this research with me and who always has been professionally and humanly deeply present. Thanks to Simona, who helped just like she does for everything. Thanks to the NES girls (!!) that are colleagues, but became very good friends with time. Thanks to all Nearlab, for being so kind to have ma around, and learn to speak my language!

Thanks to Dr Nick Ward who wanted me to come to London, taught me a lot and he was and he is able to stand an Italian hand waving tornado. Thanks to all London colleagues that adopted me for six months full of joy.

Thanks to Dr Molteni that is always full of enthusiasm for the research, and thanks to Eleonora, that has hundreds things to do, but finally everything finds its place. Thanks to Stefano e Mauro that stayed until late in the resonance room for us, always smiling. Thanks to all volunteers that accepted to help me out for free at to all patients that patiently underwent all the measures. A warm thanks to all personal of Villa Beretta Rehabilitation Centre and of Valduce Hospital.

Thanks to the girls of my apartment, to my fraternity and to all my friends, that are a lot and that really did and do a lot to my life, in every sense that is possible to think about.

Thanks to my big family and to don Fabio that are always on my side, and that are the ground of what I am now.

Thanks to Luca who will soon be my husband, who is always present, who is sharing with me this life, and who allows the life to be better!

Summary

The correct execution of a voluntary movement depends on – and is shaped by – the integration of sensory feedback or reafference. Sensorimotor integration is the brain process that dynamically combine sensory information into intentional motor response (Machado et al., 2010). Potential anatomical substrates of sensorimotor integration have been established in non-human primates (Witham et al., 2010, Jones et al., 1978; Darian-Smith et al., 1993). In humans, manipulation of proprioceptive input influences motor cortex excitability (Rosenkranz and Rothwell, 2012). Conversely, the response of somatosensory cortex neurons to proprioception is modified by the nature of the motor task (Chapman and Ageranioti-Bélanger, 1991; Cohen et al., 1994) and by motor learning (Ostry et al., 2010; Wong et al., 2011). These experiments considered sensorimotor integration as either differences (Yetkin et al., 1995; Sahyoun et al., 2004) or conjunctions (Ciccarelli et al., 2005) between active and passive tasks, but have not explicitly examined the effect of proprioceptive manipulation during an active motor task.

Functional Electrical Stimulation (FES) provides an ideal experimental model to explore sensorimotor integration because it can provide externally driven proprioceptive information that is embedded within the movement execution.

FES produces muscles contraction independently from voluntary effort but if coupled with volitional intention supplies an artificial augmentation of the sensory consequences of moving. FES stimulation of a mixed nerve activates both the efferent and the afferent fibres. Efferent fibre stimulation directly induces a muscular contraction that elicits additional proprioceptive feedback. The stimulation of the afferent fibres elicits a sensory volley that is sent to the central nervous system concurrent with the proprioceptive reafference (Bergquist et al., 2011) that contributes an additional component to proprioceptive feedback.

Moreover, it worth a note that FES is a recognised therapeutic procedure in clinic rehabilitation (Sabut et al., 2010; Pomeroy et al., 2006). In addition to the well-known peripheral effect on muscles themselves, possible mechanisms about central therapeutic benefits of FES have been already hypothesized (Rushton 2003; Everaert et al., 2010). Some hemiplegic patients treated with FES for foot drop correction during walking have shown a beneficial effect that outlasts the period of stimulation firstly observed by Liberson and collegues (Liberson, et al., 1961). This FES-induced outlasting effect is known in literature as ‘carryover effect’ (Waters et al., 1985; Merletti et al.,

1979; Rushton, 2003; Ambrosini et al., 2011). This further supports the hypothesis that FES induces some plasticity mechanisms leading to central nervous system reorganization and therefore maintenance of improvements in motor control that is worthy to be investigated.

The aim of this work is therefore to:

(i) define an experimental set-up that is suited to measure movement related cortical correlates during functional electrical stimulation;

(ii) define an experimental protocol that is suited to study sensorimotor integration during an active motor task

(iii) investigate the functional anatomy of sensorimotor integration in the human brain

(iv) investigate how functional anatomy of sensorimotor integration is affected by a brain lesion (e.g. stroke)

(i) Experimental set-up[1]

An experimental set-up to perform electrical stimulation and to monitor motor task output simultaneously with functional MRI acquisitions was proposed and tested. The experimental set-up was composed by a 1.5 T MRI scanner, a motion capture system and stimulator arranged as shown in Figure 1. The scanner used for images acquisition was a CV/I 1.5 T model (GE Cv/I^{TM}). Motion capture system is based on an optoelectronic motion analysis tool that tracks passive markers with three cameras mounted in the resonance room. The commercial motion capture system Smart μg^{TM} (BTS, Italy) was selected. Cameras have an LED enlighter emitting at 850 nm and a CCD detector sensible to infrared light. The working frequency was set to 120 Hz. Aluminium foils, connected to MR room ground, were contiguously applied to all elements in the MRI room as seen in literature (Tang et al., 2008), in order to limit the radio frequency interference. Cameras' cables were passed through the waveguide of the MRI room to reach the motion capture workstation placed in the operator room. Specific plastic markers positioning (i.e., on significant land or bone marks) depends on the goal of the study, but does not affect the experimental set-up validation. The portable stimulation device employed was the current-controlled 8-channel stimulator RehaStim pro^{TM}

[1] The work has been published in two journal paper as (i) Casellato C, Ferrante S, **Gandolla M**, Volonterio N, Ferrigno G, Baselli G, Frattini T, Martegani A, Molteni F, Pedrocchi A. Simultaneous measurements of kinematics and fMRI: compatibility assessment and case report on recovery evaluation of one stroke patient. *J Neuroeng Rehabil*. 2010; 23:7-49; and (ii) **Gandolla M**, Ferrante S, Casellato C, Ferrigno G, Molteni F, Martegani A, Frattini T, Pedrocchi A. fMRI brain mapping during motion capture and FES induced motor tasks: signal to noise ratio assessment. Med Eng Phys. 2011; 33(8): 1027-32.

(HASOMED GmbH). The stimulator device was placed in the operator room, outside the MRI room; stimulation cables passed through the waveguide to reach the subject performing fMRI exam. As seen in literature (Francis et al., 2009), two inductors were placed in series with the stimulation cables so as to filter inductive pick-up of gradient fields by the FES device. The introduction of metallic devices and of stimulation current in the MRI room could affect fMRI acquisitions so as to prevent a reliable activation maps analysis, and vice versa the strong magnetic field could affect the correct functioning of the introduced devices.

Figure 1 - Experimental set-up

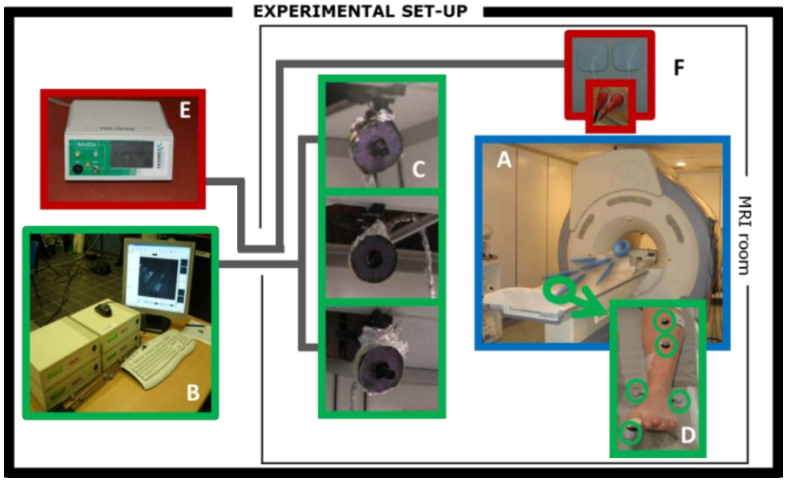

(A) MRI scanner CV/I 1.5 T; (B) motion capture system Smart µg™ with (C) three cameras and (D) reflective markers; (E) current-controlled stimulator RehaStim pro™ and (F) stimulation electrodes.

The novel experimental set-up was therefore tested and validated demonstrating that:

Proof of concept - Healthy subject sessions showed the protocols feasibility and the reliability of images analysis including the kinematic regressor. The patients' results showed that brain activation maps were more consistent when the kinematic regressor quantifying the actual executed movement (movement timing and amplitude) was included in the regression model besides the stimuli, proving a significant model improvement. Indeed, movement related activated areas were consistent with literature findings and standard neurological functional mapping.

Reliability of kinematic data acquisition - The use of three cameras allows a reliable reconstruction of 3D positions of the markers. Three cameras, even if not positioned with the optimal mutual orientations having as major priority to put them on the ceiling at the maximal distance from the magnet, represent a good compromise between the introduced noise and the reliability of markers reconstruction. Indeed, the calibration procedure for each session, estimating the reconstruction

error on a moving bar with 3 markers at fixed known distances, confirms the high accuracy of kinematics data (error < 1 mm on a working volume of 1×1×1 m). The computed mean gravity acceleration was as the expected one, hence the magnetic fields did not affect the motion capture system and camera data processing.

Reliability of stimulation signal – Electrical stimulation has been previously demonstrated to be reliable (Francis et al., 2009; Blickenstorfer et al., 2009; Iftime-Nielsen et al., 2012). The correct stimulation waveform has been checked with a phantom acquisition and visual inspection confirming literature results.

Reliability of fMRI images acquisition - The signal to noise ratio (SNR) loss introduced by the motion capture system and the electrical stimulation current was assessed through the standard index for image quality (Kaufman et al., 1989), that is the ratio between the mean signal amplitude on a homogeneous area and the standard deviation of the background signal amplitude. The recent study of Scarff and colleagues (Scarff et al., 2004) was used as reference: in simultaneous recordings of fMRI and EEG, they showed that MR image SNR, computed as in this work, decreased as the number of electrodes increased, and they fix as data quality acceptable a SNR loss on the images of 11-12%. For the proposed experimental setup including both motion capture and FES, a SNR loss equals to 2.37 ± 2.9% was assessed, that is therefore negligible.

Reliability of acquired BOLD signal – It was important to demonstrate that the Blood Oxygenation Level Dependent (BOLD) signal, marker of neural activity, could be detected within the given experimental condition and set-up. Temporal Signal to Noise Ratio (SNR) was assessed as image quality index. BOLD signal change is about 1–2% as revealed by a 1.5 T scanner (Parrish et al., 2000). This work shows that in the main cortical sensorimotor regions 1% BOLD signal change can be detected at least in the 93% of the sub-volumes, and almost 100% of the sub-volumes are suitable for 2% signal change detection.

(ii) Experimental protocol

The experimental protocol was designed so as to be able to directly investigate sensorimotor integration during an active motor task. A simple motor task such as ankle dorsiflexion has been selected, that has also been shown to be useful for assessing motor control for walking during rehabilitation (Dobkin et al., 2004).

Protocol design - A 2x2 event-related fMRI protocol with voluntary effort [V: with the levels volitional and passive] and FES [F: with the levels present and absent] as factors was performed using right ankle dorsiflexion (ADF). During a continuous 10 minutes scanning session, subjects performed 20 alternate 9 seconds OFF and 21 seconds ON blocks. Given the 2x2 factorial design, 4 conditions were performed during the ON blocks in a randomized order: (i) FV = FES-induced ADF concurrently with voluntary movement by the subject; (ii) FP = FES-induced ADF, while the subject remains relaxed; (iii) V = voluntary ADF; (iv) P = passive dorsiflexion (by the experimenter) of the subject's ankle. The dorsiflexions were paced every 3.5 seconds (for 6 repetitions) with an auditory cue. All subjects were free to choose the amplitude of their active movement to preclude fatigue. The experimenter moved the ankle to match the movements during volitional dorsiflexion.

Stimulation paradigm - FES was applied to the peroneal nerve through superficial electrodes, with biphasic balanced current pulses at 20 Hz fixed frequency. The pulse width had a trapezoidal profile and the current was set subject by subject; so as to reproduce the same movement amplitudes as during voluntary movements, within the tolerance threshold. Current and pulse width amplitudes were kept the same for both FP and FV conditions.

Kinematic measures - 3D trajectories of retro-reflective markers were acquired in order to measure the ankle angle during fMRI acquisitions and to determine the movement onsets and amplitude. Two separate acquisitions were performed in order to estimate the position of the tibia, internal and external malleoli, and internal and external metacarpi for both legs. Marker trajectories were analysed with a custom algorithm running in Matlab (Matlab R2010b). For each leg, the ADF angle was calculated as follows: the mean points between internal and external malleoli (mean malleolus) and between internal and external metacarpi (mean metacarpus) were calculated. The ADF angle was taken as the angle between the line passing through the more proximal tibial marker and the mean malleolus and the line passing through the mean malleolus and the mean metacarpus.

Contrasts of interest – Thanks to the 2x2 factorial design three contrasts of interest could be defined. The main effect of FES defined as (FV+FP)-(P+V) that identifies regions that are activated during FES induced movements (i.e. FV, FP) over and above the non-FES induced movements (i.e. V, P). The main effect of voluntary movement defined as (V+FV)-(P+FP) that identifies regions that are activated during a volitional movement (i.e. V, FV) over and above the non-voluntary movements (i.e. P, FP). The positive interaction defined as (FV-V)-(FP-P) that identifies regions

where the FES augmented proprioception in the context of volitional intent (i.e. FV-V) produced a higher activation than FES augmented proprioception in the absence of volitional movement (i.e. FP-P). The positive interaction contrast directly represents the sensorimotor integration during an active motor task, when in the brain we have the planning of the volitional movements coupled to augmented proprioceptive afferences.

(iii) Sensorimotor integration in healthy subjects[2]

The experimental set-up and the protocol were specifically designed to investigate how artificially augmented proprioceptive afferent information affects integration in the central nervous system during movement control. FES was introduced as a means of artificially supplementing proprioception during movement execution. Seventeen healthy volunteers (9 female, 8 male) with no neurological or orthopaedic impairment were studied (mean age 36±14 years, range 22-61). Experiments were conducted with approval from the Villa Beretta Rehabilitation Centre ethics committee and all subjects gave informed written consent. The four conditions of the 2x2 factorial design (i.e. V, FV, P, FP) showed clear activation in the leg sensorimotor cortex, as expected. fMRI responses during the four conditions showed activations in motor and somatosensory areas known to be involved in ADF execution and concord with previous studies (Dobkin et al., 2004; Sahyoun et al., 2004; Ciccarelli et al., 2005).

Figure 2 - Interaction contrast

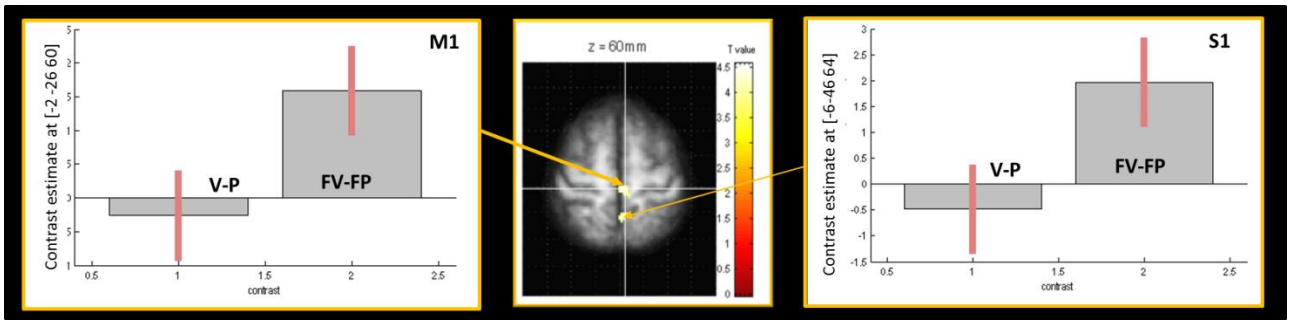

Statistical parametric maps (thresholded at p<0.001, uncorrected) showing regions activated for the positive interaction contrast (i.e. (FV-V)-(FP-P)). The slice at z = 60 mm has been chosen for display purpose only. The two plots depict the differences of FV and FP effects, under the regression model; and the difference between V and P effects for the peak voxel of each cluster (i.e. [-2, -26, 60] for M1 and [-6 -46 64] for S1). The two clusters are located anatomically in M1 (anterior cluster) and S1 (posterior cluster) leg areas. Red bars represent inter-subject variability (standard error).

[2] A journal paper on this work has been submitted to *Journal of Neuroscience* as **Gandolla M**, Ferrante S, Molteni F, Guanziroli E, Frattini T, Martegani A, Ferrigno G, Friston K, Pedrocchi A, Ward NS. The functional anatomy of sensorimotor integration in the human brain.

Positive interaction, defined as (FV-V)-(FP-P), was seen in both M1 and S1. In other words, the effect of augmented proprioception is influenced by the presence of concurrent motor signals in both M1 and S1; the activating effect of voluntary movement increases dramatically in the presence of augmented proprioceptive feedback (Figure 2).

Sensorimotor integration can be seen in terms of connectivity of input-output systems, where inputs are (ascending) sensory feedbacks or (descending) cognitive or predictive processes and outputs are (descending) information sent to the periphery or (ascending) to high levels of the sensorimotor hierarchy. Our results suggest an effect of additional (ascending) proprioceptive input during FES in M1 and S1, but not in any other brain regions.

Figure 3 - DCM model

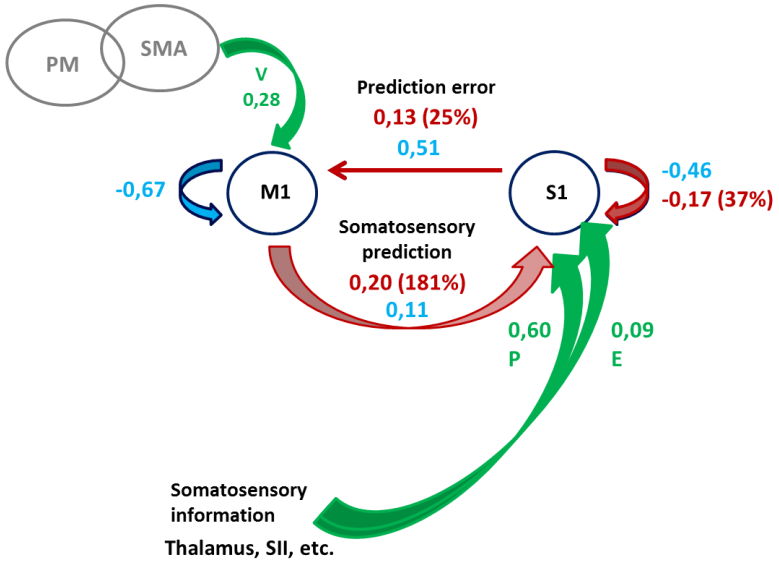

To understand how this interaction effect is generated, in terms of driving and modulatory inputs to M1 and S1, it was further investigated then with dynamic causal modelling. Using dynamic causal modelling (DCM), it was possible to show that augmented proprioception, although only slightly increasing the importance of the proprioceptive input, dramatically modulated the connections between M1 and S1, preferentially increasing the influence of M1 on S1, while attenuating the excitability of S1 (increasing self-inhibition).

Within this study, it was demonstrated that (i) changing proprioceptive input increased activations during volitional movement in, and only in, primary cortical areas (i.e. M1, S1); (ii) this interaction can be explained by an increase in the influence of M1 on S1 (as well as S1 self-connections, with less effect of S1 to M1 connections). The results clarify the functional anatomy of sensorimotor

integration and disambiguate alternative models of motor control, leaning towards an active inference view of the motor system (i.e. updating of the prediction of the sensory consequences of movement as encoded by the increase in the influence of M1 on S1). Moreover, they provide some insights into the synaptic mechanisms of sensory attenuation and may speak to potential mechanisms of action of FES in promoting motor learning in neurorehabilitation.

(iv) Sensorimotor integration in chronic stroke patients

Eleven stroke patients were recruited [range between 28 and 72 years, mean (SD) 53.2 (14.5)]. Six patients had experienced left hemiparesis and five right hemiparesis. All patients had suffered from first-ever stroke > 6 months previously, resulting in weakness of at least the tibialis anterior muscle (to <4+ on the Medical Research Council (MRC) scale). Exclusion criteria consisted of (i) impossibility to elicit an FES-induced ankle dorsiflexion of at least 10° in FES-induced ankle dorsiflexion; (ii) language or cognitive deficits sufficient to impair cooperation in the study; (iii) inability to walk even if assisted; (iv) incompatibility with MRI (e.g. pacemaker, implants, etc.); (v) high spasticity at ankle joint plantar flexor as measured by the modified Ashworth scale index, MAS > 2 (Ashworth, 1964); and (vi) brain lesion including leg primary motor cortex area.

The sensorimotor investigation in chronic stroke subjects identified brain functional reorganisation associated with ankle dorsiflexion task in chronic post-stroke patients in all conditions (i.e., V, FV, P, FP - Figure 4), encompassing primary and secondary areas known in literature to be involved in movement processing and control of ankle movement (Freund et al., 2011; Iftime-Nielsen et al., 2012; Ciccarelli et al., 2006; Wegner et al., 2008; Dobkin et al., 2004; Sahyoun et al., 2004). Patients significantly activated more than controls in a highly distributed pattern, which included regions that are activated when healthy controls perform complex or motor tasks (Ciccarelli et al., 2006; Katschnig et al., 2011). It has been suggested that this finding might be indicative of higher demand and increased effort in patients to ensure adequate motor function despite existing deficits (Katschnig et al., 2011). The conjunction analysis between patients and controls revealed clear pattern of activation in primary somatosensory cortex that has been reported to be principally involved during the same motor task execution (see point iii). This result clearly shows that although patients use a quite widespread network in order to execute even a simple movement, they also share the principal regions devoted to motor control with healthy subjects.

FES-induced ankle dorsiflexion concurrent with voluntary effort elicited a more widespread active network with respect to FES in the context of passive movement, in accord with what was found in

healthy subjects (see point (iii); Iftime-Nielsen et al., 2011; Joa et al., 2012). The differential effect of action of FES in the context of active and passive movement is confirmed by the cluster of activation revealed by the positive interaction contrast in the contralateral angular and postcentral gyrus. Postcentral gyrus has been described in literature to be active in healthy controls while executing complex or novel tasks (Sahyoun et al., 2004; Filippi et al., 2004), and angular gyrus has been suggested to be recipient of proprioceptive information encoded specifically in the postcentral gyrus (Vesia et al., 2012).

Figure 4 - Patients group analysis

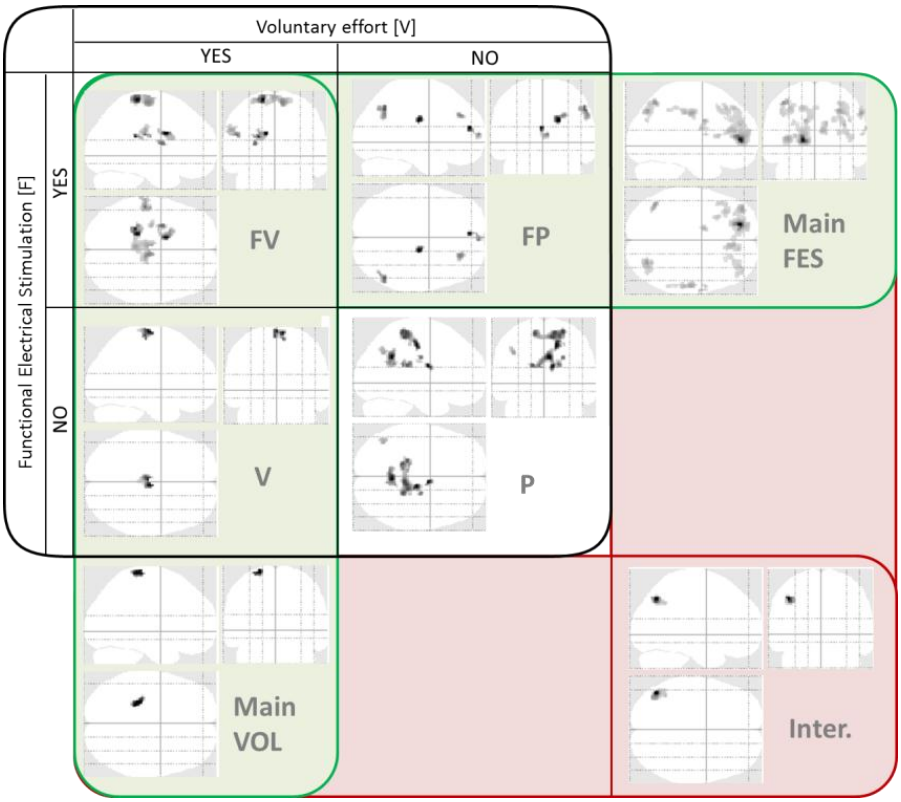

Statistical parametric maps (thresholded at p<0.005, uncorrected). FV = FES and voluntary effort; FP = FES induced movement; V = voluntary movement; P=passive movement; Main FES = main effect of FES. i.e. (FV-V)+(FP-P); main VOL = main effect of voluntary effort, i.e. (FV-FP)+(V-P); inter. = positive interaction between the factors, i.e. (FV-V)-(FP-P).

A further analysis investigated whether there was any variability in sensorimotor integration across the patient group. Here sensorimotor integration was quantified by the (voxel-wise) parameter estimates of the positive interaction contrast (see above). Motor impairment was calculated by performing a principal component analysis of the outcome measures selected to define patients' residual ability (i.e., gait velocity, endurance velocity, peak ankle angle during swing, ankle angle at initial contact, MRC index, and symmetry index). Brain regions in which there was a correlation

between sensorimotor integration and level of impairment were examined (Figure 5). Contralateral SII has been shown to be more likely to be active in more impaired patient during sensorimotor integration (i.e. interaction contrast). Iftime-Nielsen and colleagues (Iftime-Nielsen et al., 2012) suggested a sensorimotor integration role for SII in healthy subjects, that could be exploited by patients when primary sensorimotor areas (i.e., M1 and S1) are unable to provide the needed processing of information. In addition, within the interaction contrast, significant positive linear correlation was found in ipsilateral cingulate cortex, middle frontal gyrus and insula, indicating distinct networks involved in sensorimotor integration processing.

Figure 5 - Correlation analysis

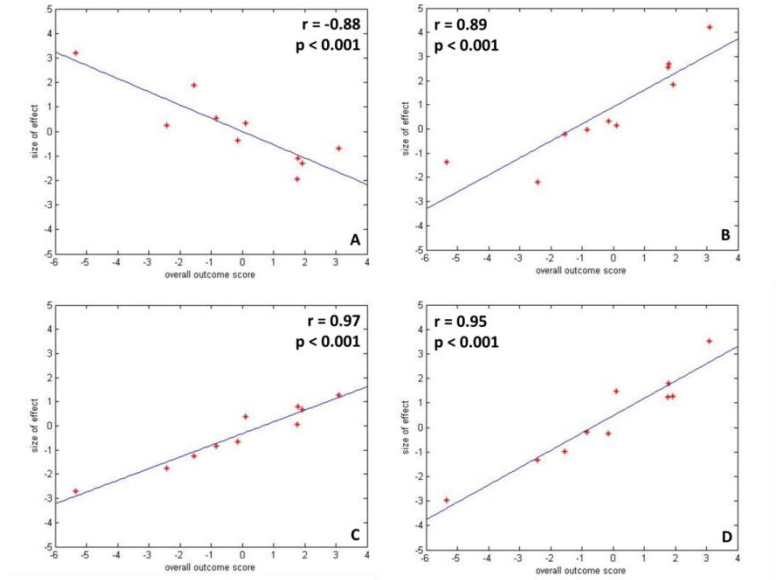

Plots of parameter estimates (size of effect) against relative overall outcome recovery score (normalized) for all stroke patients in different areas of the brain. Correlation coefficient and associated p-values for peak voxel in each region are indicated in each panel. A) contralateral SII ([-44 -44 38]); B) ipsilateral cingulate cortex ([2 36 26]); C) ipsilateral middle frontal gyrus ([40 4 36]); D) ipsilateral insula ([34 -2 10]).

Scientific and clinical impact

With this work, the feasibility of the proposed multi-modal experimental set-up was demonstrated so as to functionally electrically stimulate a subject while undergoing fMRI scanner and simultaneously record the effectively executed movement. Moreover, it has been shown that M1 and S1 exhibit a profound interaction between artificially enhanced sensory feedback and volitional movement. Changes in coupling between these regions support an active inference model of motor control. Finally sensorimotor integration in chronic stroke patients was investigated, demonstrating the feasibility and the reliability of FES cortical correlates in patients, highlighting for the first time

a clear network of activation related to FES-induced motor task in the context both of voluntary effort or passive movement. Moreover it has been shown that angular and postcentral gyri exhibit an interaction between artificially enhanced sensory feedback and volitional movement and that contralateral SII is more likely to be sensorimotor integration centre for more impaired patients.

The presented results may be important for disclose the central FES-induced mechanism that is yet not clear. These results may also have important implications for the mechanisms that underlie sensory attenuation; i.e. the decreased intensity of perceived stimulus attributes when they are the consequences of self-generated behaviour (Cardoso-Leite et al., 2010).

The present results also support the proposed mechanism of FES as a tool to promote improvement in motor function after central nervous system injury. This functional architecture and the underlying synaptic mechanisms may be important for future studies in patients during rehabilitation, by correlating changes in FES and interaction cortical correlates in a longitudinal design. Indeed the brain correlates that has been shown to have a correlation between sensorimotor integration (i.e. interaction contrast) and the degree of impairment might be important in the investigation of the carryover effect brain signature.

Organisation of the thesis

This work has been the result of the collaboration between the Nearlab at Politecnico di Milano, Villa Beretta Rehabilitation Centre and the Sobell Department of Motor Neuroscience, UCL Institute of Neurology. The thesis is organised in five chapters as following: (1) scientific context and introduction to the research; (2) design and validation of a novel experimental set-up (addressing aim (i)); (3) investigation of the functional anatomy of sensorimotor integration in the human brain (addressing aims (ii, iii)); (4) investigation of sensorimotor integration in post-stroke chronic patients (addressing aim (iv)); and (5) conclusions and vision for future.

Contents

Abbreviations

ADF – ankle dorsiflexion

AH – anterior horn

BA – Brodmann area

BOLD – blood oxygenation level dependent

c - contralateral

CNS – central nervous system

CV – coefficient of variation

DCM – dynamic causal modelling

DTI – diffusion tensor imaging

EEG – electroencephalography

EMG – electromyography

EPI – echo planar imaging

f - frequency

FES – functional electrical stimulation

fMRI – functional magnetic resonance imaging

FOV – field of view

FV - FES-induced ankle dorsiflexion concurrently with voluntary movement by the subject;

FP - FES-induced ankle doriflexion, while the subject remains relaxed

FWHM – full width half maximum

i - ipsilateral

ID – index displacement

ISD – index displacement standard deviation

LTP – long term potentiation

M1 – primary motor cortex

MAS – modified Ashworth scale

MCS – experimental condition where only Motion Capture System is working

MCS+FES – experimental condition where both motion capture system and FES are working

MEG – magnetoencephalography

MNI – Montreal Neurological Institute

MRC – Medical Research Council

MRI – magnetic resonance imaging

NIRS – near-infrared spectroscopy

S1 – primary somatosensory cortex

SII – secondary somatosensory cortex

SMA – supplementary motor area

SMC – sensorimotor cortex

SPM – statistical parametric maps

P - passive dorsiflexion (by the experimenter) of the subject's ankle

PD – pinkie displacement

PET – positron emission tomography

PM – premotor area

PSD – pinkie displacement standard deviation

PSR – paretic step ratio

PT – pyramidal tract

R index – correlation coefficient for the index finger

R pinkie – correlation coefficient for pinkie finger

ROI – region of interest

SD – standard deviation

TE – echo time

TMS – transcranial magnetic stimulation

TR – repetition time

V - voluntary ankle dorsiflexion

wLI – weighted laterality index

Chapter 1 - Introduction

Humans have the extraordinary ability to learn a vast array of motor tasks with modest amount of practice, and to effectively compensate unforeseen errors and adapt in performing those tasks. Movement is the only way to interact with the world and intentions are conveyed through muscles activations, resulting in goal-directed (functional) movements. The correct execution of a voluntary movement is therefore the result of the interplay between intention to perform a movement and its physical execution. Intention is encoded at central nervous system level, whereas execution is devoted to peripheral muscles contraction and consequent joint motion. Movement execution causes in turn sensory consequences, both intrinsic (position of the muscles etc.) and extrinsic (forces, etc.) that are conveyed back to the central nervous system to control the movement and close the loop. In fact, the quality of normal motor control is frequently lost if the motor system doesn't receive a continuous flow of sensory information: movements become inaccurate and posture unstable when somatic sensation is lost from the limbs. Loss of vestibular or visual input also impairs ability to maintain balance and orientation. The research about the sensorimotor system has always been of interest, in its developing, healthy and pathological form. In order to understand motor functions, the three levels of the sensorimotor system – limb mechanics, motor behaviour and neural control - and their interaction have to be investigated. Muscles and limb mechanics influence the translation of muscles activity to limb movement. Motor behaviour describes how the limbs or body move during a motor task, reflecting the combined action of the neural circuits that control movement and the mechanical properties of the limbs. The neural basis of movement examines how different regions of the brain and spinal cord control motor output and how they integrate somatosensory inputs.

1.1 Limb mechanics and motor behaviour

The peripheral motor system is currently well known in its anatomy and function. It can be thought as a complex filter that converts patterns of muscle activity into functional movements where the basic element is the motor unit — a motor neuron and the muscle fibres it innervates. The conversion of patterns of motor unit activity into muscle force depends on different variables including muscle fibre length, velocity, histochemical type and history-dependencies such as fatigue (Burke et al., 1973; Cheng et al., 2000; Gordon et al., 1966; Holmes, 2006; Scott et al., 1996). Muscle force is also influenced by architectural features, including tendon and fascicle length, the orientation of fibres and passive muscle elasticity (Otten, 1988; Zajac, 1989). Muscle morphometry

varies widely even across synergistic muscles (Cheng et al., 2000; Singh et al., 2002). The effective joint torque that is generated by a muscle depends on its mechanical advantage (moment arm) about that joint, which often varies with joint angle (Graham and Scott, 2003). Muscular torque at a joint depends on several parameters that relate to each segment's moment of inertia, length, mass and centre of mass position (Scott, 2000).

1.2 Neural control

Much more challenging is the investigation of neural control of movement, that was made extensively possible only from the development of non-invasive recording (e.g. EEG, NIRS) and imaging (e.g. fMRI, DTI, MEG) technologies, for obvious reasons. A recurrent feature of the early studies was the demonstration of the close relationship between motor and sensory cortical activation during motor tasks execution that was referred to as 'sensorimotor cortex' as discussed in the review authored by Rowe and Siebner (Rowe and Siebner, 2012). Sensorimotor cortex activation suggested the functional integration of these areas, thus a dynamic combination of sensory information into intentional motor response. Indeed, the two functions are intrinsically related, and the execution and control of a voluntary movement depends on and is shaped by the integration of sensory feedback, i.e. sensorimotor integration. The sensorimotor cortex is hierarchically organized, both anatomically and functionally. Successively higher levels of the motor hierarchy specify increasingly more complex aspects of a motor task. In turn, this hierarchy of motor representations depends on a parallel hierarchy of sensory input; more complex sensory information is extracted, at each level, from the spinal cord to the motor cortex (Kandel et al., 2000).

The motor system anatomically consists of four hierarchical components, as schematically depicted in Figure 1. The first one is the spinal cord that contains the neuronal circuits mediating a variety of reflexes and rhythmic automatisms (e.g. locomotion). The simplest neural circuit includes only the primary sensory neuron and the motor neuron (i.e. monosynaptic circuit). However, most reflexes are mediated by polysynaptic circuits, where one or more interneurons are interposed between the primary sensory neuron and the motor neuron. The second level, the brainstem, contains neuronal systems that are necessary for integrating motor information descending from higher levels as well as for processing information that ascends from the spinal cord. All descending motor pathways to the spinal cord originate in the brain stem with the exception of the cortico-spinal tract. The primary motor cortex (M1) represents the third level in the motor hierarchy and it is the node upon which the action of the highest levels of cortical organization converges and from which certain descending motor information requiring cortical processing are issued to the brainstem (i.e. cortico-

bulbar tract), to other sub-cortical structures, and to the spinal cord (i.e. cortico-spinal tract). The highest level of the hierarchy consists of premotor and supplementary motor cortical regions located in Brodmann's area 6. These areas act primarily on the motor cortex. In addition two other parts of the brain are important for motor functions: the cerebellum and the basal ganglia that are in charge to provide feedback circuits that regulate cortical and brain stem motor areas: they receive inputs from various areas of cortex and project to motor areas of the cortex via the thalamus. The loop circuits of these two structures flow through separate regions of the thalamus and to different cortical areas. The cerebellum and basal ganglia do not send significant output to the spinal cord, but they do act directly on motor neurons in the brain stem.

Figure 1 - The motor system (Kandel et al., 2000)

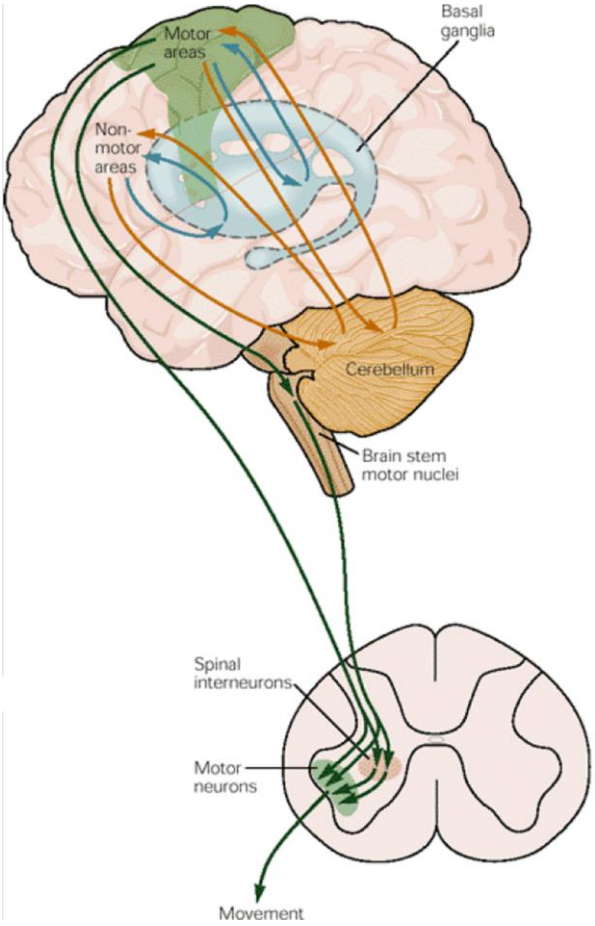

The motor areas of the cerebral cortex can influence the spinal cord either directly or through the descending system of the brain stem. Spinal cord, brain stem, brain, all receive sensory inputs and are also under the influence of two independent subcortical systems: the basal ganglia and the cerebellum. (The basal ganglia and the cerebellum act on the cerebral cortex through relay nuclei in the thalamus, which are omitted from the diagram for clarity).

The sensory system part is mainly composed by the primary somatosensory cortex (S1) that is located in the postcentral gyrus and in depth of the central sulcus. Lateral and somewhat posterior to S1 is the secondary somatosensory cortex (SII), lying in the upper bank of the Sylvian fissure. It has been shown that the afferent inputs to S1 derive entirely from the contralateral body, whereas the inputs to SII are bilateral. A third cortical region that receives somatosensory inputs is located in the posterior parietal lobe (including Brodmann's area 5 and portion of area 7). This region is a higher order sensory cortex similar in function to association cortex; it relates sensory and motor processing and is concerned with integrating the different somatic sensory modalities necessary for perception (Kandel et al., 2000). The sensory system is schematically depicted in Figure 2.

Figure 2 - Sensorimotor areas in the brain (Adapted from http://thebrain.mcgill.ca)

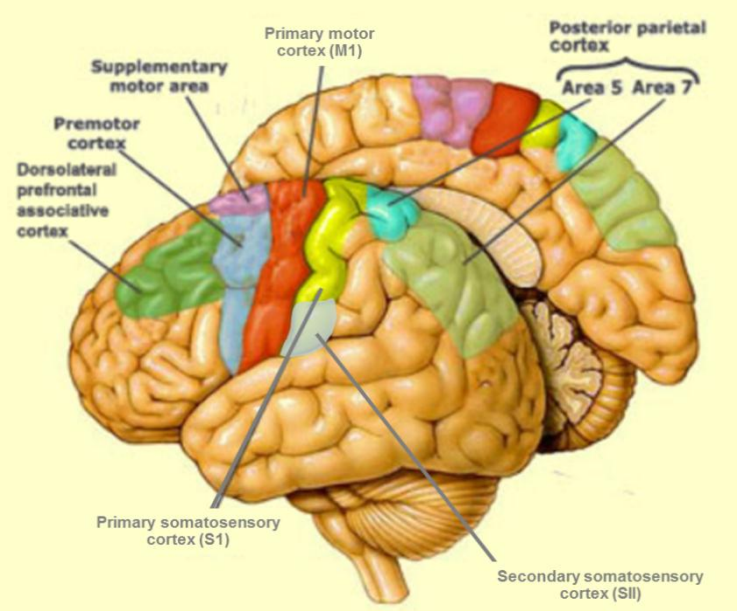

The areas of the brain devoted to sensorimotor control are schematically depicted.

As described, based on anatomical and functional criteria, the cortex of the human brain is divided in primary, secondary, and tertiary areas. The basic classical neurophysiology infers that primary cortical areas involved in the production of movements shows a somatotopic representation of the body, i.e. the relative space of human body parts occupied on the primary somatosensory cortex (S1) and on the primary motor cortex (M1), called somatosensory and motor homunculus (Penfield and Boldrey, 1937) albeit with some overlap (Schieber and Hibbard, 1993). M1 and S1 areas have the strongest anatomical connections with the limbs, and measuring cerebral activity with functional imaging tools (e.g. PET, fMRI) during a simple movement will show an activation of the primary correspondent region, irrespective of the task (Rijntjes et al., 1999). Additional involvement of secondary and tertiary cortices will depend on the complexity of the paradigm, and activation in

secondary motor cortices is generally interpreted as higher-order but still modality-specific processing, e.g., planning, preparation, imagining, selection, or internal generation of the movement (Passingham, 1993). Each level of motor control receives peripheral sensory information that is used to modify the motor output at that level. At the same time, each level contains distinct populations of neurons that project in parallel to sensory relay nuclei and other structures, including the thalamus and cerebellum.

1.3 Sensorimotor integration models

In literature, there are different hypothesis about how sensorimotor integration takes place and about the nature of the messages flowing between the different areas. Different models of sensorimotor control have been proposed, e.g. (Friston et al., 2009; Todorov, 2004). Conventional models of the sensorimotor system, as exemplified in the motor control literature (Shadmehr et al., 2010), consider descending connections to deliver driving command signals. The conventional motor control model treats the brain as an input-output system that mediates stimulus-response mappings – in which sensory signals are passed forwards to sensory to association to motor cortex and then to the spinal-cord and cranial nerve nuclei as motor commands. In computational motor control this usually involves the use of forward and inverse models, where the inverse model supplies the motor command and the forward model converts efference copy into sensory predictions (Wolpert and Kawato, 1998). These predictions are used to optimise the estimated state of the motor plant required by the inverse model. In the last ten years, the "pure" motor control theory has been substituted by the optimal motor control theory that has become a dominant model. This model was based on the work by Todorov and Jordan (Todorov and Jordan, 2002; Todorov, 2004), who showed the selective use of sensory feedback to correct deviations that interfere with task goals could account for several unexplained effects in motor control, such as the variability of task-irrelevant movement qualities (Figure 3, panel a). The concept that motor cortex could use sensory feedback contrasted with the earlier purely 'feed-forward' serial model of motor control. Optimal control needs an optimal estimate of the state of the system (state variables), which is generated from afferent feedback from sensors combined with efferent copy of motor signals. In humans, both afferent feedback and efferent copy are used to estimate on-going motor performance (Wolpert et al., 1995). It has been put forward that the presence of the rapid compensation before sensory feedback could influence motor performance as support for the presence of the efferent copy. State variables take into account not only the properties of the body, but also information related to grasped objects (Dingwell et al., 2004). The basic principle of optimal feedback control is that feedback gains are optimized on the basis of some index of performance. Such controllers

correct variations (errors) if they influence the goal of the task; otherwise, they are ignored. Optimal state estimation is created by combining feedback signals and efferent copy of motor commands. The latter uses a forward internal model to convert motor commands to state variables. Another interesting feature of optimal feedback controllers is that desired trajectories do not need to be planned explicitly but simply fallout from the feedback control laws (Scott, 2004).

One rather recent approach to describe the sensorimotor system, known in literature as active inference (Figure 3, panel b), is to consider the cortex as a hierarchical generative model, whose descending projections from primary motor cortex predict and explain sensory inputs, i.e. ascending prediction errors, to primary sensory cortex (Friston, 2010). Active inference in the context of sensorimotor system and its theoretical discussion is deeply covered in Adams and colleagues paper (Adams et al., 2012). Briefly, active inference is derived from the free-energy principle (Friston, 2010). In particular, an active agent tends to minimize free-energy or, under some simplifying assumptions, prediction error, i.e. prediction of proprioception versus actual proprioception. Active inference is the resulting interplay between action, i.e. reduction of prediction error by changing sensations (Friston, 2010) and perception, i.e. reduction of prediction error by changing predictions (Rao and Ballard, 1999). In this framework, top-down projections convey predictions, whereas bottom-up projections convey prediction errors (Friston, 2011). However, projections from cortical areas are functionally diverse; i.e. not every projection in a predictive coding hierarchy conveys either a prediction or a prediction error. For example, the information carried by S1 afferents only becomes a prediction error signal once it encounters a prediction (Adams et al., 2012).

Both models (i.e. optimal motor control and active inference) proposes the sensory inputs to motor cortex finesse its output: in optimal control theory, these inputs are state estimates that the optimal controller uses to optimise motor commands. Under active inference, these inputs are proprioceptive and somatosensory prediction errors, which a forward model uses to derive proprioceptive predictions. However, there are profound differences between the two models: a crucial difference (see Friston 2011 for further details) is that optimal control models generate motor commands by minimising a cost function associated with movement. Whereas, in active inference framework, the cost functions are replaced by prior beliefs about "desired proprioception", which emerge naturally during hierarchical perceptual inference. Conventional (computational) motor control theory uses the notion of forward-inverse models to explain how the brain generates actions from desired sensory states (the inverse model) and predicts the sensory consequences of action (the forward model).

Figure 3 - Motor control, optimal control and active inference (Adams et al., 2012)

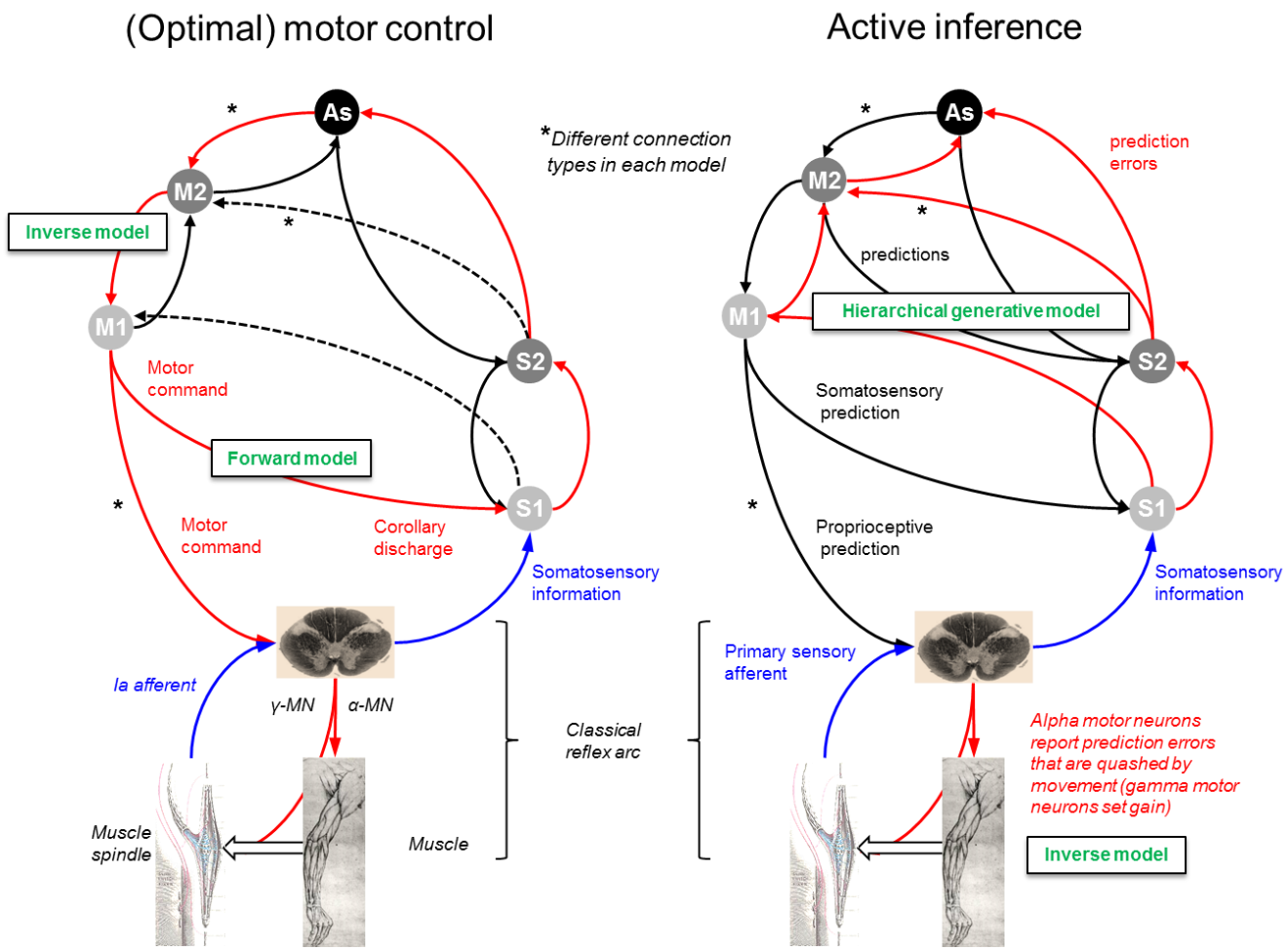

These simplified schematics ignore the contributions of spinal circuits and subcortical structures; and omit many hierarchical levels (especially on the sensory side). M1, S1, M2 and S2 signify primary and secondary motor and sensory cortex (S2 is area 5, not 'SII'), while As signifies prefrontal association cortex. Red arrows denote driving 'forward' projections, and black arrows modulatory 'backward' projections. Afferent somatosensory projections are in blue. α-MN and γ-MN signify alpha- and gamma motor neuron output. The dashed black arrows in the optimal control scheme show what is different about optimal control compared with earlier serial models of the motor system: namely, the presence of sensory feedback connections to motor cortices. This figure omits the significant contribution of the cerebellum to the forward model.

In these schemes, the inverse model has to generate a motor command from sensory cues – a complex transformation – and then a forward model uses an efference copy of this command to generate a predicted proprioceptive outcome called corollary discharge (Wolpert and Kawato, 1998). In active inference a forward or generative model generates both proprioceptive and sensory predictions – a simple transformation – and the inverse model converts a proprioceptive prediction into movement. This is a relatively well posed problem and could be implemented by spinal reflex arcs (Friston, 2010). Therefore, the nature of the descending information to the spinal cord is

different: under active inference these are proprioceptive predictions, whereas in optimal control they are motor commands. This same difference is reflected in the nature of the sensory input to motor cortex: under active inference, these ascending signals must be sensory prediction errors, whereas in optimal control are state estimates, i.e. sensory predictions. This is a key difference because in principle a motor command is a signal that drives a muscle and should not show context specificity: the command to one motor unit should not depend upon the commands to another. In contrast, a prediction of proprioceptive input encodes the consequences of a movement rather than its cause. Given that these consequences are a nonlinear function of their causes, the proprioceptive predictions for several motor units should be interdependent. The role of the spinal circuits is also different under the active inference framework. The active inference model illustrates how the classical reflex arc functions as an inverse model, mapping sensory predictions to action, i.e. motor commands (Adams et al., 2012).

Recently some arguments have been presented in literature to support the active inference theoretical framework very well discussed in Adams' paper (Adams et al., 2012). As way of example we report two considerations. Activity in motor cortex was observed during passive tasks, indicating proprioceptive responses in the precentral gyrus (Weiller et al., 1996). Moreover, the transient sensory deafferentation shows movement related activation in somatosensory cortex suggesting sensory prediction of action (Christensen et al., 2007).

1.4 Neuroscientific bases for rehabilitation

Functional brain mapping of the sensorimotor system was from the beginning strongly influenced by neurologists interested in the mechanisms of recovery after stroke (Dipiero et al., 1992; Weiller et al., 1996) and the pathophysiology of movement disorders (Jenkins et al., 1992). In fact, the aging of society and the continuously improved ability to face acute clinical interventions are enhancing the social impact of the neuro-motor disabilities, and consequently, the relevance of rehabilitation. Of particular relevance is stroke, third cause of death worldwide and the leading cause of adult disability (Lloyd-Jones, 2010). Motor impairment due to central nervous system damage is given by difficulty of the motor commands to elicit muscles contraction. This could be due to the damage of motor cortex, the damage of the pyramidal tract (PT) that conduct the stimulus from the cortex to the anterior horn (AH) or the damage to the motor neurons (AH, spinal cord level). Motor impairment is observed because the pool of neurons that usually were driving the movement are damaged (e.g. the survived neurons are not strong enough to elicit the movement). Normally, a strong volley of impulses in the PT is easily able to discharge the anterior horn cell, but following a stroke or partial spinal cord lesion, the PT population is depleted, often severely or

patchily. For many AH cells, the remaining PT innervation may be too sparse to be effective. In stroke, the ipsilateral innervation may also be too weak to regain control. In fact, for sub-cortical stroke, damages at PT have been shown to correlate to residual motor functions (Radlinska et al., 2010). Failure to regain control during the recovery period will lead to activity decorrelation and so to further synaptic weakening. Segmental and propriospinal contacts will gain control instead, occupying vacated spaces on the AH cell dendrites, and will lead to development of spasticity and associated phenomena. Deafferentation of a body part in a healthy brain enhances cortical representations of adjacent body parts, and this effect is markedly increased by voluntary activity of the adjacent part (Muellbacher et al., 2002). The underlying mechanism is thought to be what is described as "Long-Term Potentiation" (LTP), which was originally described in the hippocampus of the rabbit (Lømo, 1966; Bliss and Lømo 1973; Lømo, 2006), and was later identified as a phenomenon occurring in many other areas of the mammalian CNS, including the anterior horn of the spinal cord.

Brain functional imaging studies showed that recovery from hemiplegic strokes is associated with a brain reorganization of the activation patterns of specific brain structures (Ward, 2007) that are at the base of clinical recovery of motor functions and of sensorimotor integration for neurological patients. There is substantial evidence that chronic (> 1 year) stroke patients can show considerable motor improvement after participation in novel rehabilitation techniques (Page and Levine, 2004). Varied exercise regimens based on motor learning principles might overcome the apparent plateau often described after six months (Page and Levine, 2004). A true recovery would result in undamaged brain regions recruiting, which would generate commands to the same muscles as were used before the injury. This implies some redundancy in motor cortical areas with unmasking, through training, of pre-existing cortico-cortical connections (Jacobs and Donoghue, 1991). The compensation mechanism, in contrast, is the use of alternative muscles to accomplish the task goal (e.g. a patient with right arm plegia can compensate by using the left arm). Nevertheless, despite the clear distinction, learning is required for both true recovery and compensation. There are changes and shifts in the anatomical location of representations of motor programs as a motor behaviour progresses, through learning. Experiments in monkeys clearly demonstrate the importance of learning for the recovery of function (Nudo and Milliken, 1996). A subtotal lesion confined to a small portion of the representation of one hand resulted in further loss of hand territory in the adjacent, undamaged cortex of adult squirrel monkeys if the hand was not used. Subsequent reaching relied on compensatory proximal movements of the elbow and shoulder. Forced retraining of skilled hand use, however, prevented loss of hand territory adjacent to the infarct. In some instances, the hand representations expanded into regions formerly occupied by representations of

the elbow and shoulder. This functional reorganization in the undamaged motor cortex was accompanied by behavioural recovery of skilled hand function. These results suggest that, after local damage to the motor cortex, rehabilitative training can shape subsequent recovery-related reorganization in the adjacent intact cortex. Critically, cortical changes may only occur with learning of new skills and not just with repetitive use (Plautz et al., 2000). It is unclear at this time whether simple repetition of a task that was previously well-learned is sufficient to induce significant cortical reorganization or whether patient should be challenged on more difficult tasks. The answer may depend on the amount of salient error information provided. Sensory feedback, such as proprioception, has a crucial effect on motor ability at cortical and spinal levels as it reshapes sensorimotor integration. The neurobiology of rehabilitation-induced neural adaptations has developed from experiments in animal models and from neurophysiological and neuroimaging studies in patients after focal brain lesions. Several promising new rehabilitation approaches are based on theories of motor learning. These include impairment oriented-training, constraint induced movement therapy (Wolf et al., 2006), voluntarily assisted neuromuscular stimulation (Kraft et al., 1992), robotic interactive therapy (Lum et al., 2002) and virtual reality (Kim et al., 2009). In this work, we will focus on voluntarily assisted functional electrical stimulation.

1.5 Functional Electrical Stimulation (FES)

The term Functional Electrical Stimulation (FES) refers to the stimulation of an intact lower motor neuron to activate plegic or paretic muscles in precise sequence and magnitude so as to directly accomplish or support functional tasks.

Neurophysiological principle

The neurophysiological principle of FES is the generation of action potentials in the lower motor neurons by delivering electrical pulses to sensorimotor fibres. Electrical stimulation excites nervous fibres and not muscular fibres, because the activation threshold for eliciting a nerve fibre action potential is 100 to 1000 times less than the threshold for muscle fibre stimulation (Mortimer, 1981). For this reason, FES produces a muscular contraction only if the lower motor neurons are intact from anterior horns of the spinal cord to the neuromuscular junctions in the muscles. For what is concerning current-regulated FES systems, biphasic pulses are commonly adopted in order to balance the delivered charge. The strength of the resultant muscle contraction is regulated by three stimulus parameters: stimulus frequency, amplitude and pulse width. The product between the amplitude and pulse width defines the charge delivered by each pulse and determines the number of muscle fibres recruited (spatial summation): greater muscle force generation is accomplished by either increasing the pulse duration or stimulus amplitude to activate fibres with an higher activation

threshold (both smaller fibres and fibres at a greater distance from the electrodes). On the other hand, temporal summation is determined by the rate at which stimulus pulses are applied to muscle. The minimum stimulus frequency that generates a fused muscle response is about 12.5 Hz. Higher frequencies produce higher forces but result in faster muscle fatigue onset (Bigland-Ritchie et al., 1979). The usual parameters' set for FES delivered through surface self-adhesive electrodes are 20-50 Hz (stimulus frequency), 200-500 μs (pulse width), and 10-120 mA (current amplitude).

One of the major limitations of FES applications is the quick onset of muscular fatigue. A possible explanation can be the synchronous firing of all recruited motor neurons when electrical stimulation is applied instead of the physiological turn-over of the fibres. Another reason could be identified in the fibres recruitment order (Figure 4).

Skeletal muscle contains slow-twitch, oxidative type I fibres that generate lower forces but are fatigue resistant and fast-twitch glycolytic type II fibres that generate higher forces but fatigue more rapidly. It is well known that during voluntary contractions the motor unit recruitment order progresses as a function of increasing size, both in terms of number of muscle fibres within the motor unit and diameter of the fibres. Thus, type I fibres, characterized by a smaller diameter, are activated earlier than type II fibres. It is also well known that motor units with larger fibres are innervated by larger axons, which have a lower threshold of electrical excitability (Zajac and Faden, 1985). Therefore, it can hypothesized that during FES-induced muscle contractions larger motor units, which fatigue more quickly, might be recruited at lower stimulation levels. However, no direct evidence indicates that this is the case when surface stimulation is used. In fact, according to Knaflitz and colleagues (Knaflitz and Merletti, 1988), the geometric location and the orientation of the nerve fibres or of the terminal axonal branches in relation to the stimulating electrodes may be more important than their electrical excitability threshold in determining the motor unit recruitment order. However, it is likely that the artificial fibres recruitment order results to be less efficient both in terms of force production and fatigue onset, than the natural one. Electrical stimulation above motor threshold produces a short-latency direct motor response due to stimulation of motor axons, easily identifiable in the elecromyographic (EMG) measure, known as M-wave. In addition to the M-wave, the stimulation of a mixed nerve present the Hoffmann reflex or H-reflex (Hoffmann et al., 1910) that is elicited when the proprioceptive fibres from the muscle are stimulated. The nerve impulse travels along the fibres to the spinal cord, across the synapse located in the ventral horn of the spinal cord and finally orthodromically along the motor neuron. Hence, the H-reflex bypasses the muscle spindle and the fusimotor activity that may influence the sensitivity of the Ia afferents to engage a 'simple' reflex circuit. The H-reflex and M-wave do not recruit the same motoneurons: alpha motoneurons are recruited in an orderly fashion from smallest to largest (Henneman and

Olson, 1965). Thus, small motoneurons innervating slow motor units are recruited first in the H-reflex, while electrical stimulation that elicits the M-wave activates larger diameter axons that innervate fast motor units (Figure 5).

Figure 4 - Fibres recruitment

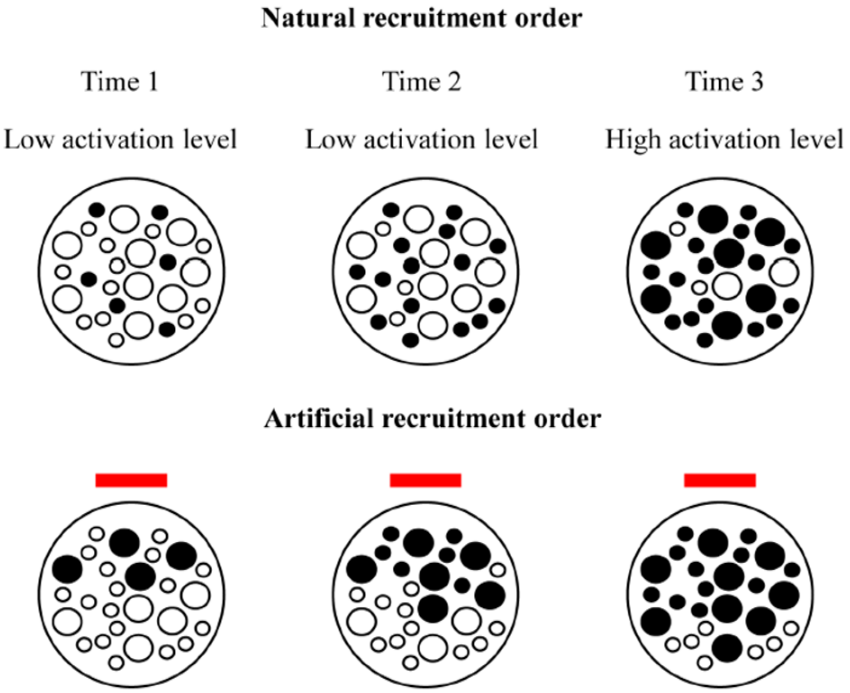

Natural (upper raw) versus artificial (lower raw) recruitment order of muscular fibres. Natural recruitment order progresses as a function of increasing size, both in terms of number of muscle fibres and diameter of the fibres; time 1: few small diameter type I fibres are recruited; time 2: quite all the small diameter type I fibres are recruited; time 3: large diameter type II fibres are also recruited. Artificial recruitment order progresses as a function of increasing electrical excitability, and proximity to the site of stimulation; time 1: larger fibres close to the site of stimulation which have a lower threshold of electrical excitability are firstly recruited; time 2: both type I and type II closer to the site of stimulation are recruited; time 3: deeper fibres are recruited (larger diameter fibres first).

Clinical efficacy

In the clinical environment, the use of electrical stimulation for functional and therapeutic applications is quite diffused in subjects with spinal cord injury or stroke; for a comprehensive review see (Sheffler and Chae, 2007). Works with multiple sclerosis (Taylor et al., 1999), traumatic brain injury (Oostra et al., 1997), and cerebral palsy (Ho et al., 2006) patients are growing in number. Electrical stimulation has known peripheral effects that include strengthening muscles, preventing muscle atrophy, preventing deep venous thrombosis, improving tissue oxygenation and peripheral hemodynamic functioning, and facilitating cardiopulmonary conditioning (Davis et al.,

2008). Of more interest in this context is the use of electrical stimulation to activate paralyzed muscles in precise sequence and magnitude to directly accomplish functional tasks is implemented thanks to a neuroprosthesis, i.e. a device or system that provides FES. The most common applications include neuroprosthesis for upper (Peckham et al., 2001) and lower limbs. The foot drop stimulator is by far the most known FES-based neuroprosthesis, since Liberson and colleagues (Liberson et al., 1961) firstly successfully applied it to a post-stroke population. FES is also used for therapeutic purposes such as motor relearning, i.e. the recovery of previously learned motor skills that have been lost following localized damage to the central nervous system. Some representative studies (Alon et al., 2011; Bogataj et al., 1995; Yan et al., 2005) assessed the efficacy of FES in improving walking ability on hemiparetic patients. Overall, these works suggested that FES applied to the lower extremity improves walking ability if applied to both post-acute and chronic phase. Two recent meta-analysis studies (Kottink et al., 2004; Robbins et al., 2006) have addressed the contributions of FES to gait rehabilitation. Kottink et al. suggested that peroneus stimulation have a beneficial effect on walking speed in stroke patients with a dropped foot. However, it is not known whether these improvements were maintained after the FES device was removed. Robbins and colleagues concluded that gait training with FES can improve gait speed following stroke; in particular, the impact of FES treatment seems to be higher in individuals at the sub-acute stage than in chronic patients, who, however, showed relative small improvements after FES training. A recent Cochrane review (Pomeroy et al., 2006), examined 24 randomized controlled trials aiming at assessing the efficacy of FES in improving the ability to move voluntarily the affected limb and/or use the affected limb in everyday activities. This review found that electrical stimulation improves some aspects of functional motor ability and motor impairment and it is acceptable to participants as assessed by the finding of no statistically significant difference between groups for withdrawal of participants during the treatment phase. The authors concluded that data are still insufficient to provide a clear evidence of the efficacy of FES on motor relearning and that further research is needed to address specific questions about the type of electrical stimulation that might be most effective, in what dose and at what time after stroke. Although more studies are needed to provide a strong evidence of the efficacy of FES-induced therapy in improving locomotor capability, the Ottawa Panel recommended using FES as a supplementary treatment to gait rehabilitation.

Figure 5 - M-wave and H-reflex (Adapted from Wynne et al., 2006).

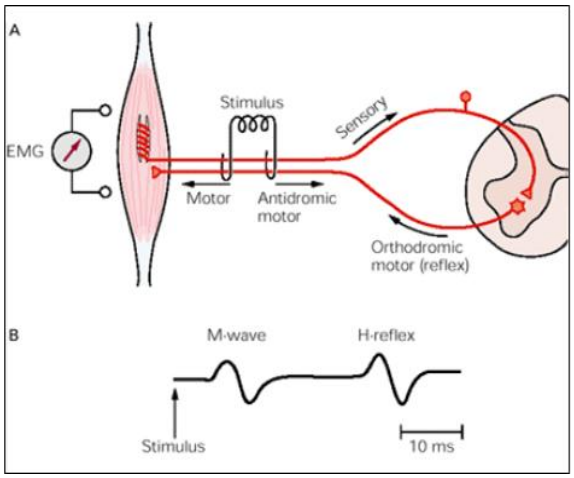

A) The H- reflex is evoked by direct stimulation of afferent sensory fibres from primary spindle endings in mixed nerve. The evoked volley in the sensory fibres monosynaptically excites alpha motor neurons, which in turn activate the muscles. Muscle activation is detected by recording EMG from the muscles. At very low stimulus strengths a pure H-reflex can be evoked because the axons from the primary spindle endings have a lower threshold for activation than all other axons. B) As the stimulus strength is increased, motor axons are excited and spindle afferents are activated. The former produces the M-wave that precedes the H-reflex in the EMG.

Central mechanisms for FES

As previously introduced, in addition to the well-known peripheral effect on muscles themselves, FES is considered to have some central therapeutic effects whose mechanisms of action are still under investigation, although possible mechanisms have been hypothesized (Bergquist et al., 2011; Rushton, 2003). Some hemiplegic patients treated with FES for foot drop correction during walking have shown a relearning effect that outlasts the period of stimulation that was firstly observed by Liberson and colleagues (Liberson et al., 1961) and it is currently known in literature as carryover effect (Ambrosini et al., 2011, 2012). However, we know from literature (Merletti et al., 1979) and from clinical practice that it is not possible to infer which patient will get the carryover effect from a peripheral evaluation. This further supports the hypothesis that FES induces some plasticity mechanisms in CNS reorganization that allows maintaining recovery of motor control.

Only recently, few studies introduced the interest on scanning subjects undergoing FES-induced motor tasks (Blickenstorfer et al., 2009; Francis et al., 2009; Iftime-Nielsen et al., 2012; Smith et al., 2003). These experiments showed that the execution of FES induced motor tasks during fMRI scanning is safe, reliable and feasible. Reproducible changes in activation in healthy subjects during FES-induced motor tasks have been observed in brain areas including primary somatosensory cortex, secondary somatosensory cortex, supplementary motor area, anterior cingulate cortex and

cerebellum both for upper (Blickenstorfer et al., 2009) and lower limbs (Francis et al., 2009). It has been suggested that FES afferent stimulation has an increased beneficial effect, if coupled with active, repetitive, and goal oriented tasks (Sheffler and Chae, 2007). Iftime-Nielsen and colleagues (Iftime-Nielsen et al., 2012) discussed fMRI grasping task brain activity when FES is combined with voluntary effort and they compared this activity to that produced when FES or voluntary movement are performed alone. FES coupled with voluntary effort revealed greater cerebellar activity compared with FES alone and reduced activity bilaterally in SII compared with voluntary movement alone. They suggest that FES modulates the sensory consequences of an internal model through SII area and the cerebellum. Transcranial Magnetic Stimulation (TMS) studies showed that FES-induced repetitive movements enhance motor cortex excitability and facilitate motor-evoked potentials of the tibialis anterior (Barsi et al., 2008; Khaslavskaia et al., 2002; Knash et al., 2003) especially in the context of ambulation (Thompson and Stein, 2004) and concurrent voluntary activation (Khaslavskaia and Sinkjaer, 2005). Cortical facilitatory and inhibitory circuits respond differently to peroneal stimulation if it is presented as an augmentation of voluntary activation (Barsi et al., 2008). Moreover, long-lasting facilitatory effects of the common peroneal nerve repetitive electrical stimulation on the tibialis anterior motor cortical excitability are focally modulated by a voluntary cortical drive (Khaslavskaia and Sinkjaer, 2005). These results suggest that the combination of voluntary effort and FES has greater potential to induce plasticity in the motor cortex. Moreover, Paired Associative Stimulation, stimulation of the common peroneal nerve paired with TMS, applied during swing phase of normal gait induced bidirectional changes in cortico-motor excitability consistent with the Hebbian principle of activity-dependent neuroplasticity (Stinear and Hornby, 2005). Asanuma and Keller (Asanuma and Keller, 1991) demonstrated that electrical stimulation of the somatosensory cortex alone or in conjunction with thalamic stimulation in an animal model induces long-term potentiation (LTP) in the motor cortex. They hypothesized that proprioceptive and cutaneous afferent impulses associated with repetitive movements induce LTP in the motor cortex, which then modify the excitability of specific motor neurons and facilitate motor relearning (Asanuma and Keller, 1991). Up to now, only few works aimed at assessing the changes in cortical activation induced by FES treatment on stroke patients. Kimberley and colleagues (Kimberley et al., 2004) performed a double-blind randomized controlled trial including 16 stroke patients to analyse the correlation between improvement in functional use of the hand and changes in cortical activation measured by fMRI during a finger-tracking task. After 3 weeks of intensive treatment, the authors observed an improvement in hand function associated with an increase of the cortical intensity index in the ipsilateral somatosensory cortex. Cortical activation, as measured by voxel count, did not change. No changes were seen in the motor

cortex in either hemisphere, suggesting that an active involvement in the therapy is needed to facilitate motor cortex plasticity. In patients with stroke, somatosensory deficits are associated with a slower recovery of motor function; therefore, an increase of the sensory input via ipsilateral pathway may be an important mechanism to improve motor recovery following CNS damage. The critical importance of sensory input to motor learning was demonstrated in an experiment in monkeys, in which the primary sensory hand area, known to have dense connections with M1, was ablated (Pavlides et al., 1993). The monkeys were able to execute previously learned tasks normally but were unable to learn new skills. Within this framework, recovery of function is analogous to acquiring a new skill. It has been suggested that repetitive movement therapy mediated by FES has the potential to facilitate motor relearning via cortical mechanisms. Importantly, it has been shown that simple suprathreshold sensory stimulation, unrelated to movement, is of limited functional value (Hummelsheim et al., 1997). It is also possible that electrical stimulation facilitates motor relearning via spinal mechanisms (Rushton, 2003). Electrical stimulation has the unique feature to activate nerve fibres both orthodromically and antidromically. The antidromic impulse in motor nerve fibres reach the AH cells, but it can go no further up the neuraxis. Rushton hypothesized that the corticospinal–anterior horn cell synapse is a Hebb-type modifiable synapse, i.e., one that is strengthened by the coincidence of pre-synaptic and post-synaptic activity. Following brain lesion, the "decorrelation" between presynaptic and post-synaptic activity might weaken the strength of the Hebb-type PT/AT synapse. FES-mediated antidromic impulses, combined with coincident voluntary effort through a damaged pyramidal motor system, could provide an artificial means to synchronize pre-synaptic and post-synaptic activity in the affected population of AH cells, helping to promote restorative synaptic modifications.

Enhanced proprioception

Strong evidences have been presented in literature to support the hypothesis that FES is particularly beneficial through a central effect and that the concurrent voluntary effort from the subject during repetitive movement training facilitates motor relearning as discussed by Sheffler and Chae (Sheffler and Chae, 2007). In order to systematically study the effects of FES at central nervous system level in this work, it has been modelled the input that FES represent in the sensorimotor system. In particular, FES is modelled as perturbation on the system as artificially induced enhanced proprioception. FES can be activated together or independently with the voluntary contraction and, if coupled with volitional descending commands, it supplies an artificial amplification of the sensory consequences of a simple motor task (Doucet et al., 2012). In fact, as previously discussed, FES activates the axons of the peroneal nerve and thus it activates both dromically and antidromically the efferent and the afferent fibres. Considering only the dromic

spikes, the ones in the efferent fibres directly induce a muscular contraction (M-wave) and this contraction then produces as consequence an extra information to be coded by the natural proprioceptive feedback. Moreover, the stimulation of the afferent fibres elicits a sensory volley that is sent to the central nervous system concurrent with the proprioceptive reafference (Burke et al., 1983) that contributes an additional component to proprioceptive feedback. If we consider two functional voluntarily induced movements kinematically comparable (e.g. 20° ankle dorsiflexion) in both conditions of presence or absence of FES, we could infer that both the motor and somatosensory consequences of the movement are amplified.

1.6 Aim and structure of the work

The aim of the present work is to address the following issues:

(i) define an experimental set-up that is suited to measure movement related cortical correlates during functional electrical stimulation;

(ii) define an experimental protocol that is suited to study sensorimotor integration during an active motor task

(iii) investigate the functional anatomy of sensorimotor integration in the human brain

(iv) investigate how functional anatomy of sensorimotor integration is affected by a brain lesion (e.g. stroke)

In order to address all presented issues, this work is organised in five chapters. (Chapter 1) The scientific context and the background literature that were the base of the novel study performed is presented and discussed. (Chapter 2) A novel experimental set-up is defined and validated. The set-up is composed by an fMRI scanner, a motion capture system to accurately detect the effectively executed movement and electrical stimulation under scanning conditions. (Chapter 3) A 2x2 factorial event-related protocol is designed and described for fMRI acquisitions with voluntary effort and FES as factors. The interaction between the two factors is defined as sensorimotor integration activity marker during a volitional motor task. The analysis of the activation maps of the interaction between the two factors, and dynamic causal modelling (Friston et al., 2003) performed on fMRI data is shown to allow to make inferences about effective connectivity between neural systems and how it is affected by experimental conditions. A functional anatomy models is proposed in the context of the active inference framework. (Chapter 4) A group of chronic post-stroke subject underwent the same experimental protocol, in order to investigate how externally

driven proprioception of the desired movement is integrated in a sensorimotor system in the attempt to execute a movement that is no longer correctly performed. (Chapter 5) The conclusion, scientific and clinical implications, and future sights of this work are finally reported and discussed.

Chapter 2 - Experimental set-up: concept and validation

In order to address the study of sensorimotor integration and how it is affected by externally triggered proprioception, a novel experimental set-up has been defined and validated. fMRI is one of the main tools to investigate brain functional responses and follow-up their evolution. However, correlating the features of the actual executed movement with the associated cortical activations can enhance the reliability of the functional Magnetic Resonance Imaging (fMRI) data interpretation. This is crucial for longitudinal evaluation of motor recovery in neurological patients and for investigating detailed mutual interactions between activation maps and movement parameters. Therefore, a new set-up has been explored combining fMRI with an optoelectronic motion capture system, which provides a multi-parameter quantification of the performed motor task. Phantom acquisitions with and without the motion capture system were performed in order to test images and kinematic data quality. An healthy subject and a neurological patient were tested with different motor task protocols in order to investigate compatibility, feasibility of different motor tasks and validity of adding kinematic data to fMRI images analysis (Casellato et al., 2010).

Furthermore, the interest of this work was about the analysis of FES effects at central nervous system level. A further methodological study was therefore performed in order to define and validate the insertion of electrical stimulation inside the MRI room. The focus point was about the Blood Oxygenation Level Dependent (BOLD) signal, marker of neural activity, could be detected within the defined experimental condition and set-up. Signal to Noise Ratio (SNR) was assessed as image quality index and an accurate analysis of the detectability of the BOLD signal within the defined experimental set-up has been performed (Gandolla et al., 2011).

In this chapter, the two steps (i.e., introduction of a motion capture system and introduction of electrical stimulation) are presented, along with their methods, results, discussion and implications for the project, and finally a general conclusion is provided.

2.1 Simultaneous measurements of kinematics and fMRI[1]

fMRI is one of the main tools to investigate brain functional responses and follow-up their evolution. Its non-invasiveness, flexibility, spatial resolution, and reference to MRI anatomical

[1] The work has been published as Casellato C, Ferrante S, **Gandolla M**, Volonterio N, Ferrigno G, Baselli G, Frattini T, Martegani A, Molteni F, Pedrocchi A. Simultaneous measurements of kinematics and fMRI: compatibility assessment and case report on recovery evaluation of one stroke patient. *J Neuroeng Rehabil*. 2010; 23:7-49.

images allows functional standard localizations. However, the analysis of fMRI performed during motor tasks in neurological patients affected by movement impairments (e.g. hemiparesis) requires an adequate monitoring of the actual executed movement performance and timing. Indeed, the required task could be incorrectly carried out and involuntary movements could occur. Moreover, longitudinal studies require repeatability of motor tasks performed in different sessions, in order to not confuse changes in the execution of the movements with evolutions in the brain functional response. Furthermore, mirror movements, i.e., unintentional and simultaneous replication on the healthy side of the intended movements performed by the paretic side, are quite common (Wittenberg et al., 2000) and can affect the interpretation of obtained images. Several studies focusing on motor protocols under fMRI examination applied different methods to acquire movement performance outcomes.

Qualitative movement inspection - Many fMRI studies used visual inspection (Cramer et al., 1997), sometimes coupled to palpation (Dobkin et al., 2004), to evaluate subject's compliance to the requested task; obviously these methods are only qualitative.

Angles measurement - Other studies used electrogoniometers (Ciccarelli et al., 2005; Enzinger et al., 2008) or ShapeTape™ (Measurand Inc., Fredericton, NB) (MacIntosh et al., 2004) to measure the angle at the ankle. Both these devices measure only in one plane, and are cumbersome and not suitable for multi-joint acquisitions. Horenstein and colleagues (Horenstein et al., 2009) recorded finger tapping performance with a MR compatible glove (Fifth Dimension Technologies, Irvine, CA); wearing a glove could, however, generate discomfort in subjects and limit their freedom in the execution of movements.

Force measurement - In some studies forces produced by the subject were recorded using a pressure transducer built in a hydraulic environment (Dai et al., 2001; Liu et al., 2000), using an MRI compatible manipulandum consisting of two force transducers (Ward et al., 2003) or using a load cell (Krainak et al., 2007). In case of force measure no free moving tasks can be executed.

Movement tracking through optical fibres - Another research group used optic fibres to monitor finger movement during writing tasks (Hauptmann et al., 2009): the recording system consisted in a plastic pen with optic fibre inside and a halogen light as power source. The movement was then tracked by a pure optical signal that did not interfere with the electromagnetic field.

Electromyography measurement: compatibility assessment - Electromyography (EMG) is a very complete method to monitor the neuro-motor output (Van Duinen et al., 2005) because even an isometric contraction and a low contraction unable to produce a visible movement can be detected.

Indeed, in most of the latest fMRI studies, EMG has been employed (Dai et al., 2001; Liu et al., 2000).

EMG measurement during fMRI acquisition implies technical issues due to the necessity of placing electrical equipment or devices that contain metal elements and conduct electrical signal inside or near the MRI scanner. Several studies acquired EMG signal outside the MRI room in the hypothesis that the movement would be the same during the scanning and outside the MRI room (Ehrsson et al., 2001; MacIntosh et al., 2004). This assumption can be made for healthy subjects, but not for impaired people because the movement is not well controlled. When simultaneous acquisitions were performed, until a few years ago, it was hard to get reliable EMG signals: indeed, the EMG recordings under the high fMRI fields were corrupted by induction artefacts, highly correlated to the movement and, thus, hardly separable from the addressed EMG. Initially, EMG was analysed only during a short inter-scan interval, when the noise on the signal was low enough, and used as a time trigger. Conventional electrode wires were connected to custom-built differential EMG amplifiers outside the MRI room (Liu et al., 2000). The critical component was identified in the preamplifier. MacIntosh and colleagues (MacIntosh et al., 2007) studied the fMRI signal contamination on EMG data for three different preamplifiers. The signal was contaminated depending on preamplifier position, along the sagittal axis of the subject (z-axis). At z=115 cm (where z=0 corresponds to the magnet iso-center), approximately the location of the lower limbs, all three amplifier configurations studied showed a minimum. The preamplifier is therefore usually placed at the level of subject's legs. fMRI images were shown to be free from artefacts due to EMG acquisition device. Recently (Van Duinen et al., 2005; MacIntosh et al., 2007), new artefacts correction techniques for EMG post-processing have been validated, leading to achieve a reliable EMG signal recorded even during scanning periods (Van Rootselaar et al., 2007). A recent study validated an accurate algorithm so as to clean the EMG signal in real time during fMRI (Ganesh et al., 2007), in order to allow a good estimation of EMG during the acquisition itself.

Electromyography measurement: EMG-related brain activation - Moreover, Van Duinen et al. (Van Duinen et al., 2008) and Van Roostelaar et al. (Van Rootselaar et al., 2007) used EMG recordings not only to verify which muscles are effectively activated, but they actually focused their analysis on brain activations that correlate with EMG activity. Van Duinen et al. (Van Duinen et al., 2008) distinguished between brain areas in which activity was modulated by the amount of EMG and areas that were active during the task but in which the activity was not modulated. They found that activity in motor areas (contralateral sensorimotor cortex, premotor areas and ipsilateral cerebellum) was strongly correlated with the amount of EMG. In contrast, activity in frontal and parietal areas (inferior part of the right precentral sulcus, ipsilateral Supramarginal gyrus, bilateral

inferior parietal lobule, bilateral putamen and insular cortex) was correlated with activation per se, independently on the amount of EMG. Whereas, Van Roostelaar and colleagues (Van Rootselaar et al., 2007) focused on EMG-based regressors definition, so as to directly integrate them into fMRI statistical analysis. They showed that EMG power variability was well correlated with activity in brain areas known to be involved in movement modulation. This demonstrates the possibility of deep analyses on how muscle activation affects activation maps and not only a check on correct movement execution. Nonetheless, EMG could have potential risks for the subjects due to the contact of skin with metallic parts inside time-varying magnetic field and the MR compatibility leads to a significant rising of costs. Moreover, inter-session repeatability of EMG signal recorded in MRI environment is very limited, mainly because it strongly depends on electrode placement, and multi-segment motor tasks could involve different muscular groups, not easy to be detected by surface EMG.

Movement kinematic measurement - Exploring a different approach to the same goal, this study intended to develop a new set-up which combines an fMRI system with an optical motion capture system. The motion capture system records 3-D trajectories of passive markers with high accuracy (Borghese and Ferrigno, 1990). The proposed integrated system has different advantages with respect to the commonly used technologies. First, it allows to calibrate wide working volume so to acquire multi-segment tasks. Second, the only direct contact elements with the patient are small, light and plastic markers, which do not limit spontaneous movement execution and do not carry any potential risk for the subject. Third, the recorded trajectories of the markers are very reliable and highly accurate and well established data processing permit to calculate angular ranges of motions, velocities and accelerations in 3-D of all the segments, enriching the fMRI activation maps with a complete description of the kinematics of the motor output. Fourth, markers placement is very reliable assuring the intersession repeatability. It does not imply any risk for the subject since it is based on plastic markers and it does not create any encumbrance to the movement; it allows both body sides acquisitions and it guarantees an optimal repeatability of markers placements across different sessions and across more subjects. It provides, without any complex data processing, a complete description of motion, by computing accurate parameters, which can represent possible regressors to be introduced into the image analysis. Therefore, it allows to investigate how movement outcome is related to cortical activations and not just to check the meeting of protocol requirements, as explained above for EMG-fMRI studies. In this way, the neurophysiological and biomechanical levels of neuromotor control are simultaneously investigated.

The aim is therefore to prove the mutual compatibility of using a motion capture system inside the MRI bore, by phantom tests and healthy subject acquisitions before and after motion capture

insertion. Secondly, it aims at proposing a method to utilize the recorded kinematics parameters into the fMRI model design, adding movement output as regressor, and to demonstrate the possible positive impact, especially in a neurological (partly collaborative) subject at different stages of rehabilitation.

2.1.1 Methods

Participants

An healthy subject (24 years old, male, right-handed) was recruited, both to assess compatibility between the motion capture and fMRI and to evaluate the feasibility of different motor tasks as clinical protocols.

Moreover, an hemiparetic subject was recruited to validate the clinical usefulness of the setup. The patient (61 years old, female, right-handed) suffered from an ischemic stroke 4 weeks before the acquisition session. The lesion was located on the right hemisphere and covered the insula and temporal cortex. She was not claustrophobic and she had no implanted devices incompatible with MR. fMRI acquisitions were performed at the hospitalization (t=1) and after one month of rehabilitation therapy (t=2). She underwent standard rehabilitation treatment (i.e., physical therapy, including stretching, muscular conditioning, exercises for trunk control, standing, and walking training) and 20 functional electrical stimulation cycling sessions (Ferrante et al., 2008).

Some clinical scores, representative of her motor impairment, are reported (Table 1). This study was undertaken with the understanding and written consent of each subject, with the approval of the Ethical Board of Villa Beretta Rehabilitation Centre.

Table 1 - Clinical scores

Measure	t=1	t=2
Motricity Index (lower limbs)	26	45
Quadriceps MVC (right)	112 N	140 N
Quadriceps MVC (left)	13 N	52 N

fMRI

MRI was performed on a GE Cv/I™ 1.5 T scanner. Subjects anatomy was acquired with a 3D spoiled gradient echo sequence T1-weighted; echo time (TE) = 6.9 ms; automatic repetition time (TR) = 15.9 ms; flip angle = 15 °; matrix 256x256; field of view = 26 cm; voxel

size = 1x1x0.8 mm. For functional imaging sessions a gradient EPI sequence T2-weighted was used; TE = 50 ms; TR = 3 s; flip angle = 90 °; matrix 128x128; FOV = 24 cm; voxel size = 1.8x1.8x4 mm. Each functional acquisition included 100 volumes of 22 images, for a total of 2200 scans acquired in a single run lasting 5 minutes.

Motion Capture System

A motion capture system, Smart μg™ (BTS, Italy), was used to measure kinematics. Cameras have a CCD detector sensible to infrared and a LED enlighter emitting at 850 nm; the working frequency was set to 60 Hz. The system works with passive plastic retroreflective markers, which reflect the near-infrared light allowing the cameras to detect their 2D projection on the sensor planes. From the calibration parameters of each camera and the marker 2D coordinates coming from at least two cameras sensors at the same time instant, the system algorithm is able to provide the absolute 3D position of each marker, by collinearity equations (Borghese and Ferrigno, 1990). Then, the tracking procedure is performed by the operator, using a system-specific software (SmartTracker®), in order to associate the 3D reconstructed data with the markers model, along all acquired frames.

In the present set-up three cameras were bounded to the MR room ceiling (SuperClamp 035™ and 804RC2™ heads Manfrotto, Italy), inside the Radio-Frequency (RF) shield, with one camera centred above the axis of the bore and the other two 1.0 m apart on each side, at the maximum possible distance from the bore (about 3 m). The working volume was about 1x1x1 m, the accuracy reconstruction was less than 1 mm. A fourth camera, outside the MRI room, was used to capture an active infrared LED, which was switched on simultaneously with the fMRI scanning start, in order to synchronize the fMRI protocol and the kinematics acquisition. Also the controller pc was placed outside the shielded room, next to the radiologist desk. Cables connecting the controller pc and the cameras located inside the MR room passed the RF shield across a waveguide (Figure 7, panel A). The motion analyser was calibrated with the shielded door opened; after calibration the door was closed and the fourth camera, used only for synchronization and not for movement reconstruction, was moved to capture the synchronizing LED.

Cameras, heads, clamps and cables are metallic; cameras and enlighters contain printed circuits which are sources of electromagnetic noise, as well as the cables. For this reason the integration of the two systems could introduce both RF noise and inhomogeneity in the main static magnetic field. On the other hand, the optical components could be affected by the static magnetic field, provoking for instance a focalization degradation, and the electrical components could be compromised by the magnetic noise. As seen in literature (Tang et al., 2008), in order to limit the RF interference introduced into the MR images by electronic devices, aluminium foils, connected to MR room

ground, were contiguously applied to the cables connecting cameras and CPU. Enlighters, as well, were partially covered with grounded aluminium foils.

Compatibility test

In order to evaluate the interference between the two systems, MR images of a phantom were acquired with (i.e. reference condition) and without the working motion capture system inside the MR room (i.e. integrated set-up). A standard phantom with one-compartment of aqueous paramagnetic solutions was used. 30 seconds EPI sequence acquisitions were performed (with the parameters described above in *fMRI*), thereby 10 volumes of 22 images each were obtained.

The Signal-to-Noise Ratio (SNR) was calculated on each slice for all volumes. We used the standard index for image quality (Kaufman et al., 1989), that is the ratio between the mean signal amplitude on a homogeneous area and the standard deviation of the background signal amplitude. Therefore, the ratio between the mean value of a small region placed in the most homogeneous area of phantom (around the barycentre) with high signal intensity and the mean of standard deviations for four areas placed outside the object in the image background was computed (Figure 6).

Figure 6 – Illustration of SNR calculation

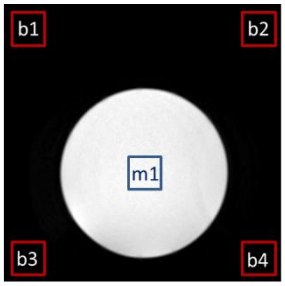

$$SNR = \frac{mean(m_1)}{mean(std(b_1), std(b_2), std(b_3), std(b_4))}$$

On the left hand side representation of a slice of the homogeneous phantom with indicated the regions for SNR calculation (the figure has illustration purposes only). m1 = area in the most homogeneous area of phantom (around the barycentre); b1/b2/b3/b4 = areas in the background of the images (four corners). On the right hand side the equation for SNR calculation is indicated.

Afterwards, for each slice, the loss of SNR percentage was computed as following:

$$\Delta SNR = \frac{SNR_{ref} - SNR_{system}}{SNR_{ref}} * 100$$

where SNR_{ref} corresponds to the reference condition and SNR_{system} to the integrated set-up.

Moreover, in order to establish possible effects of magnetic fields on the recording accuracy of the motion capture system, tests on kinematic data were performed. A marker was repeatedly launched

vertically during a phantom fMRI session (N=4). The equation of uniformly accelerated linear motion was applied on the descending tracks of the falling down marker: knowing, from recorded kinematic data, the displacement and duration, the mean value of acceleration was computed.

Protocol procedures

Subjects were instructed to keep eyes closed to avoid activations of visual cortex. Head movements were minimized with rubber pads and straps. To ensure minimum transmission of movements to the head across the spine, knees were bent and legs lied on a pillow. Participants wore earphone and microphone to communicate with the operator who gave them oral commands, triggering the task temporal sequence (start and stop of each 30 s block). The fMRI paradigm consisted of a 30 seconds block design alternated with 30 seconds rest blocks.

The healthy subject was tested during two different tasks, to evaluate the compatibility between the two systems and a preliminary clinical feasibility (Table 2). The first (H1, H2) was a finger tapping task, performed with both hands in separate sessions. It was chosen because it is a well-established task and it leads to the activation of well-defined areas (Liu et al., 2000), easy to be localized. The healthy subject was asked to tap the thumb with the pulp of each finger in turn, starting from the index finger; no constraints were imposed on the frequency of execution. The second task (H3, H4) was self-paced ankle dorsal- plantar-flexion. The subject performed the protocols alternatively with both sides, in separate sessions.

For the hemiparetic patient only the ankle dorsal- plantar-flexion on both sides was chosen as clinical protocol for evaluation, since fine hand control was not completely recovered at the considered rehabilitation stage. The patient was tested before and after an FES-based rehabilitation treatment.

In order to get confident with the required motor task, prior to each MRI acquisition, the subjects underwent a training that replied, out of magnetic resonance room, the conditions of the examination. During this training, along with ankle angles of both limbs, superficial EMG activity from soleus, gastrocnemius lateralis and tibialis anterior muscles was acquired for the patient, in order to exclude mirror isometric contractions, which the kinematics system would not have detected.

Table 2 - Tested protocols

Subject	Executed protocols
Healthy subject	H1. Right (dominant) finger tapping protocol
	H2. Left (non-dominant) finger tapping protocol
	H3. Righ (domainant) ankle plantar-dorsi-flexion protocol
	H4. Left (non-dominant) ankle plantar-dorsi-flexion protocol
Neurological subject	P1. Right ankle plantar-dorsi-flexion protocol; pre-treatment
	P2. Left (paretic) ankle plantar-dorsi-flexion protocol; pre-treatment
	P3. Right ankle plantar-dorsi-flexion protocol; post-treatment
	P4. Left (paretic) ankle plantar-dorsi-flexion protocol; post-treatment

Kinematics acquisition and data analysis for finger tapping

Markers were placed on the top of the index and pinkie fingers and dorsally on the wrist (Figure 7, panel B) of both hands. A plastic support with two markers identified each thumb; this solution was adopted to avoid uncorrected reconstructions, due to the compromising of markers visibility during the touching phases between fingers. Three fingers for each hand were considered sufficient for a validation acquisition on an healthy subject; indeed, desired movement parameters, as the frequency and the movement amplitude for each cycle were computable.

The reconstructed trajectories were filtered with a fifth-order Butterworth low-pass filter (cut-off frequency = 5 Hz) and 3D displacements of index and pinkie fingers were analysed. For each active period, considering all cycles, the mean Displacements of moving Index (i.e., index displacement - ID) and of moving Pinkie (i.e., pinkie displacement - PD) were computed. The frequency (f) of movement (number of cycles/30 s block) was calculated; the same number of repetitions for the two analysed fingers is a proof of correct task execution. The displacements for index and pinkie fingers not involved in the task were estimated by standard deviations (i.e., index standard deviation – ISD; pinkie standard deviation - PSD). So as to assess the presence of mirror movements, the correlation coefficients between the two hands fingers (i.e., R index and R pinkie) were computed. Movements of the hand not required to perform the task were considered to be significant when standard deviation > 0.5 cm, and were considered mirror movements when correlation coefficient > 0.5.

Kinematics acquisition and data analysis for ankle dorsal- plantar-flexion

Two markers, distal and proximal, were placed on the tibia and a third one was placed on the top of the toe (Figure 7, panel C). Ankle angle was approximated with the angle α defined by the line

passing through the two markers placed on the tibia and the line joining the marker on the toe and the projection of malleolus on the tibia-line. The values are shifted considering 0 ° as the perpendicular condition. In order to reconstruct the ankle angle, a fifth-order Butterworth low-pass filter (cut-off frequency = 5 Hz) smoothed the recorded trajectories and data were projected on the plane that carried most information about the movement, identified with principal components analysis (Baroni et al., 2001). For each acquisition the Mean Amplitude (MA) and the frequency (f) of the dorsal- plantar-flexion movement were calculated during active blocks. The angular displacement for the foot not performing the task during activation epochs was estimated by the Standard Deviation of α (SD) in order to verify the correct fulfilment of the task. To assess if the involuntary movement was a mirror movement or not, the correlation coefficient (R) between the angles at the two ankles was computed. Relying on values found for the healthy subject, movements of the foot which was required to stand still were considered significant when SD > 4 °, which means > 5 % of the moving ankle range of motion, and were considered mirror movements when R > 0.5. The training outside the bore was also used to validate the chosen landmarks as representative of the movement protocol.

Figure 7 - Experimental set-up

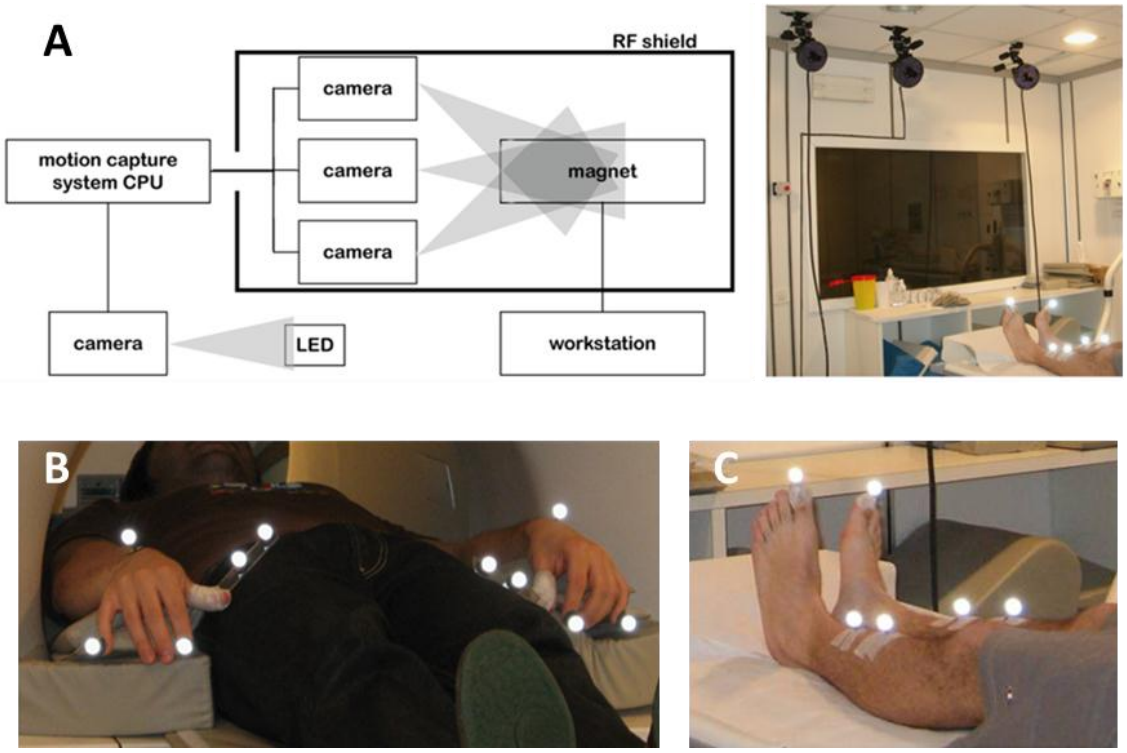

A) a scheme and a picture of the integrated experimental setup; B) position of the markers for finger tapping acquisitions; C) position of the markers for ankle dorsal- plantar-flexion acquisitions.

fMRI data analysis

Functional images were converted from DICOM to Analyse format with the MRIcro software (Rorden and Brett, 2000). Pre-processing and statistical analysis were carried out with SPM5® (Wellcome Trust Centre for Neuroimaging, London, UK, http://www.fil.ion.ucl.ac.uk/spm/) running on Matlab® (2007a, The MathWorks, Natick, MA). Images were corrected for slice timing and realigned to the first image of each respective acquisition. The first acquired image is reliable because it is the first one afterward a 30 s "preparation phase", aiming at getting a steady-state magnetization. The motion correction algorithm, as a standard processing step from SPM5, was run (Friston et al., 1996). As demonstrated by Johnstone and colleagues (Johnstone et al., 2006), in a block design, or more generally a design in which head motion parameters are even moderately correlated (correlation coefficient 0.2 or greater) with the model, including the head motion parameters as covariates of no interest has a deleterious impact reducing the sensitivity for detecting true activations. Since our experimental design and the not negligible correlation of head motion with the required movement protocol, we chose to not insert the realignment parameters as covariates in the design matrix. Images were then normalized on the Montreal Neurological Institute (MNI) standard brain (Mazziotta et al., 2001). Finally, they were spatially smoothed with a Gaussian kernel homogeneous in the three spatial directions, with a Full Width Half Maximum Gaussian filter of 6 mm, to increase the signal-to-noise ratio.

For each experimental session, a general linear model was employed (Friston et al., 1995), performing each analysis with two different types of model design. In the first design, i.e. the standard block design, only the stimuli was modelled with a conventional boxcar function as five rest periods of 30 s alternating with five active periods of 30 s. In the second one, a user defined kinematic regressor describing the actually executed movement was added into the design matrix besides the stimuli. The kinematic regressor was the amplitude along time, computed from recorded kinematic coordinates. This way kinematic regressor comprises both different amplitude of tasks execution as well as timing of task execution not coherent with the request. The effect of inserting the actual kinematics parameters in the generation of cortical activation maps was evaluated comparing the two models.

A high-pass filter was automatically included in the analysis by SPM5 (cut-off time constant = 128 s). Statistical analysis was accomplished using a p-value < 0.01 with Family Wise Error correction and extent threshold of 100 voxels.

Four ROIs were defined, two of them matching the representation of ankle in the sensorimotor cortex for each hemisphere and two matching the hand mapping areas. Coordinates in MNI

reference system for the centre (for the foot: x = ±6 mm, y = -37 mm, z = 70 mm; for the hand: x = ±36 mm, y = -22 mm, z = 58 mm) and extension of the ROIs were obtained from literature (Alkadhi et al., 2002). To define such ROIs, we used the standard software WFU PickAltas, which provides a tool for generating ROI masks based on the Talairach Daemon database; this method is an automated coordinate-based system which retrieves brain labels from the 1988 Talaraich Atlas (Lancaster et al., 1997).

For each acquisition, the centre of mass of activated areas was calculated, weighting the intensity, of each cluster of voxels included into the areas of interest (motor ROIs).

To estimate inter-hemispheric balance, weighted laterality index (wLI) (Calautti et al., 2007) was calculated from the sum of t-values across all active voxels in each ROI according to the formula:

$$wLI = \frac{(\sum t_c - \sum t_I)}{(\sum t_c + \sum t_I)}$$

where t_C are t-values of voxels lying in the ROI in the contralateral hemisphere and t_I are t-values of voxels lying in the ROI in the ipsilateral hemisphere. wLI ranges from -1, which stands for a totally ipsilateral activation, to 1, totally contralateral.

2.1.2 Results

Compatibility test

The computed SNR values were compared between the two experimental conditions: without (i.e. reference condition) and with three working cameras of the motion capture system within the scanner room (i.e. integrated set-up). SNR values for the two experimental conditions are reported in Figure 8: the time profile inside one volume (22 slices) and along the acquired 30 s was the same with and without motion system, showing an analogous reduced SNR at the first slices for each volume. The relative ΔSNR between the two conditions, averaged among volumes, was 2.37 ± 2.9 %.

Concerning the kinematic data reliability, the acceleration value, averaged among four trials, was 9.92 ± 0.26 m/s^2 , as expected in standard condition.

Figure 8 - SNR evaluation

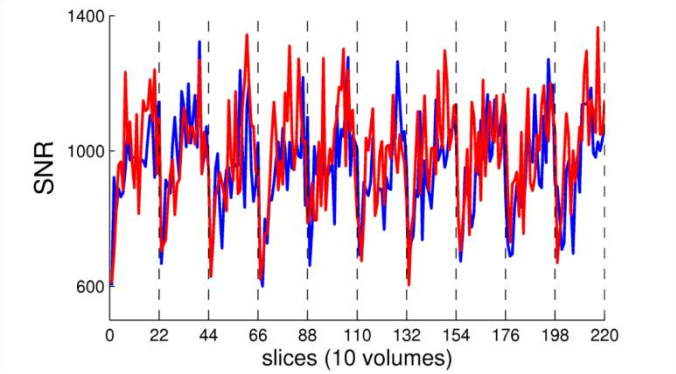

SNR along with the 220 slices, split up into 10 volumes (vertical dashed lines). Red: reference condition; Blue: with motion capture system working within the scanner room.

Realignment parameters assessment

The measure of the realignment parameters showed that the worst case (i.e. maximum displacement) was observed in the rotational parameters during the P2 session (i.e. pre-treatment ankle plantar-dorsiflexion paradigm with the paretic leg); indeed she could not realize any movement and her efforts could be the main reason of these higher movements. Since this session was not used for cortical maps comparisons because of absence of any performed movement, all other absolute values of translation indexes were less than 1.89 mm (maximum around z-axis) and rotation angles less than 2 ° (maximum for the pitch angle). Even if an acceptance threshold is not officially defined, these values are plentifully under thresholds already reported in literature, e.g. 4 mm translation and 5 ° rotation (Johnstone et al., 2006).

Healthy subject acquisition

Healthy subject anatomical and functional images showed a similar increase in broadband noise. On the reference anatomical images, we could see narrow zippers artefacts. As explained by Heiland in (Heiland, 2008) they are caused by RF signals leaking into the receiver of the MR scanner and appear as bright lines in MR images. Their positions within the image depend on the frequency of the RF source that causes the artefact (not-completely shielded equipment inside the scanner room), as well as on readout bandwidth and field of view. Within the functional images, these zippers are not visible. This probably means that in functional images, the low resolution leaded to the RF noise aliasing. A basic evaluation of this the RF noise distributed on the fMRI image is represented by the SNR reduction on the phantom images.

Finger tapping task (H1, H2)

Concerning the right finger tapping task, subject correctly respected the temporal sequence and performed the task with almost constant movement extent and rhythm. The significant kinematic parameters are reported in Table 3. No involuntary movement, nor mirror movement were observed for the resting hand. As expected since the accomplishment of the required protocol, the analysis with the design matrix including the kinematic regressor (index displacement along time) yielded analogous activation maps compared with the standard design matrix analysis, in terms of both localization and extensions even if it yielded to better statistics (i.e. higher t-values) due to a better modelling. Activated areas were mainly located in the contralateral sensorimotor cortex and pre-motor cortex, a few lied in Brodmann's Areas (BA) 5 and 7 too. Activation was totally contralateral (wLI=1) and the activation barycentre was at [-37 -27 52] mm, consistent with the homunculus topography for hand. Left side provided analogous results (and it is not reported in Table 3).

Ankle dorsal- plantar-flexion task (H3, H4)

Kinematic data for the healthy subject, right and left ankle, are reported in Table 3. The planarity of movement was verified for all the acquisitions by principal component analysis: at least 98% of information related to trajectories lied on the plane chosen for projection. The subject correctly respected the temporal sequence of the task. Accordingly to the fact that the kinematic regressor (ankle angle along time) follows the pre-defined stimuli, the two analyses yielded to similar activation maps, for both sides. Activated voxels were located in contralateral sensorimotor cortex and pre-motor cortex for right ankle plantar- dorsi-flexion (Figure 9, panel A). When executing the task with the left foot some active voxels were found in contralateral BA 5, too (Figure 9, panel B). Activations were highly contralateral for both sides (wLI > 0.86). For both protocols, kinematic data provided the demonstration that healthy subject performed the tasks meeting the required timing and using a comparable amplitude and frequency of execution along the different blocks, as expected.

Table 3 - Kinematic data

	1st block	2nd block	3rd block	4th block	5th block	Mean
H1. Right (dominant) finger tapping protocol						
ID [cm]	3.5± 2	6.3 ± 2.8	8.2 ± 2.5	6.2 ± 1.6	3.8±1.6	5.6 ± 2.1
PD [cm]	1.7±0.9	3.3±0.8	3.9±0.9	3.1±0.8	2.8±0.4	3±0.7
f [Hz]	0.33	0.37	0.33	0.37	0.4	0.36±0.03
ISD [cm]	0.02	0.03	0.02	0.01	0.01	0.016±0.01
PSD [cm]	0.04	0.01	0.02	0.03	0.02	0.025±0.01
H3. Right (dominant) ankle plantar-dorsi-flexion protocol						
MA [°]	37.89±5.61	38.53±4.8	43±8.6	46.32±10.32	49.15±11.91	42.98 ± 8.24
SD [°]	0.81	0.3	0.43	0.46	0.2	0.45 ± 023
f [Hz]	0.57	0.47	0.47	0.53	0.5	0.51 ± 0.04
R	0.07	-0.2	0.35	-0.24	-0.33	-0.07 ± 0.28
H4. Left (non-dominant) ankle plantar-dorsi-flexion protocol						
MA [°]	46.28 ± 5.57	43.01± 8.16	42.39±7.33	43.77 ± 7.35	44.25±6.84	43.94 ± 7.05
SD [°]	0.89	0.99	0.48	0.49	0.45	0.66 ± 0.26
f [Hz]	0.47	0.63	0.53	0.50	0.56	0.54 ± 0.06
R	0.15	-0.05	0.08	-0.01	0.14	0.06 ± 0.09
P1. Patient healthy foot at hospitalization						
MA [°]	27.11 ± 7.70	29.88 ± 6.25	31.29 ± 5.91	31.8 ± 7.63	31.02±7.38	30.23 ± 6.99
SD [°]	0.11	0.04	0.04	0.08	0.06	0.07 ± 0.28
f [Hz]	0.4	0.43	0.43	0.53	0.43	0.45 ± 0.05
R	-0.2	0.32	0.49	-0.07	0	0.11 ± 0.29
P3. Patient healthy foot after one month						
MA [°]	46.47±7.17	44.41±9.71	54.11±18.37	59.95±19.47	63.36±18.82	53.69±14.71
SD [°]	0.3	0.19	0.2	0.07	0.13	0.18 ± 0.33
f [Hz]	0.8	0.9	0.87	0.93	0.9	0.88 ± 0.05
R	-0.18	0.13	-0.07	-0.01	0.29	0.03 ± 0.18
P4. Patient paretic foot after one month						
MA [°]	9.91 ± 6.05	9.64 ± 4.7	9.74 ± 3.86	10.55 ± 4.1	11.06±18.82	10.18 ± 4.72
SD [°]	7.8	7.77	4.93	5.6	5.34	6.58 ± 1.38
f [Hz]	0.13	0.16	0.13	0.3	0.13	0.17 ± 0.07
R	0.59	-0.05	0.75	0.16	0.18	0.33 ± 0.33

Kinematic data measured when the healthy subject was performing the finger tapping with the right hand - ID: Index Displacement; PD: Pinkie Displacement; f: frequency; ISD: rest Index Standard Deviation; PSD: rest Pinkie Standard Deviation. Kinematic data measured during the ankle dorsiflexion task - MA: ankle angle mean amplitude; SD: standard deviation of the resting ankle; R: correlation with the resting leg motion; F = frequency of the movement.

Figure 9 - Cortical maps for right and left ankle dorsi-flexion of healthy subject

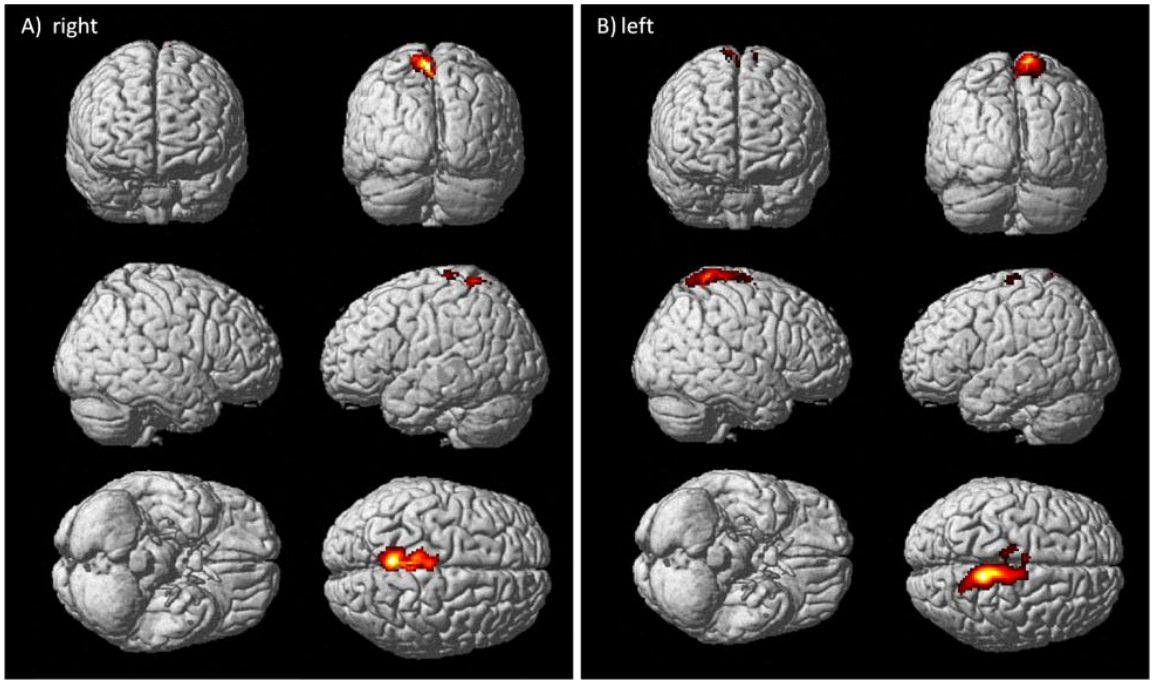

Activations, rendering 3D, for healthy subject, right ankle protocol (panel A) and left ankle protocol (panel B), both analysed with the model design including the kinematic regressor.

Hemiparetic subject acquisition

Pre-rehabilitation acquisition (P1, P2)

At the hospitalization the patient needed a wheelchair and could not perform any movement with the paretic limb: kinematic data did not show any significant angle variation for the paretic limb. No active voxels were found while she was trying to execute the task with the paretic foot, even when limits on cluster extension were removed and significant threshold on p-value increased till 0.05. It could hypothesized that if imagery-related activations were present, they were disorganized so as to be not visible (acute phase at hospitalization). Instead, with the healthy foot, she was able to perform the required movement, but she did not manage to meet time triggering imposed by the operator. She kept moving after stop signals in third and fourth active blocks (Figure 10). Kinematic data are reported in Table 3.

Figure 10 - Kinematic regressor of patient's healthy foot pre-rehabilitation (P1)

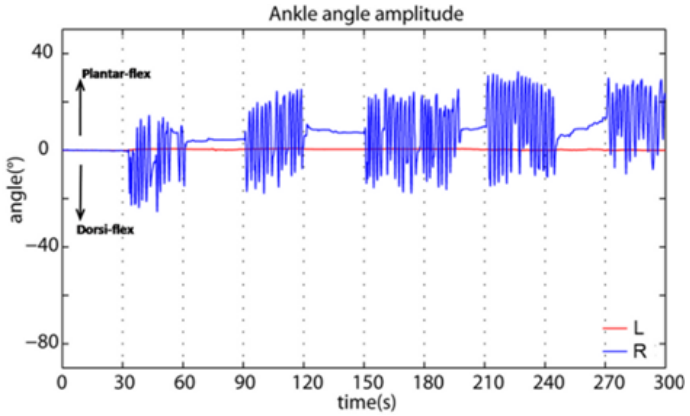

Ankle angle amplitude of patient's healthy foot (right) at hospitalization (the bar at the bottom of the figure highlights the actual timing). It was sampled for matching with the scans number and then inserted into the design matrix as kinematic regressor.

In such case, given the difference between the stimuli and the kinematic performance (ankle angle along time), a modified outcome due to the kinematic regressor was expected.

Figure 11 shows the comparison between the statistical analysis using the predefined standard block design matrix (panel A) and the matrix including the regressor with the actual kinematics (panel B). The latter led to a better model of the data as it can be observed by the extent of the activated area and from the more significant t scores due to better variance explanation (Table 4). The wLI was accordingly different (0.64 with predefined design matrix and 0.72 with kinematics regressor), being the extent of activations almost doubled. The position of activated areas barycentre was only slightly affected ([-4 -30 71] mm with predefined design matrix and [-5 -31 70] mm with kinematics regressor). Active areas were identified in the primary sensorimotor cortex and BA 5 and 7. The two involved lobes are the parietal and the frontal ones in both analyses, even if the use of kinematic regressor allows to almost duplicate the significant activated voxels in both lobes. In particular, the increased activated cortical functional BAs are within the somatosensory cortex (BA 2,3,5,7) and the motor cortex (BA 4, 6). The wider activation of BA6 indicates the strong involvement of premotor cortex (PM) and supplementary motor area (SMA).

Post-rehabilitation acquisition (P3, P4)

After one month of rehabilitation, for the not impaired limb, the patient achieved a good fulfilment of temporal sequence; the ankle motion was quite repeatable in between blocks (Table 3). As a consequence, the model design with the addition of the kinematic regressor did not modify significantly the activation maps. Primary sensorimotor cortex and BA 7 (

Figure 11, panel C), prevalently in the contralateral hemisphere (wLI = 0.84), were activated. Compared to the pre-rehabilitation session of the same foot, these findings highlighted a globally larger activated area and a slight improving of the contralaterality.

After one month of rehabilitation the patient was able to move again the paretic side. With the paretic limb the patient executed a movement. Nevertheless the patient did not manage either to meet the task timing or to keep the right foot still, as requested by the protocol (Table 3). The activations obtained from the two model designs were therefore different. In particular, the standard design yielded to small clusters (all less than 25 voxels) and all in the ipsilateral hemisphere. Instead, inserting the actual kinematics regressor into the design matrix yielded to more meaningful activation maps, i.e. wider clusters and even in the contralateral hemisphere (

Figure 11, panel D).

Table 4 - Activated voxels for not paretic pre-rehabilitation ankle plantar-dorsi-flexion session, comparing the two model designs

Region	**# voxels**	
	With predefined design matrix	**With re-defined design matrix**
TOTAL # VOXELS	228	451
Left cerebrum	155	336
Parietal lobe	103	227
Paracentral_Lobule_L (aal)	103	212
Postcentral gyrus	83	188
White matter	87	179
Gray matter	52	128
Frontal lobe	52	112
Precuneus_L (aal)	27	88
Paracentral lobule	35	78
Precentral gyrus	31	58
Brodmann area 4	16	43
Brodmann area 3	18	32
Brodmann area 6	4	26
Inter-hemispheric	11	22
Postcentral_L (aal)	14	20
Brodmann area 5	9	19
Medial frontal gyrus	6	15
Paracentral_Lobule_R (aal)	9	13
Brodmann area 2	5	6
Parietal_Sup_L (aal)	3	5
Supp_Motor_Area_R (aal)		3
Right Cerebrum		3
Brodmann area 7		2

Figure 11 - Cortical maps of patient

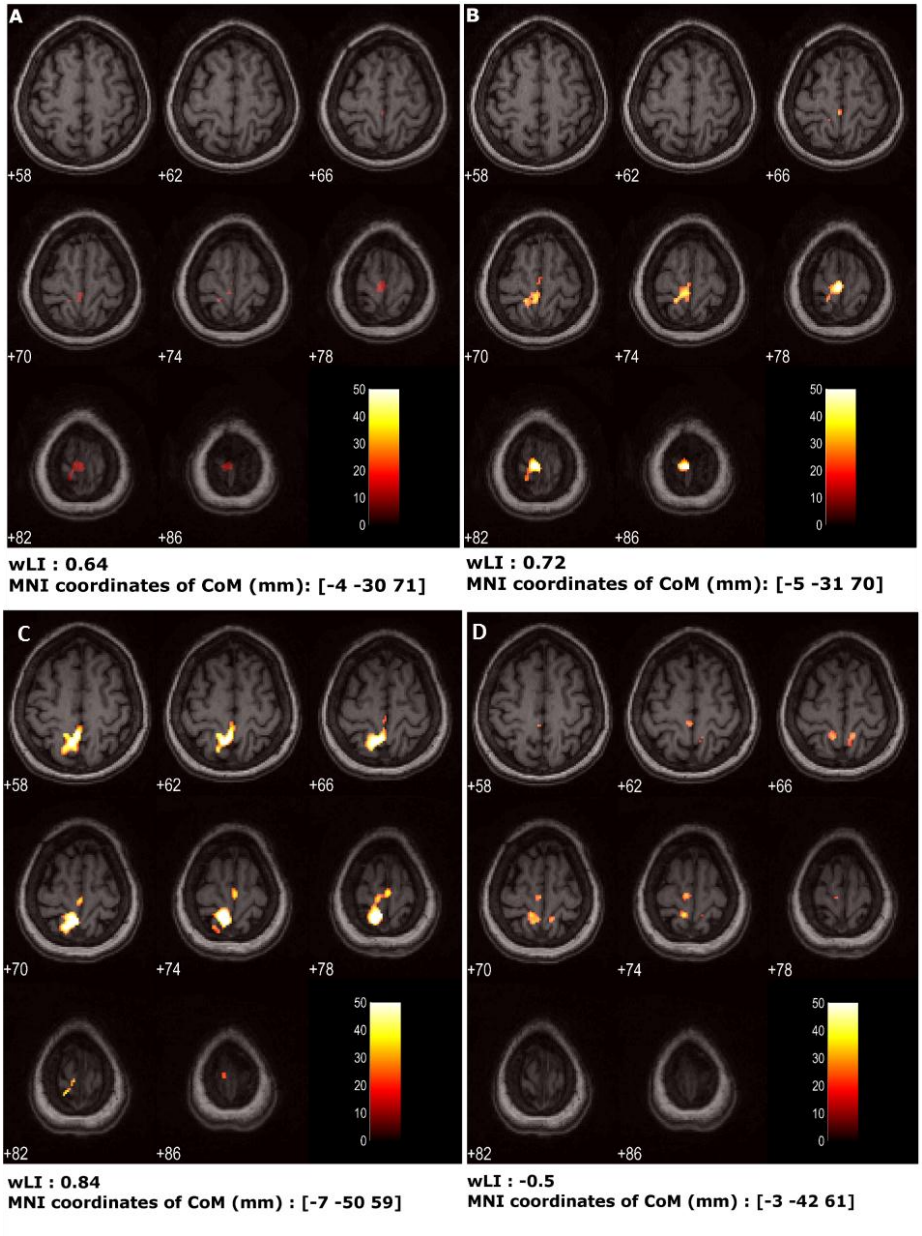

Activation for patient's healthy foot at hospitalization, seven transversal slices centred around z = 70 mm are shown (slice thickness = 4 mm). A) P1 (i.e. non-paretic plantar ankle plantar-dorsiflexion pre-treatment) protocol; activation maps using standard design matrix for statistical analysis; B) P1 protocol; activation maps using design matrix with the kinematic regressor; C) P3 (i.e. non-paretic plantar ankle plantar-dorsiflexion post-treatment) protocol; activation maps using design matrix with the kinematic regressor; D) P4 (i.e. paretic plantar ankle plantar-dorsiflexion post-treatment) protocol; activation maps using design matrix with the kinematic regressor. Under each one, wLI and coordinates of the centre of mass of activated areas are reported. Note that the colour scale was set equal for both panels.

2.1.3 Discussion

Compatibility test

The loss of SNR introduced by the motion system (2.37 ± 2.9 %) can be considered as negligible. Indeed, we can use as reference the recent study of Scarff and colleagues (Scarff et al., 2004): in simultaneous recordings of fMRI and EEG, they showed that MR image SNR, computed as we did, decreased as the number of electrodes increased, and they fix as data quality acceptable a SNR loss on the images of 11-12%. Their value originates from completely different device components, more complex and necessarily closer to the MR scanner; anyway, it can be considered a general reference (worst case) about the additive noise on the fMRI images due to a new device. Other studies (Chaudhary et al., 2010; Glover and Law, 2001) using similar parameters (e.g. signal to noise fluctuation ratio) assessed the reliability of fMRI images finding a relative SNR loss with respect to the standard condition of 2.75%. Mullinger and colleagues (Mullinger et al., 2008) evaluated on a phantom the effect of the conducting materials in the EEG-caps with 1.5 T acquisitions, accepting a SNR reduction of 27 % with 32 electrodes. The use of three cameras allows a reliable reconstruction of 3D positions of the markers. Three cameras, even if not positioned with the optimal mutual orientations having as major priority to put them on the ceiling at the maximal distance from the bore, represent a good compromise between the introduced noise and the reliability of markers reconstruction. Indeed, the calibration procedure for each session, estimating the reconstruction error on a moving bar with 3 markers at fixed known distances, confirms the high accuracy of kinematic data (in our case, accepted error < 1 mm on a working volume of 1x1x1 m). The computed mean gravity acceleration was as the expected one, hence the magnetic fields did not affect the motion capture system and camera data processing. Feasibility of methodology was therefore demonstrated.

Healthy subject acquisition

Both the hands and the legs were visible; thus, excluding the part inserted into the bore, it was demonstrated the possibility of acquiring a great number of multi-segment motor tasks. Since the easiness and the not invasiveness of markers positioning, the landmarks definition can be customized depending on the patient's specific movement skills and the segments involvement in the movement execution. For instance, depending on the goals of study, it could be necessary, for a finger tapping task, to monitor each individual finger. Smaller markers and not cumbersome rigid structures could represent valid solutions, but the working volume extent, the distance between cameras and bore and the reconstruction error have to be specifically evaluated.

On the healthy subject anatomical image two narrowband "zippers" appeared. Because of their position and size, no problem occurred for image processing. However, loss of significance could not be completely excluded due to pixels covered by zippers.

For both the tested protocols on the healthy subject, the proposed method has been implemented including the actual kinematics into the protocol model. As expected for healthy subject, who correctly meet the request, the kinematic parameter did not add new information with respect to the pre-defined stimuli and the cortical maps did not experience any significant changes.

The activation maps areas, the position of clusters barycentre and the level of contralaterality were in both tests consistent with the literature. Comparing the obtained functional areas between the two motor tasks, it was highlighted an additional activation of BA 5 and 7 for finger tapping compared to ankle dorsal- plantar-flexion. Indeed, these areas are involved in maintaining a spatial reference system during execution of fine and complex tasks, by coordinating movement and proprioception, hence when the involved degrees of freedom are numerous. The hand has a larger cortical representation, especially in the pre- and postcentral gyri, compared to lower limb representations (Lotze et al., 2000; MacIntosh et al., 2004), as expected by literature.

Hemiparetic subject acquisition

The healthy foot pre-rehabilitation and the paretic foot post-rehabilitation sessions confirmed the usefulness of design matrix redefinition with the inclusion of the kinematic data. In the latter, only with such model optimization activation maps showed significant activation clusters, making the cortical map consistent with the performed bilateral modest movements.

Furthermore, for healthy foot post-rehabilitation session, a greater extension of activations was obtained, in the same areas, compared to the ones found at hospitalization, before the rehabilitation treatment. The quantitative measurements of movement amplitude and frequency obtained with motion capture system provide information that could be precious to relate difference in activation characteristics to difference in the movement parameters. A recent study (Luft et al., 2005) evidenced that post-stroke modifications in neuronal networks controlling the paretic limb, especially compensatory recruitment of the non-lesioned hemisphere, may affect cortical areas in control of the non-paretic limb. Moreover, non-use of both lower extremities due to impaired walking or altered limb kinematics and body posture due to hemiparesis may induce neural adaptations in networks controlling the intact limb. Hence, quantifying mirror movements and movement extent, both for paretic and healthy sides, is crucial to interpret what is due to bilateral movements, what is due to larger movements and what is an expression of neural plasticity: indeed,

depending on lesion location, a compensatory recruitment of bilateral cortical regions can be part of the motor recovery.

The standard statistical analysis of fMRI images, usually employed in clinical examinations, is based on the repeatability of protocol blocks, in terms of both periods duration and execution parameters (amplitude and frequency). This hypothesis is actually the main limitation of fMRI exploitation for motor recovery evaluation; indeed, this repeatability is not quantitatively verified, thus the resulting cortical maps are affected by possible variations of the task execution. This repeatability assumption becomes even weaker for neurological patients than for healthy subjects. The possible poor matching among protocol blocks parameters can affect the intra-session analysis. This non-repeatability increases when considering different sessions of the patient at different stages of the rehabilitative pathway; this element needs therefore to be monitored for longitudinal studies aimed at the evaluation of rehabilitative process. This loss of comparability turns out to be even more significant for inter-subjects studies, where, for instance, a specific rehabilitation treatment is under test.

The repeatability of the markers placement and the comparability of motion parameters represent the main advantage of using motion capture system with respect to EMG, where the level of noise of the recorded signal and the criticality of electrodes positions strongly limit the possibility to compare consistently muscles activation profiles between different experimental sessions. Further, when the interest is on movement execution, the correct single subject choice of muscles to be studied can complicate because of synergism, while kinematics offer a simple, reliable and general picture of motion. On the contrary, when the study is focused on presence of isometric contractions, kinematics is not at all suitable, or when different muscles strategies are investigated only EMG could provide detailed analysis.

The present work demonstrates the availability of the possible simultaneous measure of kinematic data and fMRI, offering an innovative and extremely flexible experimental set-up for a better understanding of neural correlates of motor tasks.

As initial step, here the kinematic data have been successfully adopted to enrich the design matrix by including the representative parameters of the performed movement in the boxcar function used during fMRI block statistical processing; it means to take into account both the movement extent within and between blocks and the actual specific segmentation of task-execution periods and rest periods. The utility of design matrix re-definition for fMRI statistical processing have been recently demonstrated also by Krainak and colleagues (Krainak et al., 2007): the mechanical motor output was measured in terms of force and torque, by a MR compatible 6-degree of freedom load cell, and

the torque signal was used to identify the onset and the end of each single trial; the set-up permitted nevertheless only isometric protocols for upper limbs. Our combined methodology allows, indeed, recording of multi-joint dynamic motor tasks and there are not any constraints about the duration of trials, which can be defined for both block or event-related protocols.

Moreover, the use of motion capture allows to track a huge number of markers in the calibrated working volume, permitting synchronized quantitative information about movements of multiple segments. This aspect strongly impacts on mirror movements monitoring, which allows to correctly interpret possible ipsilateral activations, distinguishing between activations due to movements of the limb which was asked to be still and activations due to a cortical reorganization as form of motor recovery. The accuracy of the motion system allows to detect even mirror movements with amplitude smaller than 0.5 cm, i.e. angles about < 2 °; therefore also not visible movements, almost flickers, are turned out by the system. Recently, Enzinger and colleagues (Enzinger et al., 2008) carried out an fMRI ankle dorsiflexion paradigm to test for cortical reorganization in patients with chronic stroke with varying degrees of residual gait impairment. A wooden ankle support with an electrogoniometer was used. Since the most interesting results concerned the increased cortical activation in the unlesioned hemisphere (ipsilateral to paretic limb), it could be very enriching to apply a complete kinematic analysis, able to provide a quantification of probable mirror movements and a global 3-dimensional multi-segment measurement of lower limbs.

Another challenging application of fMRI simultaneous kinematic analysis could be in the investigations of functional properties of brain areas associated with motor execution and imagery (Hanakawa et al., 2003), with the final goal to understand the effectiveness of motor imagery to enhance the recovery. The kinematics recordings could provide a method solving the main issue concerning the feedback of motor imagery task accuracy; indeed, it could verify the absence of any actual movement, even if isometric contractions not resulting in motion could be masked by kinematic acquisitions.

In order to systematically verify correlations between motor output and cortical activations, more complex protocols should be employed, with more detailed instructions to the subject: established frequencies and amplitudes should be kept constant for defined sessions or systematically changed as request. Such complexity could be unfeasible for many neurologic patients and a quantitative instrumentation for objective movement monitoring is needed, able to detect even undesired or unconscious variations in the motor task.

A complete and structured analysis of the effects of motor execution parameters to the activation maps in healthy and in pathological subjects will be necessary to provide reliable information for

the clinical massive use of motor fMRI acquisitions. Whether and in which extent there could be a relation between kinematics parameters and activation area will be the object of following deeper experimental studies. In literature the amplitude effect was studied, e.g. with a simple finger tapping test (Waldvogel et al., 1999), supporting the hypothesis that a larger amplitude of the task would correspond to a larger BOLD signal. Similar suggestions came from MachIntosh's studies on ankle dorsiflexion, measured by fibre-optic device on one joint: large-amplitude movements yielded to less lateralized activation compared to small-amplitude movements, after verification of no difference in relative head motions (MacIntosh et al., 2004). Multi-segment and bilateral kinematics monitoring could add useful information to these hypotheses. Frequency parameter on movement execution is more popular in literature even if opposing results were asserted. Some studies did not find any relationship between frequency and activation areas (Diciotti et al., 2007), on the contrary others (Lutz et al., 2005) demonstrated the parallel increasing of movement frequency and BOLD signal; finally, Sadato et al (Sadato et al., 1997) showed the size of activated area increased with higher frequencies only up to 2 Hz. There is still great uncertainty concerning these relationships, analyzing different motor tasks.

Our proposed combined recording of motor output and neural correlates performs a continuous movement monitoring, including different time-varying kinematics parameters as regressors in the fMRI processing, so optimizing the protocol model with the movement output (Francis et al., 2009). This methodology should provide a more precise reduction in the number of uncontrolled variables, enhancing the capability to discern the causes of different cerebral activations: motor performance characteristics or cortical reorganization.

2.2 fMRI brain mapping during motion capture and FES induced motor tasks[2]

The experimental set-up to monitor motor task output by a motion capture system simultaneously with functional MRI acquisitions was tested. Only recently few people scanned subjects undergoing FES induced tasks (Blickenstorfer et al., 2009; Francis et al., 2009; Han et al., 2003; Iftime-Nielsen et al., 2012). For safety, two inductances were added on the stimulation wires to absorb unexpected changes in the current (Francis et al., 2009). These studies showed that FES during fMRI scanning is safe, reliable and feasible. However, any study about image quality assessment was found in literature.

[2] This work has been published as **Gandolla M**, Ferrante S, Casellato C, Ferrigno G, Molteni F, Martegani A, Frattini T, Pedrocchi A. fMRI brain mapping during motion capture and FES induced motor tasks: signal to noise ratio assessment. Med Eng Phys. 2011; 33(8): 1027-32.

A quantitative evaluation of BOLD image quality was addressed, both with the introduction of motion capture cameras and FES stimulation. The introduction of these devices with metal parts inside the MRI room (motion capture system) as well as the use of currents on stimulation wires inside the bore could affect the quality of acquired images. As seen in literature (Van Duinen et al., 2005; Krakow et al., 2000; Lazeyras et al., 2001), the analysis of signal drop and SNR loss during multi-modal acquisitions, such as EMG and EEG recording during fMRI, is performed so as to address the compatibility assessment of the integrated set-up. SNR loss is eventually expected due to conductors affecting the sensitivity of the coil as a result of RF interaction. Moreover, in the case of FES, the relevance of temporal assessment of noise is crucial, because variable current is injected during the acquisition. As long the interest was in preserving signal change detection over the time course of the images acquisition, temporal SNR calculation is proposed, as in (Parrish et al., 2000). The brain signal change during activation as detected by 1.5 T scanner is quite small: about 1-2%, as reported by Parrish and colleagues (Parrish et al., 2000). What is needed to be demonstrated while perturbing the MRI room static magnetic field is that the brain signal change could be detected. Therefore, it will not be here demonstrated that SNR absolute value is not affected by our integrated experimental set-up, while the focus will be on BOLD signal detectability in the obtained fMRI images. Thanks to Parrish and colleagues' work (Parrish et al., 2000), an absolute reference is defined for checking the detectability of BOLD signal (1-2% signal change), based on temporal SNR calculus.

2.2.1 Methods

Subjects

Two healthy female right handed volunteers (37 and 28 years old) were scanned. Experiments were conducted at Valduce hospital (Como, Italy) with the approval of the Ethical Board of Villa Beretta Rehabilitation Centre. Each subject gave informed written consent.

Experimental set-up

The experimental set-up was composed by a 1.5T MRI scanner, the motion capture system and FES device arranged as shown in Figure 12 and previously described, with the addition of the stimulator. The portable stimulation device employed was the current-controlled 8-channel stimulator RehaStim pro^{TM} (HASOMED GmbH). The stimulator device was placed in the operator room, outside the RF shield, thus it was not affecting the static magnetic field. Stimulation cables passed through the wave guide to reach the subject performing fMRI exam. As seen in literature (Francis et al., 2009), two inductors were placed in series with the stimulation cables so as to filter inductive pick-up of gradient fields by the FES device. Since ankle dorsiflexion (ADF) was selected as

representative motor task (see next paragraph), five passive markers for movement tracking were placed on both legs, for a total of ten markers: two markers were placed on the tibia axis, one in correspondence of the medial malleolus, one in correspondence of the lateral malleolus and the last one on the toe. Specific markers positioning depends on the goal of the study but does not affect the present evaluation.

Figure 12 - Experimental set-up

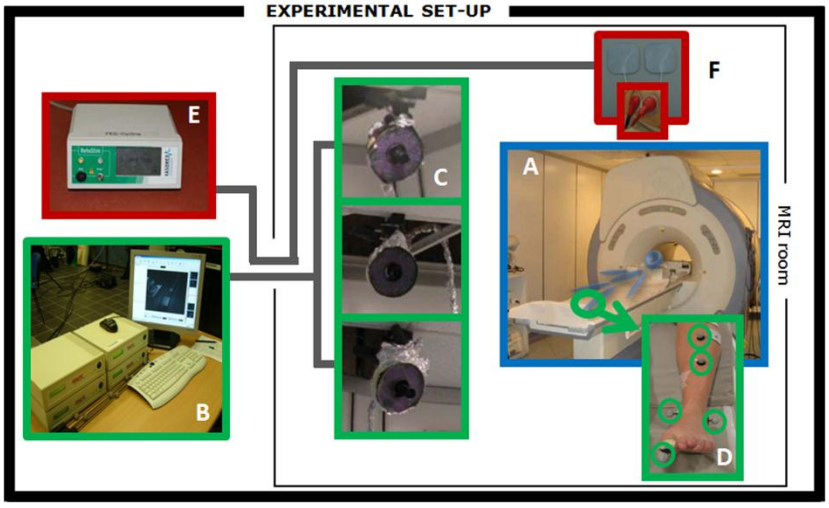

A) MRI scanner CV/I 1.5T; B) motion capture system Smart µg™ with C) three cameras and D) reflective markers; E) FES current-controlled stimulator RehaStim pro™ and F) stimulation electrodes.

Experimental protocol

The proposed fMRI protocol was a 30 seconds block design protocol, with alternate ON and OFF blocks. Each acquisition was composed by 10 alternate ON and OFF blocks, and therefore the total duration of each acquisition was 5 minutes. ADF was selected as exemplifying motor task. Two movement modalities were proposed during ON blocks: voluntary active (Active) and FES induced (FES) ADF, so as to assess the effect of motion capture system and electrical stimulation on image quality. During both movement modalities, the motion capture system was working, recording kinematic data. The two experimental conditions will be referred to as as MCS (only Motion Capture System working, i.e. Active movement modality) and MCS+FES (both motion capture system and FES device working, i.e. FES movement modality). During Active movement modality, the subject was asked to dorsiflex his/her ankle at a self-paced amplitude and frequency, whereas during FES movement modality the subject was asked to be relaxed and to not contribute voluntarily to the movement, while the stimulation was inducing his/her ankle to dorsiflex. During OFF blocks, no movement was performed (Rest). ON and OFF blocks timing were auditory cued by the operator outside the MRI room, thus an operator was directly telling the subject when each

block was starting or ending. The experimental protocol is shown in Figure 13. Each of the two subjects repeated the protocol three times for each movement modality, thus 6 trials for each

Figure 13 - Experimental protocol

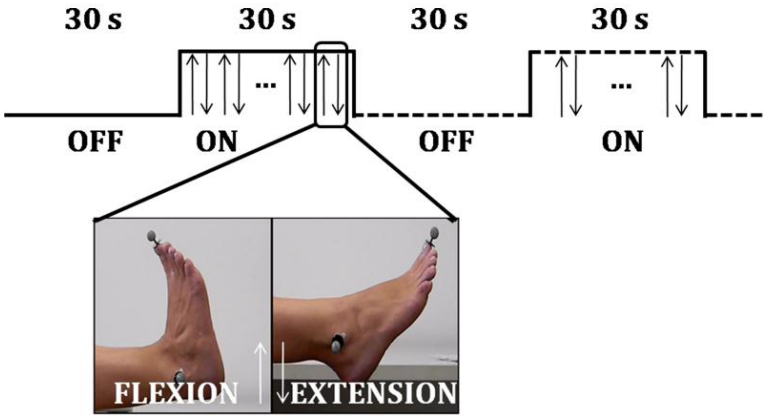

30 seconds block design. Each acquisition was composed by 10 alternate ON and OFF blocks, and therefore the total duration of each acquisition was 5 minutes.

movement modality were recorded (N=6). The order of the movement modalities was randomly assigned for each subject.

FES stimulation paradigm

To obtain ADF, stimulation was applied to the tibialis anterior muscle with biphasic balanced current impulses at 20 Hz fixed frequency. The pulse width had a trapezoidal profile (maximum pulse width 400 μs) and the current was set subject by subject so as to produce a muscle contraction associated to a movement amplitude comparable to the self-paced active movement.

fMRI images acquisition

First acquired image was an anatomic MRI so as to make possible subject-specific analysis. For functional imaging sessions a gradient EPI sequence weighted on T2* was used; TE = 50 ms; TR = 3 s; flip angle = 90°; matrix 128x128; FOV=24 cm; voxel size=1.8x1.8x4 mm. Pads were placed around the subject's head to minimize head motion. The subject had flexed knees and the thigh supported in order to reduce mechanical perturbation to the head.

SNR calculation

fMRI images underwent a standard pre-processing analysis carried out with SPM8® (Wellcome Trust Centre for Neuroimaging, London UK). Images were realigned to first scan of each acquisition and realignment parameters were assessed for excessive motion. Exclusion threshold was set as 3 mm for the linear translation (Van Rootselaar et al., 2007). None of the trials was

excluded from this study. Data from all acquired sessions were then normalized to standard Montreal Neurological Institute (MNI) space. Spatial smoothing was performed using a Full-Width Half-Maximum (FWHM) Gaussian filter of 8 mm. Separately for each subject and each trial, SNR was determined independently for each voxel time series as the mean signal of the entire realigned, normalized and smoothed time series divided by its standard deviation. A temporal SNR volume resulted for each acquired session for a total number of 6 SNR volumes for each movement modality.

SNR data reproducibility

To assess intra-subject and inter-subjects variability of SNR values collected, the Coefficient of Variation (CV) was calculated for four considered Regions Of Interest (ROIs) for both subjects across all three trials of each movement modality (Tjandra et al., 2005; Francis et al., 2009). The four identified regions were primary motor cortex (M1), premotor and supplementary motor cortex (PM/SMA), primary somatosensory cortex (S1), and second somatosensory area (SII). The regions have been identified in the standardized MNI brain through Brodmann areas, namely M1 corresponds to Brodmann area 4 (b4), PM/SMA to b6, S1 to b2 and b3, and SII to b5 and b7. The CV for a given ROI (number of voxels = 3633 for M1; 11120 for PM/SMA; 4823 for S1; 7839 for SII) was defined as the standard deviation of the SNR values ($\hat{\sigma}$) over their mean ($\bar{x}$) in terms of a percentage:

$$CV = \frac{\hat{\sigma}}{\bar{x}} * 100$$

The three trials were averaged separately for each ROI, and the resulting averaged CVs were compared between the two subjects with a non-parametric Mann-Whitney test. If the Mann-Whitney test resulted to be not significant, then there would not be evidences for SNR data differences between the two subjects. Then, the median and the first and third quartiles of these CV values obtained by both subjects can be calculated. The CV median, for a given ROI and a given condition, represents the homogeneity of the considered voxels in terms of SNR; with a low value being indicative of good homogeneity. The CV interquartile interval provides a measure of the reproducibility of such homogeneity across subjects and trials; with a low value being indicative of good reproducibility.

SNR data analysis

In order to determine if the resulting SNR in each voxel was high enough to detect BOLD signal changes (e.g. to detect activation), the SNR values were compared with a threshold as calculated in

literature through computer simulations (Parrish et al., 2000). As broadly explained in the reference study (Parrish et al., 2000), SNR can be defined as follows:

$$\mathrm{SNR} = \frac{2t}{\Delta S\sqrt{N}}$$

where t is the t-value threshold used to determine the significance of signal changes related to brain activation; ΔS is the percentage BOLD signal change due to neural activation (recalling that in fMRI, ΔS can be substituted for the difference in means if the data are mean corrected and normalized); and N is the total number of images acquired in the time series. In this formulation type I error (α) can be directly controlled thanks to the t-value selected, whereas type II error (β) cannot be directly controlled. This is why Parrish and colleagues performed a computer simulation study so as to define the minimum SNR required for specific experimental and statistical parameters, i.e. the confidence level (t-value), power level (β), expected percent signal change (ΔS), and number of samples collected (N). Minimum SNR is independent from acquisition parameters and it is affected only by the number of samples for each voxel, which corresponds to the number of acquired volumes. The computed SNR values can be therefore be compared with the proposed threshold and it can stated that, if the SNR value is over the threshold, then it can be detected ΔS percentage signal change with a probability to incorrectly reject the null hypothesis when it is in fact true (type I error) defined by α value and a detection rate (probability to not reject the null hypothesis despite being false) defined by β value, with a given number of samples (N). In this specific study the parameters were set as following: $\alpha = 0.05$, $\beta = 0.95$, and $N = 100$. Five signal change sensitivity levels (ΔS) were initially considered: 2%, 1%, 0.75%, 0.5% and 0.25% and five levels sensitivity maps were obtained by simply thresholding the SNR volumes at a level determined by the computed thresholds for the five specific considered signal changes, as seen in literature (Bonakdarpour et al., 2007; Parrish et al., 2000; Royet et al., 2003; Small et al., 2004; Williams et al., 2006). Afterwards, because the signal change of interest was the BOLD signal change that corresponds to about ΔS = 1-2%, the percentage of total voxels where 1% and 2% of signal change could be detected was determined. The main sensorimotor regions described before, critical for motor tasks mapping, have been considered in detail. For each sub-volume, the median and the first and third quartile of the percentage of total voxels where 1% and 2% of signal change can be detected among the 6 trials for each movement modality were computed.

2.2.2 Results

SNR data reproducibility

Figure 14 shows the CVs (median and first and third quartiles) for the selected ROIs (M1, PM/SMA, S1, SII) for the two subjects. S1 in both conditions led to the lowest CV, whereas SII led to the highest. Maximum CV, 37.5%, is shown in SII area for the MCS condition for subject 1. The non-parametric Mann-Whitney test for the assessment of variability across the two subjects demonstrated that there is not any evidence for differences between subjects (all obtained p-values were not significant [p-value>0.05]), and therefore good inter-subject reproducibility can be considered to be achieved. The CV medians (%) (interquartile interval (%)) across both subjects for MCS condition resulted to be 29.4 (4), 29.9 (6), 21.7 (3), and 37 (4) respectively for M1, PM/SMA, S1, and SII areas. For what is concerning MCS+FES condition, the CV medians (%) (interquartile interval (%)) were 24.3 (2), 22.2 (6), 19.8 (2), and 33.7 (4) for the same cortical areas. Median CVs are all under 30% for both conditions, except for SII area that presents CV equals to 37% and 33.7% for MCS and MCS+FES condition respectively. The data reproducibility has been verified by the interquartile intervals (always lower than 6%).

Figure 14 - Coefficient of variation

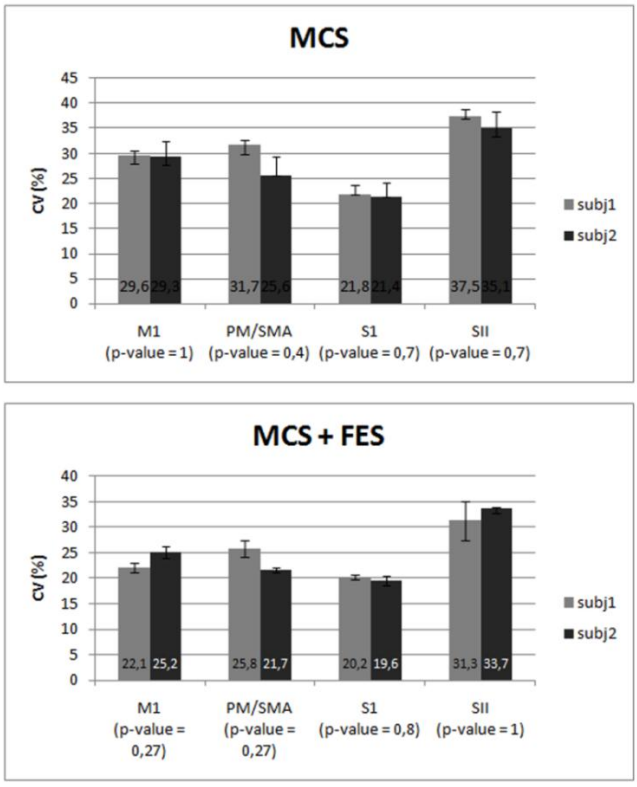

Coefficient of variation (median and fist and third quartile) for the selected ROIs (M1, PM/SMA, S1, SII) for the two subjects.

SNR data analysis

SNR maps with five sensitivity levels were determined. The minimum temporal SNR required to detect changes in the BOLD signal was calculated based on Parrish et colleagues' work (Parrish et al., 2000) so as to detect 2%, 1%, 0.75%, 0.5% and 0.25% (Table 5).

Maps from different trials and different subjects resulted to be quite similar as expected, due to data reproducibility and ROIs homogeneity shown in the previous paragraph. By way of example, an SNR map for both analysed movement conditions is shown in Figure 15. As it can be noticed, detectable signal change drops in correspondence with the skull.

Figure 15 - SNR sensitivity maps

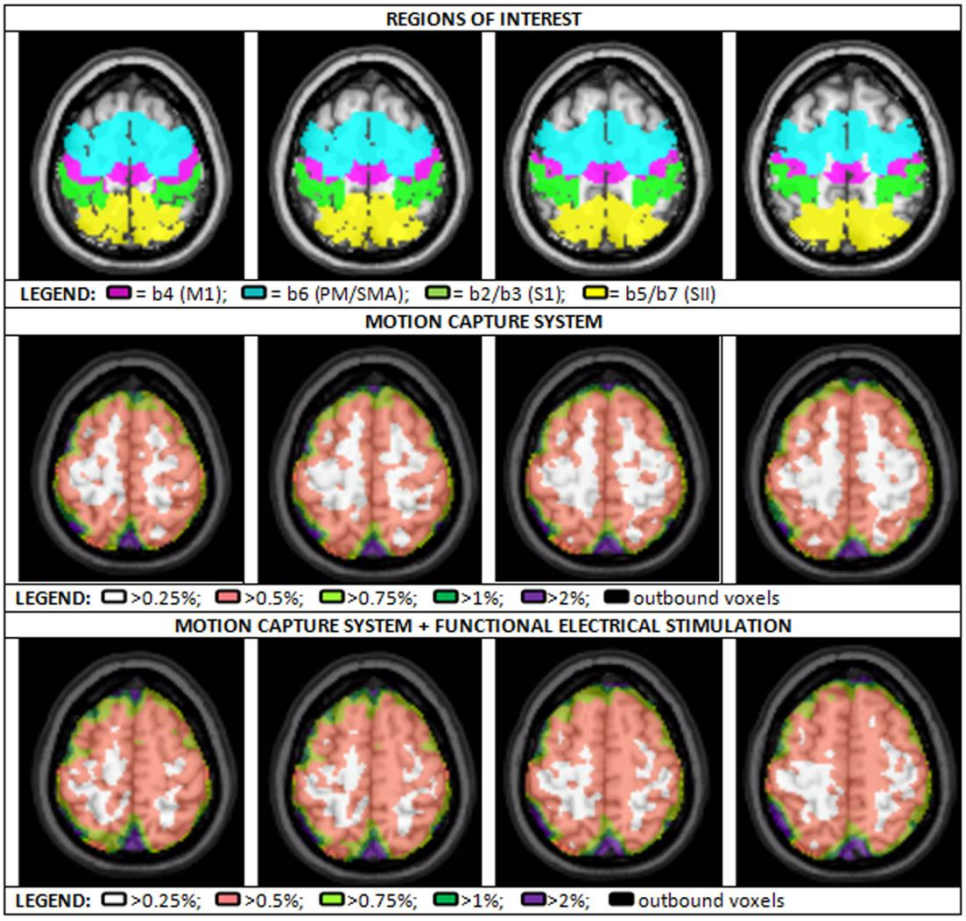

SNR sensitivity maps for both experimental conditions (single subject): only motion capture system working and motion capture system working with simultaneous functional electrical stimulation. The slices shown in figure corresponds to Z = 57 (first column), Z = 56 (second column), Z = 55 (third column), and Z = 54 (fourth column). b4 = Brodmann area 4; M1 = primary motor cortex; b6 = Brodmann area 6; PM/SMA = premotor and supplementary motor cortex; b2/b3 = Brodmann area 2 + Brodmann area 3; S1 = primary somatosensory cortex; b5/b7 = Brodmann area 5 + Brodmann area 7; SII = second somatosensory area.

Table 5 - SNR values

Change in BOLD signal (ΔS) (%)	SNRmin
2	36
1	73
0.75	97
0.5	146
0.25	293

Minimum SNR values required to detect associated BOLD signal change. ΔS = change in BOLD signal; SNR_{min} = minimum SNR required to detect a given change in signal. SNR_{min} was calculated with fixed parameters: number of volumes (N) = 100, $\alpha = 0.05$ and $\beta = 0.95$.

Despite a signal drop at the brain boundary, it can observed that the considered brain areas are well over threshold in both conditions so as to allow BOLD signal detection. Most internal regions are more sensitive and less affected by any kind of noise in both conditions. MCS+FES condition has a slight drop in SNR value as it can be noticed by the smaller white area with respect to MCS condition (Figure 15). The median and the first and third quartile of the percentage of volume where 1% and 2% signal change is detectable are shown in Table 6. For the considered regions, 1% BOLD signal change can be detected at least in the 93% of the sub-volumes, for both movement modalities. Moreover, almost 100% of the sub-volumes are suitable for 2% signal change detection.

Table 6 - Percentage of ROIs volume where 1% and 2% signal change is detectable

		MCS			**MCS+FES**		
		median	1st IQ	3rd IQ	median	1st IQ	3rd IQ
M1 (b4)	**1%**	99.34462	98.92818	99.78007	99.59039	99.13981	99.77381
	2%	100	100	100	100	100	100
PM/SMA (b6)	**1%**	98.71903	97.69667	99.61165	99.53102	99.36981	99.70852
	2%	99.9723	99.94416	99.99551	100	100	100
S1(b2-b3)	**1%**	95.69664	94.38002	98.40089	99.92745	99.75643	99.98964
	2%	100	100	100	100	100	100
SII	**1%**	94.74959	92.85344	95.80061	93.03555	92.82528	95.14624
(b5-b7)	**2%**	99.96813	99.90108	99.90108	99.57309	99.33733	99.67492

Percentage of ROIs volume where 1% and 2% signal change is detectable. Sample data equals to six (N = 6) for both conditions. MCS = only motion capture system working, MCS+FES = motion capture system and FES stimulation working, M1 = primary motor cortex, PM/SMA = premotor and supplementary motor cortex, S1 = primary somatosensory cortex, SII = second somatosensory area, b = Brodmann area, IQ = inter-quartile. For the considered regions, 1% BOLD signal change can be detected at least in the 93% of the sub-volumes, for both movement modalities. Moreover, almost 100% of the sub-volumes are suitable for 2% signal change detection.

2.2.3 Discussion

Two subjects underwent two experimental protocols: fMRI scanning with only motion capture system working (MCS) and with motion capture system and FES simultaneously working (MCS+FES). Each subject repeated the protocol three times for both experimental conditions. SNR data homogeneity and repeatability across trials and across subjects have been demonstrated through CVs analysis for all considered ROIs. Thresholded SNR maps have been created for each trial at five different sensitivity levels: 0.25%, 0.5%, 0.75%, 1% and 2%. They showed better detection sensitivity in the most internal brain regions, whereas they showed a signal drop close to the external part, next to the skull. Such SNR loss at brain edges could be mainly due to motion artefacts (e.g. head motion, but also respiratory artefacts). Therefore possible activations revealed close to the edges should not be trusted, as they could represent "false positives", i.e. they could be caused by presumed signal changes due to neuronal activity that is instead just due to motion. This result supports what has been already found in literature (Parrish et al., 2000). A 1-2% detectable signal change volume has been created so as to determine regions where BOLD signal change could be detected. If sensorimotor regions are considered, at least in the 93% of the selected sub-volumes 1% signal change can be detected, and almost in the whole considered volume, 2% signal change can be revealed, for both movement modalities. In fact, as described before, signal sensitivity drops in correspondence with the skull and, even if sensorimotor regions are located in the brain cortex, they maintain enough sensitivity to allow BOLD signal detection. The most affected region resulted to be SII area that is the most occipital one, the closest to the brain boundary, and included a significant portion of less sensitive area (>2% signal change detection) in the detectability maps (Figure 15). This is confirmed by the data repeatability analysis that shows SII area to be the most variable among trials and subjects (Figure 14). Even if widely used in literature (Bonakdarpour et al., 2007; Royet et al., 2003; Small et al., 2004; Williams et al., 2006), a limitation of the present approach can be identified in the lack of multiple correction during threshold definition. Signal detection does depend on the application of multiple test correction and therefore, without correction, the number of false positives may increase. However, the present approach is used so as to assess whether each voxel independently has a SNR high enough to detect BOLD signal. The resulting maps will be used to eventually reduce the number of voxels being considered for fMRI standard analysis. Hence, the consequent activation maps will be corrected for multiple comparison. On the other hand, the possibility to correct for multiple comparison when thresholding SNR maps does not allow it to be generalized because the correction factor for the threshold would strongly depend on processing parameters (e.g. smoothing parameters). In any case, it has to be noted that in

the comparison between the two experimental conditions MCS and MCS+FES, this issue does not have an impact, as both situations are equally processed.

It is not here demonstrated that SNR is not affected at all by the introduction of external devices in the MRI room; the point is that, in any experimental condition, SNR value has to be greater than the significant threshold (Parrish et al., 2000) in order to detect the signal of interest (e.g. BOLD signal). This is what has been assessed during this work. Thus these results demonstrated the feasibility of BOLD signal detection with the integrated experimental set-up previously described. Image quality assessment completed the analysis of mutual device interaction in order to not misinterpret brain activation maps just because the signal is not detected and at the same time to not consider as brain activation presumed signal changes not due to neuronal activity. Namely, the aim of the work was to demonstrate that image acquisition with the selected integrated system (fMRI with motion capture system) during FES induced motor tasks was feasible as seen in literature, but, most of all, reliable for what is concerning BOLD signal detection, which was instead taken for granted by previous works. The integrated system will therefore allow to detect FES induced fMRI maps simultaneously with kinematic acquisitions so as to investigate FES contribution to CNS plasticity during rehabilitation treatment.

2.3 General conclusions

The concept and the validation of a novel experimental set-up have been discussed in this chapter. The experimental set-up is composed by an fMRI scanner, a motion capture system and a stimulation device. Since metallic materials and time-dependent current were inserted into the scanner, stimulation current, motion capture system measures and image quality (i.e. BOLD signal detectability) had to be carefully checked. Recently few people scanned subjects undergoing FES induced tasks, performing the only hardware modification of two inductances on the stimulation wires to absorb unexpected changes in the current (Blickenstorfer et al., 2009; Francis et al., 2009; Han et al., 2003; Smith et al., 2003). These studies showed that FES during fMRI scanning is safe, reliable and feasible, and therefore only a qualitative check to assure a correct muscle stimulation during scanning was performed. Motion capture system measures have been successfully validated through the comparison between real and measured gravity acceleration. Image quality has been assessed both through phantom acquisitions and though temporal SNR analysis.

With respect to the current most established technique for motor output assessment during fMRI, i.e. MR-compatible EMG acquisition (e.g. Van Duinen et al., 2008; Van Roostelar et al., 2007; Francis et al., 2009), some advantages have been highlighted which could promote the use of motion capture system to enrich EMG data or to substitute EMG, depending on the research goals.

Firstly, since the kinematics is well known to be much reliable in terms of markers positioning, both intra-subject and inter-subjects, the motion analysis during fMRI can be well applicable to different subjects and to different experimental conditions, allowing solid comparisons. EMG data are difficult to be repeatable even on the same subject, as extremely affected by electrodes placement. Moreover, significantly different muscular synergies could be adopted by subjects, leading to the need of detecting many muscles to get a complete information about performed movement. Secondly, kinematic allows multi-segments acquisitions, providing a bilateral and complete description of motor task execution, through quantified parameters such as start and end instants of movement, amplitude, frequency, and verification of mirror movements. On the other hand, there are some technical disadvantages for kinematics versus EMG. The first is the loss of isometric contractions; to overcome this issue, it is possible or to verify before the fMRI protocol the existence of isometric contractions (as in this work), or to couple EMG and kinematics, exploiting the strength points of each methodology, during the fMRI examination. Similarly, when muscles synergies are under investigation only EMG is feasible. A further weak issue concerning kinematics is that the scientific community in neuroimage is now acquainted to EMG, and the comparison between EMG studies and kinematic parameters is not immediate and requires some preliminary investigations. The integration method revealed itself to be useful to investigate functional neural control of actual movement. It, therefore, represents a basis that can be enriched depending on the investigation goals, such as the study on movement modalities effectiveness, crucial for optimizing motor recovery.

The presented results demonstrated the feasibility of the proposed multi-modal experimental set-up so as to functionally electrically stimulate the subject while undergoing fMRI scanner and simultaneously record the effectively executed movement.

Chapter 3 – The functional anatomy of sensorimotor integration in the human brain[3]

3.1 Introduction

The correct execution of a voluntary movement depends on – and is shaped by – the integration of sensory feedback or reafference. Sensorimotor integration is the brain process that dynamically combine sensory information into intentional motor response (Machado et al., 2010). Potential anatomical substrates for this aspect of sensorimotor integration have been established in non-human primates. Specifically, part of the primary sensory cortex, Brodman area (BA) 3a, receives substantial input from muscle proprioceptors (Schwarz et al., 1973) and there are direct connections between primary sensory and motor areas of the brain (Darian-Smith et al., 1993; Jones et al., 1978; Witham et al., 2010). In humans, manipulation of proprioceptive input influences motor cortex excitability (Rosenkranz and Rothwell, 2012). Conversely, the response of somatosensory cortex neurons to proprioception is modified by the nature of the motor task (Chapman and Ageranioti-Bélanger, 1991; Cohen et al., 1994) and by motor learning (Ostry et al., 2010; Wong et al., 2011).

Each level of the motor system receives peripheral sensory information that is used to modify the output at that level (Kandel et al., 2000), suggesting additional involvement of non-primary regions in sensorimotor integration. Secondary somatosensory area (SII) has been selectively linked to proprioceptive processing and integration (Hinkley et al., 2007), attention to proprioceptive stimuli (Chen et al., 2010), painful and non-painful stimulus processing (Ferretti et al., 2004) and complex object manipulation (Binkofski et al., 1999). In addition to SII, precuneus area (BA7b) and parietal rostroventral area (PR) have been identified as potential sites of sensorimotor integration (Hinkley et al., 2007) by virtue of their anatomical connections with premotor and primary motor cortices (Disbrow et al., 2003; Padberg et al., 2005). These experiments considered sensorimotor integration as either differences (Sahyoun et al., 2004; Yetkin et al., 1995) or conjunctions (Ciccarelli et al., 2005) between active and passive tasks, but have not explicitly examined the effect of proprioceptive manipulation during an active motor task.

Functional Electrical Stimulation (FES) provides an ideal experimental model to explore sensorimotor integration because it can provide externally driven proprioceptive information that is embedded within the movement execution.

[3] A journal paper on this work has been submitted to *Journal of Neuroscience* as **Gandolla M**, Ferrante S, Molteni F, Guanziroli E, Frattini T, Martegani A, Ferrigno G, Friston K, Pedrocchi A, Ward NS. The functional anatomy of sensorimotor integration in the human brain.

FES produces muscles contraction independently from voluntary effort but if coupled with volitional intention supplies an artificial augmentation of the sensory consequences of moving. FES stimulation of a mixed nerve activates both the efferent and the afferent fibres. Efferent fibre stimulation directly induces a muscular contraction that elicits additional proprioceptive feedback. The stimulation of the afferent fibres elicits a sensory volley that is sent to the central nervous system concurrent with the proprioceptive reafference (Bergquist et al., 2011) that contributes an additional component to proprioceptive feedback.

Our aim was to use FES during functional magnetic resonance imaging (fMRI) to (i) explore the effect of concurrent voluntary movement on brain regions receiving afferent proprioceptive signals; and (ii) determine how the coupling or directed (effective) connectivity between these regions is influenced by proprioception.

3.2 Materials and methods

Participants - Seventeen healthy volunteers (9 female, 8 male) with no neurological or orthopaedic impairment were studied (mean age 36±14 years, range 22-61). Experiments were conducted with approval from the Villa Beretta Rehabilitation Centre ethics committee and all subjects gave informed written consent.

Experimental set up - The experimental set-up was comprised a 1.5 T MRI scanner (GE Cv/I™), a motion capture system (Smart μg™; BTS) and an electrical stimulator (RehaStim pro™; HASOMED GmbH), as previously described and validated (Casellato et al., 2010; Gandolla et al., 2011).

fMRI task design – A 2x2 event-related fMRI protocol with voluntary effort [V: with the levels volitional and passive] and FES [F: with the levels present and absent] as factors was performed using right ankle dorsiflexion (ADF). During a continuous 10 minutes scanning session, subjects performed 20 alternate 9 seconds OFF and 21 seconds ON blocks. Given the 2x2 factorial design, 4 conditions were performed during the ON blocks in a randomized order: (i) FV = FES-induced ADF concurrently with voluntary movement by the subject; (ii) FP = FES-induced ADF, while the subject remains relaxed; (iii) V = voluntary ADF; (iv) P = passive dorsiflexion (by the experimenter) of the subject's ankle. The dorsiflexions were paced every 3.5 seconds (for 6 repetitions) with an auditory cue. Prior to scanning, subjects practiced the protocol until comfortable with the task. All subjects were free to choose the amplitude of their active movement to preclude fatigue. The experimenter moved the ankle to match to the movements during volitional dorsiflexion.

FES stimulation paradigm - Functional electrical stimulation was applied to the peroneal nerve through superficial electrodes, with biphasic balanced current pulses at 20 Hz fixed frequency. The pulse width had a trapezoidal profile (maximum pulse width 400 μs) and the current amplitude was set subject by subject; so as to reproduce the same movement amplitudes as during voluntary movements, within the tolerance threshold. Current amplitude and pulse width were kept the same for both FP and FV conditions.

Data acquisition - A GE Cv/I system, operating at 1.5 T was used to acquire both T1-weigthed anatomical images (0.94 x 0.94 x 4 mm voxels) and T2*-weighted MRI transverse echo-planar images (1.8 x 1.8 x 4 mm voxels, T_E = 50 ms) with blood oxygenation level dependent contrast. Each echoplanar image comprised 22 contiguous axial slices, positioned to cover the temporo-parietal and occipital lobes, with an effective repetition time of 3 seconds per volume. The first six volumes were discarded to allow for T1 equilibration effects. A total of 200 brain volumes were acquired in a single run lasting 10 minutes.

Kinematic measures and analysis – 3D trajectories of retro-reflective markers were acquired in order to measure the ankle angle during fMRI acquisitions and to determine the movement onset for event-related fMRI time series analysis. Two separate acquisition sessions were performed. The first was a static acquisition performed before the scanning, but while lying in the scanner, to estimate the coordinates of the internal and external malleoli for both lower limbs. The reason for doing this in a separate acquisition was that the malleoli markers were often covered during movement. During the static acquisition, a plate with 3 markers was placed on each tibia and 4 sticks with two markers each were placed on the four malleoli (Figure 16, panel A). The relative positions of the malleoli with respect to the plates (i.e. left and right plates) were computed and the transformation matrices were estimated under the assumption that tibia and malleoli were rigidly connected. The second acquisition, dynamic acquisition, was performed during the fMRI scanning. Only the two plates on the tibia were used to estimate the tibia 3D position and the malleoli. Four additional markers were placed over the four metacarpi (Figure 16, panel B). In this configuration, markers were always visible during ADF. The sampling frequency was set at 120 Hz. The synchronisation between the kinematic measures and the fMRI acquisitions was implemented using a further marker that was held by an operator in the cameras' field of view until the proper fMRI protocol started.

Markers trajectories were analysed with a custom algorithm running in Matlab (Matlab R2010b). Trajectories from both static and dynamic acquisitions were interpolated with cubic splines and filtered with a second-order Butterworth low-pass filter (cut-off frequency = 1 Hz). For each leg, the ADF angle was calculated as follows: the mean points between internal and external malleoli

(mean malleolus) and between internal and external metacarpi (mean metacarpus) were calculated. The ADF angle was taken as the angle between the line passing through the more proximal tibial marker and the mean malleolus and the line passing through the mean malleolus and the mean metacarpus. The automatic detection of onsets and amplitude measurements was checked carefully after acquisition.

Figure 16 - Markers disposition

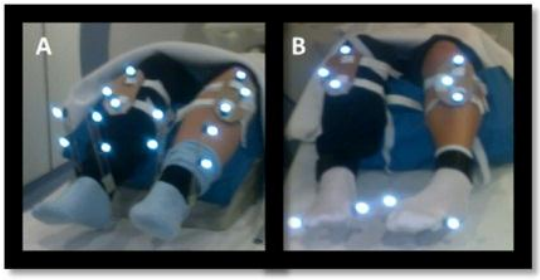

(A) Static acquisition: disposition of the 7 markers for each leg. Markers were placed on each tibia and 4 sticks with two markers each were placed on the four malleoli. (B) Dynamic acquisition: disposition of the 5 markers for each leg. The markers on the tibias were left in the same position as (A), 4 markers were placed on the 4 metacarpi.

fMRI data preprocessing - Imaging data were analysed using Statistical Parametric Mapping (SPM8, Wellcome Department of Imaging Neuroscience, http://www.fil.ion.ucl.ac.uk/spm/) implemented in Matlab (MatlabR2010b). A skull strip procedure on the structural image for each subject was performed to improve the coregistration of functional and structural images. All fMRI volumes were then realigned, and realignment parameters were assessed for excessive motion. A threshold of 4 mm in translation and 5º in rotation was applied (Johnstone et al., 2006). To suppress task related motion artefacts, realigned images were also unwarped (Andersson et al., 2001). The skull stripped structural image was then coregistered to the mean image of the functional realigned volumes, and segmented. The normalisation transformation to the Montreal Neurological Institute (MNI) reference brain in Talairach space (Talairach and Tournoux, 1998) was then estimated using the segmented structural image. The structural image and functional volumes were normalised and resampled to 2 mm x 2 mm x 2 mm voxels. Functional normalised images were then smoothed with an isotropic 8 mm full-width half-maximum kernel (Friston et al., 1995). The time series in each voxel were high pass filtered at (1/128) Hz during subsequent modelling to remove low frequency confounds.

Statistical analysis - Statistical analysis was performed in two stages using the standard summary statistic approach. In the first stage, functional images were analysed separately for each subject.

From the kinematic measures, both the onset and the amplitude for each ankle dorsiflexion were extracted. Two ADF covariates were defined for each condition (i.e. FV, V, FP, P): onsets and amplitude covariates. All ADF onsets belonging to the same condition were defined as a single event type and modelled as delta (stick) functions in the corresponding stimulus function. A second stimulus function for each condition (amplitude covariate) was defined as a delta function scaled by the actual amplitude of each ADF for each condition. The amplitude covariate was mean corrected and orthogonalised with respect to the correspondent onset covariate (Ward et al., 2008). All onset and amplitude stimulus functions were then convolved with a canonical hemodynamic response function, together with its temporal and dispersion derivatives (Friston et al., 1998) and used as regressors in a general linear model of the observed fMRI time series. Thus, for each subject, voxel-wise parameter estimates for each regressor were obtained. Linear contrasts of parameter estimates (reflecting mean effects and interactions) were generated for each subject (i.e. contrast images) and used for the creation of statistical parametric maps at the second (between subject) level.

Contrast images for each subject were entered into a one sample t-test for each effect of interest and were initially thresholded at $p < 0.001$ uncorrected for inspection. However, we were specifically interested in brain responses in contralateral primary motor cortex (M1) and primary sensory (S1) leg areas, and in bilateral secondary somatosensory cortices (SII). M1 and S1 regions of interest (ROI) were defined as a 10 mm spheres cantered respectively on [x = -6, y = -28, z = 60] and [x = -4, y = -46, z = 62] in the MNI coordinates system (Freund et al., 2011), whereas bilateral SII areas were defined as 12 mm spheres cantered on [x = ±58; y = -27; z = 30] as previously described (Ciccarelli et al., 2006; Iftime-Nielsen et al., 2012). Results were thresholded at $p < 0.05$ corrected for multiple comparisons within the ROIs (i.e. small volume correction).

Three contrasts of interest were tested: the main effect of FES, the main effect of voluntary movement and their interaction. The main effect of FES was defined as (FV+FP)-(P+V) and identifies regions that are activated during FES induced movements (i.e. FV, FP) over and above the non-FES induced movements (i.e. V, P). The main effect of voluntary movement was defined as (V+FV)-(P+FP) and identifies regions that are activated during a volitional movement (i.e. V, FV) over and above the non-voluntary movements (i.e. P, FP). The interaction was defined as (FV-V)-(FP-P) and identifies regions where the FES augmented proprioception in the context of volitional intent (i.e. FV-V) produced a higher activation than FES augmented proprioception in the absence of volitional movement (i.e. FP-P). Anatomical attribution was performed carefully by superimposing the maxima of significant effects both on the MNI brain and on the normalized structural images averaged across all subjects, and then labelling with the aid of the atlas of Duvernoy (Duvernoy 1991).

Dynamic Causal Modelling (DCM) analysis – The functional images were smoothed with an isotropic 4 mm full-width maximum kernel for dynamic causal modelling (Friston et al., 2003) as implemented in SPM8 software (DCM10). The observed fMRI time series are used to estimate directed (effective) connectivity among regions or nodes, as described in literature (Friston et al., 2003) assuming neuronal activity conforms to the following bilinear approximation:

$$\dot{\boldsymbol{x}} = \left[\boldsymbol{A} + \sum_{\boldsymbol{j=1}}^{\boldsymbol{m}} \boldsymbol{u_j B^j}\right] * \boldsymbol{x} + \boldsymbol{Cu}$$

Here, x represents the neuronal activity in a given ROI (e.g. M1), and therefore this equation describes the evolution of neuronal activity in terms of a mixture of inputs from other areas and experimental input, where u represents the experimental input to the system (this input corresponds exactly to the stimulus functions described under the general linear model above). The model parameters in the *A* matrix describe the average connectivity among brain regions during the experiment, irrespective of task modulation (endogenous connections). The model parameters of the *B* matrix represent the change in endogenous connections that can be elicited by an experimental variable (modulatory inputs). The model parameters in the *C* matrix represent the direct influences of an experimental variable on specific regions (driving inputs). Non-zero entries in the matrices [*A, B, C*] specify our assumptions about model structure. DCM parameters define the functional architecture and interactions among brain regions at a neuronal level. This model is supplemented with a forward model of how neuronal activity is transformed into the measured fMRI response (Friston et al., 2003). Estimated connectivity parameters describe the direction and strength of influence among brain regions. In addition to providing Bayesian estimates of the model parameters, model inversion provides an approximation to model evidence. This free energy approximation can be used to identify the model that is most likely given the observed data, using Bayesian model selection (Penny et al., 2004; Penny et al., 2010).

The results of the general linear model (standard SPM) analysis described above and our a priori hypotheses motivated a DCM that focused on modelling activity in M1 and S1 in terms of task-dependent changes in connectivity (i.e. x1 = M1; x2 = S1). In terms of summarising the regional activity of each subject, regional time series were selected, using the following anatomical and functional criteria: functionally, the choice of subject-specific coordinates was informed by the location of the group maxima (see Table 7). Subject-specific maxima in regions that were within 5 mm of the group maxima and within the same gyrus were selected. For each subject, data from the M1 and S1 were extracted as the first eigenvariate of a 4 mm sphere centred in the subject-specific maxima. A simplified general linear model was defined as follows, in order to specify the

driving and modulatory experimental inputs. These comprised a stimulus function representing the effect of voluntary effort – V (onsets from V and FV conditions; i.e. u1); a second input encoding the contribution of functional electrical stimulation to proprioceptive input – E (onsets from FV and FP conditions; i.e. u2); a third input representing underlying proprioceptive input from all movements – P (onsets from all conditions; i.e. u3). A basic two-area DCM was specified with bidirectional endogenous connections between the regions (M1, S1) and self-connections (i.e. A matrix = [1 1; 1 1]) as it is known from literature that M1 and S1 areas are reciprocally connected (Jones et al., 1978). The effects of experimental inputs (i.e. C matrix structure) was based upon prior knowledge about functional anatomy: V was assumed to drive the system from M1, modelling top-down intentional signals during voluntary movements from pre-motor and supplementary motor cortices (i.e. C11 = 1); indeed, it is known that premotor areas project in M1 supragranular layers of M1 (Donoghue and Parham, 1983). P was assumed to drive S1 (i.e. $C_{23} = 1$), modelling the proprioceptive and somatosensory consequences of movement (e.g. ascending afferents from muscle spindles, Golgi tendon, etc.) that are known to convey information to sensory areas (Schwarz et al., 1973); E was specified to enter S1 as well (i.e. $C_{22} = 1$), modelling the further sensory contribution due electrical stimulation (Figure 17).

Figure 17 - Base DCM

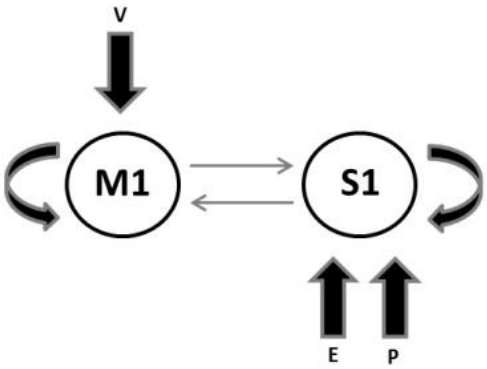

Base two-area DCM with reciprocal connections between the regions (M1, S1). V (effect of voluntary - FV and V onsets) was assumed to drive the system from M1. P (proprioception - all onsets) conveyed information to S1. E (effect of FES – FV and FP onsets) drove S1 as well.

Crucially, E was also allowed to modulate connections or neuronal excitability. Therefore the base model produced 15 variants, allowing all endogenous connections (including self-connections) and their combinations to be modulated by the E (i.e. all different possible combinations of the B^1 matrix). The rationale for exploring the modulatory effects of E is that both the driving effects of stimulation and activity-dependent effects on cortical excitability or gain were of interest for

examination. For example, augmented proprioceptive input may simply drive S1 to produce a greater activation. In addition, it may change the sensitivity of neuronal populations in S1 to intrinsic (from S1) or extrinsic (from M1) afferents.

Figure 18 - Activation maps for the experimental conditions

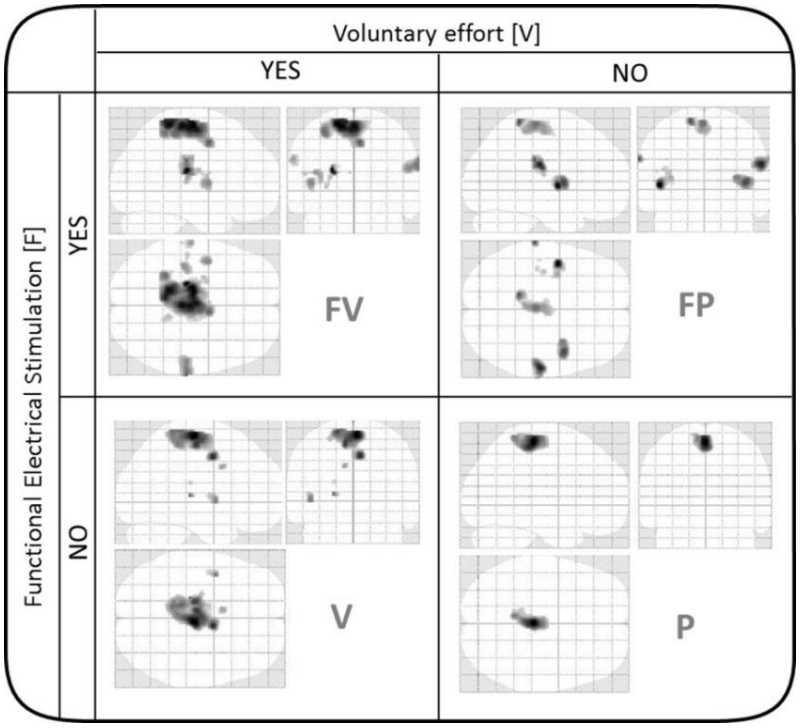

Statistical parametric maps (thresholded at p<0.001, uncorrected) showing regions activated in the four conditions using a maximum intensity projection format. FV = FES and voluntary effort; FP = FES induced movement; V = voluntary movement; P=passive movement.

3.3 Results

Group fMRI effects - Realignment parameters were assessed for excessive motion, and only one subject violated our criteria. This subject was therefore discarded from the group analysis. Figure 18reports thresholded SPMs at $p < 0.001$ (uncorrected) for each condition (i.e. V, FV, FP, P). All four conditions show clear activation in the leg sensorimotor cortex, as expected. fMRI responses during the four conditions showed activations in motor and somatosensory areas known to be involved in ADF execution and concord with previous studies (Ciccarelli et al., 2005; Dobkin et al., 2004; Sahyoun et al., 2004). Specific peaks of activation are reported in Table 7 and Table 8.

Figure 19 - Interaction contrast illustration

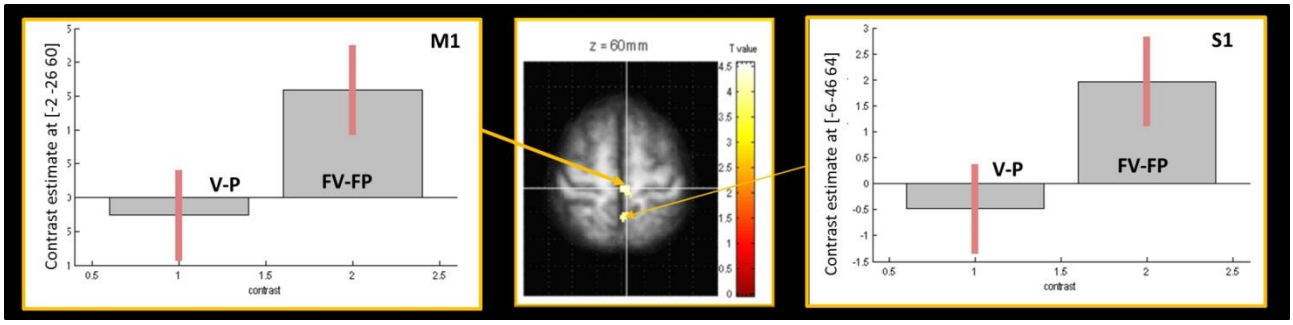

Statistical parametric maps (thresholded at p<0.001, uncorrected) showing regions activated for the positive interaction contrast (i.e. (FV-V)-(FP-P)). The slice at z = 60 mm has been chosen for display purpose only. The two plots depict the differences of FV and FP effects, under the regression model; and the difference between V and P effects for the peak voxel of each cluster (i.e. [-2, -26, 60] for M1 and [-6 -46 64] for S1). The two clusters are located anatomically in M1 (anterior cluster) and S1 (posterior cluster) leg areas. Red bars represent inter-subject variability (standard error).

Table 7 - Peaks of activation in the defined ROIs

	MNI coordinates					
	x	**y**	**z**	**T**	**side**	**region**
FV>V	-64	-20	28	3,78	c	SII
	66	-20	26	5,12	i	SII
FP>P	-66	-26	34	5,26	c	SII
P>FP	0	-46	56	3,86	c	S1
FV>FP	-8	-30	62	5,06	c	M1
	-6	-46	60	3,76	c	S1
main effect Voluntary (V+FV)-(P+FP)	-12	-26	66	4,41	c	M1
main effect FES (FV+FP)-(V+P)	-64	-18	24	6,59	c	SII
	60	-18	28	4,07	i	SII
Interaction	-2	-26	60	4,06	c	M1
	-6	-46	64	4,18	c	S1

Peaks of activation in the defined ROIs (i.e. primary motor cortex – M1, primary sensory cortex - S1, contralateral secondary sensory cortex - cSII, ipsilateral secondary sensory cortex - iSII) at threshold p<0.05 FWE corrected (for predefined ROIs). c = contralateral side; i = ipsilateral side.

Table 8 - Cortical and subcortical significantly activated regions

	MNI coordinates					
	x	**y**	**z**	**T**	**side**	**region**
V>Rest	-8	-16	58	7.55 (+)	c	SMA
	-16	-18	68	7.27 (+)	c	SMC (paracentral lobule)
	4	-20	64	7.19 (+)	i	SMA
	0	-22	64	6.62 (*)	c	M1 (precentral gyrus)
	-12	-42	66	5.80 (*)	c	S1 (postcentral gyrus)
	8	-2	44	6.64	i	median cingulate gyrus
	-44	2	2	5.34	c	insula
	-20	-22	6	4.85	c	thalamus
	-18	-24	20	4.56	c	caudate nucleus
	-28	-6	6	4.12	c	putamen
FV>Rest	-14	-16	64	9.51 (+)	c	SMC (paracentral lobule)
	0	-26	64	8.09 (+)(*)	c	M1 (precentral gyrus)
	-8	-44	68	4.85 (+)(*)	c	S1 (postcetral gyrus)
	-40	-24	18	5.52	c	Rolandic operculum
	68	-22	30	6.36 (*)	i	SII
	-62	-18	32	5.47 (*)	c	SII
	-44	-2	8	4.9	c	Insula
	-24	-2	14	4.57	c	Putamen
	12	-42	64	4.37	i	Precuneus
FP>Rest	58	-18	24	7.59 (+)(*)	i	SII
	-46	-2	4	6.79	c	Insula
	-14	-42	70	6.04	c	Precuneus
	0	-26	66	5.44 (*)	c	M1 (precentral gyrus)
	-12	-42	66	5.65 (*)	c	S1 (postcetral gyrus)
	-66	-26	30	5.95 (*)	c	SII
	42	4	6	5.78	i	Insula
	-38	-16	16	4.69	c	Rolandic operculum
P>Rest	0	-26	62	6.65 (*)	c	M1 (precentral gyrus)
	-4	-38	60	5.07 (*)	c	S1 (postcetral gyrus)
	-6	-44	66	5.05	c	Precuneus
	54	-24	26	3.95 (*)	i	SII

Cortical and subcortical regions significantly activated during V, FV, P and FP conditions (uncorrected $p<0.001$). (+): significant activation at FWE corrected $p<0.05$ at the whole brain level. (*): significant activation at FWE corrected $p<0.05$ within predefined ROIs. c = contralateral side; i = ipsilateral side.

A positive interaction was seen in both M1 and S1. In other words, the effect of augmented proprioception depends on the presence of concurrent motor signals in both M1 and S1. Alternatively, the activating effect of voluntary movement increases dramatically in the presence of stimulation augmented proprioceptive feedback (Table 7, Table 8 and Figure 19). To understand how these interaction effects are generated, in terms of driving and modulatory inputs to M1 and S1, the results of dynamic causal modelling will now be described.

DCM results – The coordinates of the extracted ROIs were consistent across subjects and in agreement with the previous literature e.g. (Boudrias et al., 2012). The average coordinates, along with their variability in terms of standard deviation (±) were as follows. For M1 area x = -2 ± 1.75; y = -26 ± 3.01; z = 62 ± 2.91, whereas for S1 area x = -7 ± 2.62; y = -44 ± 2.37; z = 66 ± 1.86. The winning model (Figure 20) suggests that E exerts a modulatory effect on the reciprocal connections between M1 and S1 and S1 self-connection. The posterior probability of this winning model over alternative models was 0.97. In other words, assuming uniform priors over the 15 models, we can be 97% certain that the model in Figure 20 is the most likely model, following Bayesian model selection.

In terms of endogenous connectivity (Figure 20, blue numbers), it can be seen that M1 and S1 self-connections have negative values (-0.67 Hz and -0.46 Hz respectively), this reflects self-inhibition, as required for system stability. In contrast, the reciprocal connections between the M1 and S1 have positive values (reflecting an excitatory influence). In particular, the M1 to S1 connection is 0.11 Hz and S1 to M1 is 0.51 Hz. This means the connection from sensory to motor cortex is about five times stronger than the reciprocal connection. When considering the driving inputs (Figure 20, green numbers), top-down corollary discharge (V) to M1 has a positive value: 0.28 Hz. Proprioception (P) discharge to S1 has a high impact on the system (0.6 Hz) and it is further increased by the effect of stimulation (E) by about 15%.

The modulatory effect of augmented proprioceptive input (Figure 20, red numbers) indicates which connections are modulated by E; i.e., context-dependent changes in endogenous connectivity. The modulatory effects indicate that there is an overall increased sensorimotor integration. In particular, the change of the sensitivity of inhibitory recurrent effects of S1 is quite sensible (+37%). It appears that M1 is not directly modulated by E, which is again sensible because E does not have a direct access to M1. These results suggest a quite impressive increase of the influence of M1 on S1 with a 181% increase in the sensitivity of S1 population to M1 afferents. In addition, there is an increase in S1 to M1 connection, namely the outgoing information of S1 has a greater influence (+25%) over M1 during concurrent functional electrical stimulation. In summary, the most prescient influence of electrical stimulation was to massively and selectively increase the sensitivity of S1 populations to

projections from M1 that, presumably, convey corollary discharge – or the predicted sensory consequences of movement.

Figure 20 - Winning DCM among the 15 competing models

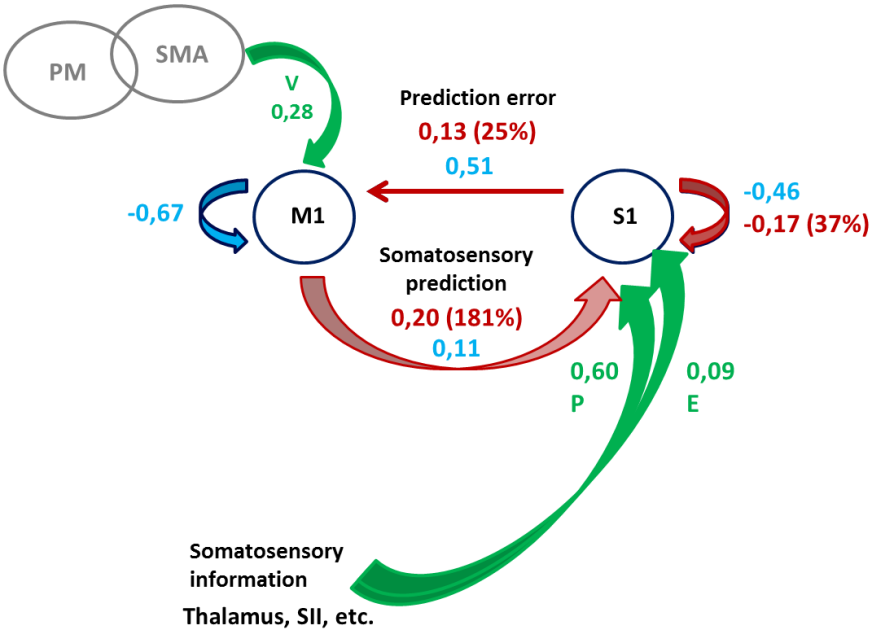

3.4 Discussion

The aim of the present study was to explore sensorimotor integration at the cortical level during a simple motor task. The interest was in the investigation on how artificially augmented proprioceptive afferent information effects integration in the central nervous system during movement control. FES was introduced as a means of artificially supplementing proprioception during movement execution. It has been demonstrated that (i) changing proprioceptive input increased activations during volitional movement in, and only in, primary cortical areas (i.e. M1, S1); (ii) this interaction can be explained by an increase in the influence of M1 on S1 (as well as S1 self-connections, with less effect on S1 to M1 connections).

Sensorimotor integration can be seen in terms of input-output systems, where inputs are (ascending) sensory feedbacks or (descending) cognitive or predictive processes and outputs are (descending) information sent to the periphery or (ascending) to high levels of the sensorimotor hierarchy. Our results suggest an effect of additional (ascending) proprioceptive input during FES in M1 and S1, but not in any other brain regions. Others showed reduced activation in SII for active compared to passive movement during stimulation (i.e. FV compared to FP in our study) suggesting that SII might be involved in the matching of an internal model with the sensory input (Iftime-Nielsen et al.,

2012). However, in our study SII activity was greater in the stimulation conditions compared to no stimulation, suggesting that SII is the recipient of the FES stimuli (Chen et al., 2008; Francis et al., 2009). Our subjects were naïve to FES and SII activation may simply reflect the increased attentional load to proprioceptive stimuli (Chen et al., 2010; Hinkley et al., 2007) in both FV and FP conditions. Precuneus was active in all conditions suggesting that it is a recipient and processor of proprioception stimuli, but not selectively devoted to sensorimotor interaction, as previously suggested (Hinkley et al., 2007).

Sensorimotor integration was further investigated with DCM (Friston et al., 2003), which served to compare the relative plausibility of alternative neurophysiological mechanisms that may have caused the effects it has been established using conventional analyses (Stephan and Roebroeck, 2012). DCM provided plausible results for intrinsic connectivity: the presence of the positive (descending) input to M1 is likely to represent projections from higher order areas, including premotor areas and supplementary motor area (Kandel et al., 2000). Updating of motor plans (or predictions) should be mediated by sensory areas, which is reflected in the excitatory S1-M1 connection. S1 activity is dominated by the external inputs: S1 granular layer receives ascending inputs from spinal circuits, typically through the thalamic pathway (Padberg et al., 2005) and is reflected in the positive inputs to S1. Our main aim was to examine how this directed connectivity was modulated by proprioception augmentation. Two main effects of proprioceptive augmentation were observed: (i) an increase in S1 self-inhibition, indicating a decrease in sensitivity to non-specific afferents and (ii) a large increase in the facilitatory effect of M1 on S1, reflecting a large and selective increase in the gain of S1 to M1 afferents. The increase of influence of S1 on M1 was by contrast small, probably because the proprioceptive inputs are passed from S1 to M1, even if a clear prediction of the sensory consequences of the movement has not been made. Crucially, the fact that augmented proprioception selectively increased input to S1 from M1 suggests that effect of stimulation depends upon the presence of top-down volitional or intentional signals. This is because the primary determinant of M1 activity is an effect of volitional movement. In this context, one can regard the modulation of the M1 to S1 connection as mediating the interaction between augmented proprioception and volitional movement (as encoded by the activity of M1).

It is interesting to consider these results in the context of proposed models of motor control. Optimal control theory suggests that M1 is responsible for generating the descending motor commands to produce a desired trajectory (i.e. model inversion) (Todorov, 2004). Active inference on the other hand suggests that M1 is part of a hierarchical generative model that sends predictions of the sensory consequences of a movement to the periphery (Friston et al., 2009). Therefore, the information sent from M1 to S1 would be different under the two models. Namely, in active

inference, it is a prediction of the sensory consequences of movement; i.e. proprioception prediction or corollary discharge; whereas in optimal control it is the copy of the motor command sent to muscles to execute the movement (efference copy). Proprioceptive prediction has a "sensory" nature, whereas motor commands are signals that drive muscles. The motor command needed to perform ADF should be the same regardless of the presence of any augmented proprioception, whereas the proprioception prediction should be modified according to the actual proprioception state (i.e. it depends on whether FES is present or not). The DCM results support an active inference view of the motor system, since the update of the generative model; i.e., update of the proprioceptive prediction occurs via the modulation of the influence of M1 on S1. In the optimal control view, this efference copy would have been in the motor command framework and the best place to integrate new inputs would have been in M1 (where the inverse model is located), or in the cerebellum, where coding of the sensory and the motor commands are co-localised (Blakemore et al., 2001). The author suggests that the differential effect of proprioception during concurrent voluntary movement in healthy subjects enhances the influence of M1 on S1, thereby amplifying the gain of the somatosensory prediction to S1.

Our results may also have important implications for the mechanisms that underlie sensory attenuation; i.e. the decreased intensity of perceived stimulus attributes when they are the consequences of self-generated behaviour. Under active inference, sensory attenuation corresponds to the attenuation of the precision of (ascending) sensory information that allows top-down predictions to produce a movement through classical reflex arcs (Brown et al. – submitted). At the synaptic level, precision is thought to be encoded by the postsynaptic gain of units reporting prediction error. Our results are exactly consistent with sensory attenuation in the following sense: the selective increase in sensitivity or postsynaptic gain to descending M1 inputs produced by (unpredicted) stimulation appears to attenuate the gain of S1 units, while selectively enhancing the gain to top-down (predictive) inputs. This is precisely the pattern of gain control that would be required by sensory attenuation; namely the suppression of (unpredicted) proprioceptive input that might otherwise subvert or override top-down predictions driving volitional movement.

The present results also support the proposed mechanism of FES as a tool to promote improvement in motor function after central nervous system injury. TMS studies show that FES-induced repetitive movements enhance motor cortex excitability and facilitate motor-evoked potentials of the tibialis anterior (Knash et al., 2003), especially in the context of ambulation (Thompson and Stein, 2004) and concurrent voluntary activation (Barsi et al., 2008), presenting long-lasting facilitatory effects focally modulated by a voluntary cortical drive (Khaslavskaia and Sinkjaer, 2005). Stimulation of the common peroneal nerve paired with TMS, applied during swing phase of

gait induced bidirectional changes in cortico-motor excitability consistent with the Hebbian principle of activity-dependent neuroplasticity (Stinear and Hornby, 2005). FES seems to be particularly effective when augmenting attempted volitional movement, although the mechanism is not yet clear. On the basis of the results here, the author hypothesises that FES interacts with attempted volitional movement to produce long lasting motor improvement (in dorsiflexion) by increasing the influence of M1 on S1.

A significant limitation of this study was the inability to collect data from the cerebellum. The cerebellum is thought to be part of the motor control loop, and it has been shown to be differentially involved during voluntary and non-voluntary FES (Iftime-Nielsen et al., 2012). It has been tried to overcome this limit as far as possible by properly training the subjects outside the scanner so that the subjects were familiar with the stimulus during both FES conditions. The executed movement during scanning to control for movement parameters across sessions was measured. Movement rate has been set at 0.3 Hz (Ciccarelli et al., 2005), and the amplitude was left free to be determined by the subject, as an egocentric reference task: this led to a broad range of amplitudes (10°-71°). However, Ciccarelli and colleagues (Ciccarelli et al., 2005) did not find any effect of movement amplitude (10°-55°), suggesting that if the movement is egocentric and self-paced, there is no difference in associated cortical activity. Having said this, movement amplitude was included as covariate in our analysis, to ensure our analyses were robust to possible differences across subjects, specifically due to this parameter.

The presented study has highlighted that M1 and S1 exhibit a profound interaction between artificially enhanced sensory feedback and volitional movement. Changes in coupling between these regions support an active inference model of motor control. This functional architecture and the underlying synaptic mechanisms may be important for future studies in healthy ageing individuals or patients (e.g. stroke); or indeed during rehabilitation.

Chapter 4 – Sensorimotor integration in chronic stroke subjects

4.1 Introduction

The aging of society and the continuously improved ability to face acute clinical interventions are enhancing the social impact of the neuro-motor disabilities, and consequently, the relevance of rehabilitation. Stroke is the second leading cause of death and one of the leading causes of adult disability (Gresham et al., 1997). Although there are evidences that behavioural motor therapy plays a role in promoting contra- and ipsilesional plastic changes after stroke, the functional outcomes are often of limited practical significance and after completing standard rehabilitation approximately 50–60% of patients still exhibit some degrees of motor impairment and require at least partial assistance in activities of day living (Bolognini et al., 2009). Therefore, investigation of novel approaches to promote the recovery of motor impairments is essential.

It has been suggested that increase in somatosensory inputs in the affected area could be an important strategy to enhance functionally relevant human brain reorganisation after injury (Ward and Cohen, 2004). It has been demonstrated that primary sensorimotor areas are influenced by artificially enhanced sensory feedback as induced by functional electrical stimulation and proprioception prediction. Moreover, a mechanism of action of FES on central nervous system has been proposed through a connectivity model: augmented proprioception preferentially increases the influence of M1 on S1 as well as S1 self-connections, with far less effect on S1 to M1 connections (see chapter 3 for a detailed discussion). As previously introduced, these results could provide an hypothesis for the underlying mechanism of action for the use of artificially increased proprioception techniques together with the subject's voluntary contribution during rehabilitation (e.g. Sheffler and Chae, 2007). In fact, enhanced proprioception has been implemented though FES which is a recognised therapeutic procedure in clinic rehabilitation (Pomeroy et al., 2006; Sabut et al., 2010; Alon et al., 2011; Bogataj et al., 1995; Yan et al., 2005). In addition to the well-known peripheral effect on muscles themselves, possible mechanisms about central therapeutic benefits of FES have been already hypothesized (Everaert et al., 2010; Rushton, 2003; Sheffler and Chae, 2007; Bergquist et al., 2011). Some hemiplegic patients treated with FES for foot drop correction during walking have shown a beneficial effect that outlasts the period of stimulation firstly observed by Liberson and colleagues when using a stimulator for foot drop correction (Liberson et al., 1961). This FES-induced outlasting effect is known in literature as 'carryover effect' (Ambrosini et al.,

2011; Burridge, 2001; Merletti et al., 1979; Waters et al., 1985). This further supports the hypothesis that FES induces some plasticity mechanisms leading to central nervous system reorganization and therefore maintenance of improvements in motor control. Our aim was therefore to use FES during functional magnetic resonance imaging to explore (i) the effect of concurrent voluntary movement on brain regions receiving afferent proprioceptive signals in post-stroke patients, and (ii) compare the sensorimotor integration processing adopted by patients with respect to control subjects. To our knowledge, this is the first study directly investigating FES brain functional correlates in post-stroke patients as revealed by fMRI analysis.

4.2 Methods

Participants

Patients were recruited from the outpatient and inpatient services at the Villa Beretta Rehabilitation Centre (Costamasnaga, LC, Italy). All patients had suffered from first-ever stroke > 6 months previously, resulting in weakness of at least the tibialis anterior muscle (to <4+ on the Medical Research Council (MRC) scale). Exclusion criteria consisted of (i) impossibility to elicit an FES-induced ankle dorsiflexion of at least 10° in FES-induced ankle dorsiflexion; (ii) language or cognitive deficits sufficient to impair cooperation in the study; (iii) inability to walk even if assisted; (iv) incompatibility with MRI (e.g. pacemaker, implants, etc.); (v) high spasticity at ankle joint plantar flexor as measured by the modified Ashworth scale index, MAS > 2 (Ashworth, 1964); and (vi) brain lesion including leg primary motor cortex area. All patients received post-stroke rehabilitation therapy appropriate to their clinical needs. The age-matched control group was recruited from volunteers. Their results have been fully reported previously (i.e., see chapter 3). Experiments were conducted with approval from the Villa Beretta Rehabilitation Centre ethics committee and all subjects gave informed written consent.

Clinical and instrumental measures

Patients that met the inclusion criteria were recruited for the study. At the time of recruitment for this study, patients impairment was evaluated using clinical and instrumental tests. In particular, (i) a gait analysis test following the standard Davis evaluation protocol (Davis et al., 1991) in the "Gait Lab" at Villa Beretta Rehabilitation Centre; (ii) and the 6 minutes walking test were performed. Moreover patients were scored by the clinicians on the (iii) MRC scale index at tibialis anterior muscle (Medical Research Council. Aids to the examination of the peripheral nervous system, Memorandum no. 45. Her Majesty's Stationery Office, London, 1981). A set of outcome measures derived from the evaluation tests was designed to assess different aspects of patients' functional condition at the time of recruitment. All patients were therefore scored on the following outcome

measures within 3 days before the MRI test: (i) gait velocity (Perry et al., 1995; Vonschroeder et al., 1995), (ii) ankle angle during swing (Kesar et al., 2011), (iii) ankle angle at initial contact (Kesar et al., 2011), and (iv) step length symmetry index – paretic step ratio (PSR - Balasubramanian et al., 2007), as measured during the gait analysis test; (v) endurance velocity, as calculated during the 6 minutes walking test; (vi) MRC index.

In order to obtain one representative vector of outcome scores (overall outcome score), a principal components analysis has been performed on the whole data set. So as to perform a correct analysis, each set of the six outcome measures was standardised (giving unit variance and zero mean) and all considered outcome measures were converted such that increasing score reflected minor residual disability (i.e. increasing in the outcome measure reflected improvement). All selected outcome measures, but the PSR index reflect an improvement when the value is increasing, wheras PSR index reflects a physiological condition when is equals to 50, i.e. symmetric gait. Both PSR index increasing or reduction from 50 represent moving away from the physiological condition. Therefore, the PSR index (i.e. length of the paretic step normalised with respect to the sum of the paretic and non-paretic step-length) was converted such that an increasing score reflected improvement. In particular it has been computed as following:

$$PSR_{mod} = 50 - abs\left[50 - \left(\frac{paretic\ step\ length}{paretic\ step\ length + non\ paretic\ step\ length} * 100\right)\right]$$

With this transformation, an unbalanced PSR was accounted the same both if the paretic step length was longer or shorter with respect to the non-paretic one.

The principal components were summed up until the 90% of the variability of the data was explained. The selected principal components were then considered as the vector representing the impairment across the patient group.

Measures and procedures

The experimental set up, the fMRI task design, the FES stimulation paradigm, data acquisition processing, kinematic measures and analysis, and fMRI data preporcessing were kept the same as for controls. All procedures are detailed in chapter 3 – *experimental set-up; fMRI task design; FES stimulation paradigm; data acquisition; kinematic measures and analysis; fMRI data preprocessing*.

Statistical analysis

Statistical analysis was performed in two stages (i.e., single subject level and group level) using the standard summary statistic approach. In the first stage (i.e., single subject analysis), functional images were analysed separately for each patient with the same approach discussed for the healthy

controls. Linear contrasts of parameter estimates (reflecting mean effects and interactions) were generated for each subject (i.e. contrast images) and used for the creation of statistical parametric maps at the second (between subjects) level. Besides the main effect of each condition (i.e. V, FV, P, FP), three contrasts of interest were tested as in healthy controls (chapter 3 – *statistical analysis*): the main effect of FES, the main effect of voluntary movement and their positive interaction. For all group analyses, the images of patients with right-sided infarcts (left-foot weakness) were flipped about the mid-sagittal line, such that all subjects were considered to have right-sided infarcts. All statistical parametric maps (i.e. maps of the t-statistic) were initially thresholded at $p < 0.001$ and $p < 0.005$ uncorrected for inspection. However, the specific interest was about brain responses in brain regions (ROIs) which are known to be part of the motor network (Table 9) and were reported to be significant in previous publications investigating ankle movement (Ciccarelli et al., 2006; Freund et al., 2011; Iftime-Nielsen et al., 2012; Wegner et al., 2008). Results were therefore thresholded at $p < 0.05$ corrected for multiple comparisons within the ROIs (i.e. FWE small volume correction). Anatomical attribution was performed carefully by superimposing the maxima of significant effects both on the MNI brain and on the normalized structural images averaged across all subjects, and then it was labelled with the aid of the atlas of Duvernoy (Duvernoy 1991).

Group fMRI effects

The second stage of the analysis (i.e. group analysis) included four different aspects.

(i) Patients' main effects - To investigate the behaviour of the fMRI response into the population from which our sample was drawn, i.e. group fMRI effects, contrast images for each subject were entered into a one sample t-test for each contrast of interest (Figure 21, panel A).

(ii) Comparison between patients and controls groups – So as to investigate differences in the fMRI response between the group of patients and controls, the contrast images for all patients were entered into a two-sample t-test (control group compared with patient group – Figure 21, panel B). The data for this analysis were the pooled parameter estimates for the covariate representing the main effect of each condition and each contrast of interest across control subjects; and the parameter estimates for the same covariate in patients. Moreover, a conjunction analysis has been performed so as to identify brain regions that were commonly activated between the two groups.

(iii) Comparison of single patient with control group - Because it cannot be kept for granted that all patients recruit the same areas following the lesion, random effects analyses were performed (Friston et al., 1999) in order to test if there was no difference in the task-related activation pattern in an individual patient compared with the control group (Ward et al., 2003). The data for this analysis comprised two samples: the pooled parameter estimates the representing the main effects

for each condition across control subjects; and the parameter estimates for the same covariate in a single patient. Thus, contrast images were entered into two-sample t tests (control group compared with a single patient - Figure 21, panel C).

(iv) *Correlation between recovery score and sensorimotor integration across stroke patients* - The fourth experimental question was related to whether the sensorimotor integration was impairment – dependent in our group of patients. Therefore, the correlation between the voxel-wise task-related change in BOLD signal in the interaction contrast and the overall outcome score (i.e. taking into account all aspects of impairment) across subjects was investigated. Indeed, in the random effects model, a linear correlation analysis has been performed in which the variables consisted in the contrast images for the positive interaction contrast for each patient and the mean-corrected outcome measure (i.e. overall outcome score - Figure 21, panel D). For significant voxels, the correlation coefficient of parameter estimates against recovery for each patient, along with the corresponding p-value was calculated.

Figure 21 - Design matrices

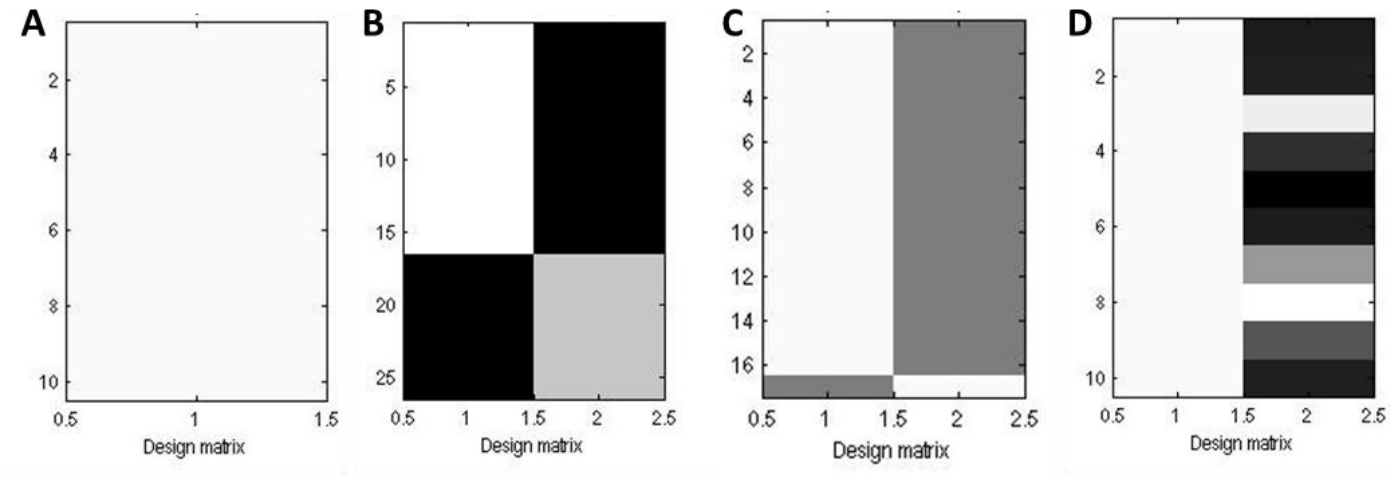

Design matrices for the second level analysis (i.e. group analysis). A) one sample t-test for main effect investigation in the patients group; B) two-sample t-test to investigate differences between patients and control groups; C) two-sample t-test to investigate differences between single patient and control group; D) correlation analysis between interaction contrast and overall outcome score in patients group.

Table 9 - ROIs defined a priori from literature for patients analysis

Regions	Shape and radius	Coordinates of the centre		
		X	y	z
M1	Sphere, r = 10 mm	±6	-28	60
S1	Sphere, r = 10 mm	±4	46	62
SII	Sphere, r = 12 mm	±58	27	30
Postcentral gyrus (b5; b7)	Sphere, r = 12 mm	±20	-36	72
SMA	Sphere, r = 15 mm	±8	-6	64
PM	Sphere, r = 15 mm	±20	-8	64
Superior frontal gyrus (b10)	Sphere, r = 12 mm	±28	60	13
Middle frontal gyrus	Sphere, r = 12 mm	±37	34	40
Inferior frontal gyrus	Sphere, r = 12 mm	±46	31	12
Rolandic operculum	Sphere, r = 12 mm	±55	9	4
Middle cingulate cortex	Sphere, r = 12 mm	±7	-12	44
Inferior parietal gyrus	Sphere, r = 12 mm	±48	-24	20
Superior temporal gyrus	Sphere, r = 10 mm	±54	15	-12
Precuneus	Sphere, r = 15 mm	±8	-54	64
Insula	Sphere, r = 10 mm	±44	12	-2
Thalamus	Sphere, r = 12 mm	±13	-17	7
Posterior putamen	Sphere, r = 12 mm	±30	0	9
Caudate	Sphere, r = 12 mm	±13	13	13
Angular gyrus	Sphere, r = 12 mm	±40	-58	50
Supramarginal gyrus	Sphere, r = 12 mm	±48	-48	34

M1 = primary motor cortex; S1 = primary somatosensory cortex; SII = secondary somatosensory cortex; b = Brodmann area; SMA = supplementary motor area; PM = premotor cortex. All coordinates are given in the Montreal Neurological Institute (MNI) reference brain in Talairach space (Talairach and Tournoux, 1998).

2.3 Results

Clinical and instrumental measures

The control group was composed by seventeen subjects, aged between 21 and 61 years (mean 36±14 years - see chapter 3 for details). Eleven stroke patients were recruited aged between 28 and 72 years (mean 53.2±14.5 years). There was no significant difference in age between patients and controls, as assessed by the Mann-Whitney U-test. Patients' characteristics are listed in Table 10.

Six patients had experienced left hemiparesis and five right hemiparesis. The site of cerebral infarction was determined from the T_1-weighted structural MRI. Five patients were found to have had infarcts involving the middle cerebral artery territory, particularly in the Sylvian part, and one involving the anterior cerebral artery territory. In addition, four patients had suffered from a lesion involving the Globus Pallidus and one the caudate nucleus (Figure 22). No patients had lesions involving the leg representation of the primary motor cortex (M1). The degree of functional recovery at the time of scanning was variable, as measured by the selected outcome scores (Table

11). The first three principal components of the data set comprising scores for each outcome measure across patients accounted for 90.7% of the variance within this data set. Therefore the sum of the projection of the data on the first three principal components was taken as the vector of the overall degree of residual ability across the group.

Table 10 - Patients characteristics

Patient	Age (years)	Sex (M/F)	Affected leg (R/L)	Site of lesion	Type of stroke	Time to scan (months)
PP	37	F	L	R ACA	Hemorrhagic	10
AF	23	M	L	R MCA	TCE	23
SF	38	F	L	R globus pallidus	Ischemic	23
EM	64	F	R	L MCA	Hemorrhagic+ Ischemic	13
MT	19	M	R	L MCA	Hemorrhagic	44
RM	47	F	R	L Globus pallidus	Hemorrhagic	44
MF	25	F	L	R MCA	Ischemic	30
SB	46	M	L	R globus pallidus	Ischemic	13
LL	57	M	R	L Caudate nucleus	Ischemic	6
GR	53	M	R	L Globus pallidus	Hemorrhagic	37
PR	49	M	L	R MCA	Ischemic	89

(*) Initial severity refers to the MRC grade for ankle dorsiflexion as recorded at the time of the stroke. M = male; F = female; R = right; L = left; MCA = middle cerebral artery; ACA = anterior cerebral artery.

Figure 22 - Axial structural T1-weighted MRI scans at the level of maximum infarct volume for each patient performed at the time of the fMRI.

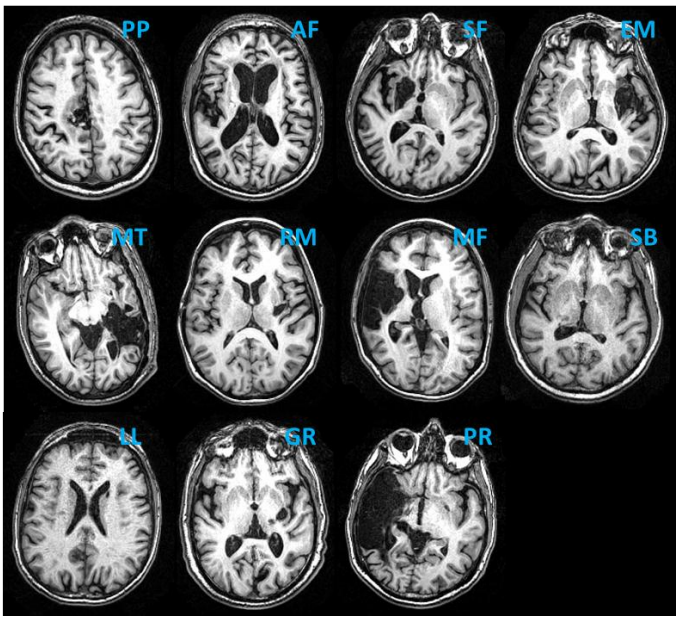

Table 11 - Patients outcome measures

Patient	Gait velocity (m/s)	Ankle angle swing (°)	Ankle angle initial contact (°)	PSR (0-100%)	Endurance velocity (m/s)	MRC (1-5)	Overall outcome score
PP	0.49	-12.67	-12.14	47.2	0.51	1	1.78
AF	0.64	-4.91	-11.61	53.4	0.82	3	1.92
SF	0.25	2.75	7.48	38.3	0.28	2	-5.35
EM	0.32	-7.09	-10.11	59.4	0.5	3	-2.42
MT	0.82	-5.77	-15.12	46.1	1.01	3	3.1
RM	0.52	3.05	-12.0	57	0.82	3	-0.14
MF	0.7	2.77	-0.43	57.1	0.98	3	0.11
SB	0.49	10.6	8.6	45.4	0.58	3	-1.55
LL	0.33	0.8	-6.7	44.9	0.50	2	-0.83
GR	0.43	11.10	4.3	50	1.02	3	1.64
PR	0.33	-6.5	-11.6	50.7	0.58	2	1.75

Minimum to maximum scores (or units) are expressed under each outcome score. MRC = Medical Research Council scale index.

(i) Patient's main effects

Realignment parameters were assessed for excessive motion, and only one subject violated our criteria (chapter 3 – *fMRI data preprocessing*). This subject was therefore discarded from the group analysis. Figure 23 reports thresholded SPMs at $p < 0.005$ (uncorrected) for each condition (i.e. V, FV, FP, P), for visual inspection only.

fMRI responses during the four conditions showed activations in motor and somatosensory areas known to be involved in ADF execution. Specific peaks of activation are reported inTable 12. A significant positive interaction was seen in angular and postcentral gyri where the effect of augmented proprioception depends on the presence of concurrent motor signals.

Figure 23 - Group fMRI effects

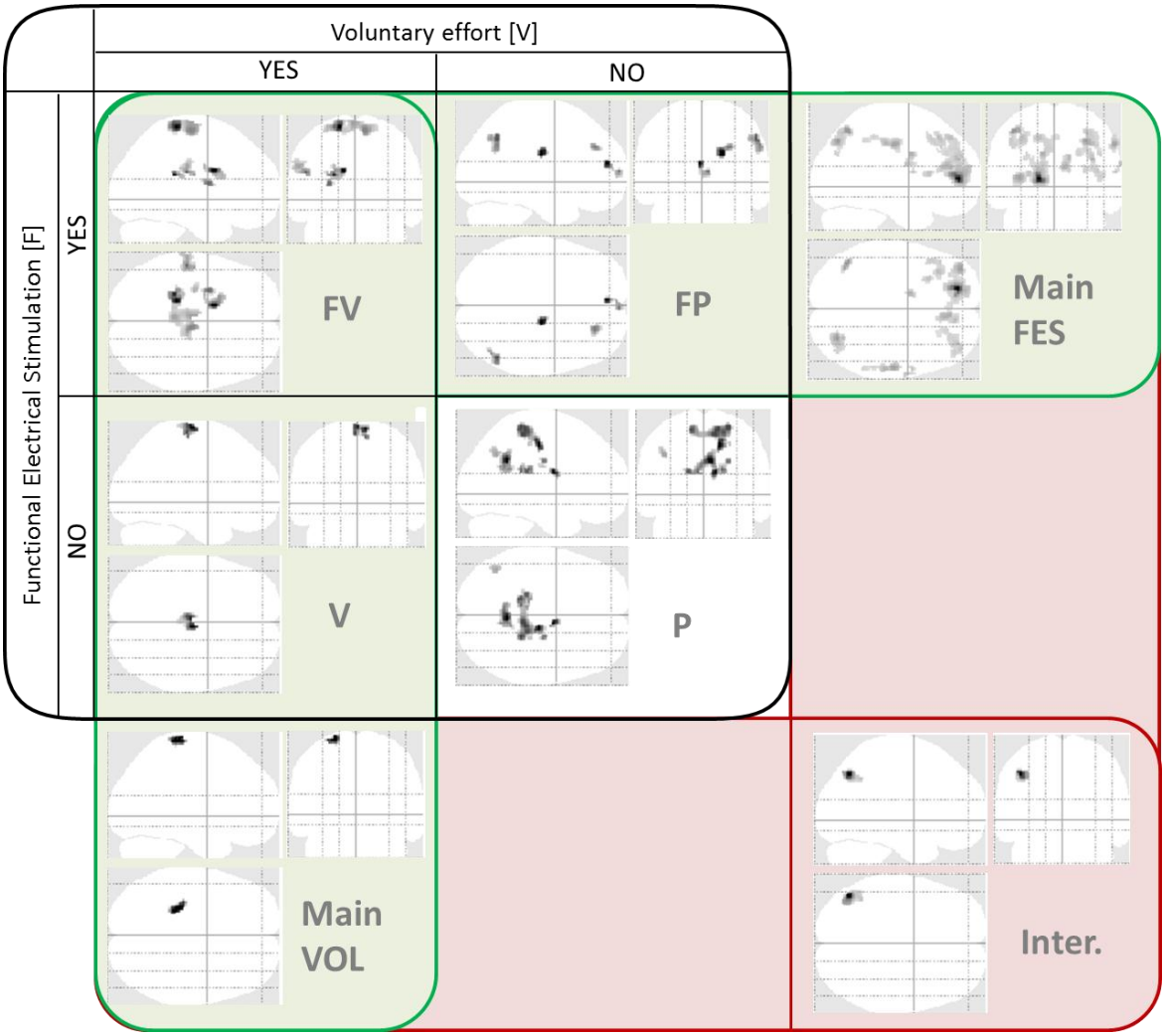

Statistical parametric maps (thresholded at $p<0.005$, uncorrected) showing regions activated in the four conditions and the three contrasts of interest using a maximum intensity projection format. FV = FES and voluntary effort; FP = FES induced movement; V = voluntary movement; P=passive movement; Main FES = main effect of FES. i.e. (FV-V)+(FP-P); main VOL = main effect of voluntary effort, i.e. (FV-FP)+(V-P); inter. = positive interaction between the factors, i.e. (FV-V)-(FP-P).

Table 12 - Group main effect peaks of activation

	MNI coordinates			Z	Side	Region
	x	y	z			
V > rest	6	16	30	3.27 (§)	i	Median cingulate gyrus
	-4	-24	66	2.90 (+)	c	M1
	6	-22	62	2.84 (+)	i	M1
FV > rest	8	-20	66	3.41 (*)	i	M1
	-6	-22	68	2.95 (+)	c	M1
	-4	-36	68	3.98 (+)	c	S1
	-52	-24	24	3.61 (*)	c	SII
	-18	-34	68	4.19 (*)	c	Postcentral gyrus
	8	-2	66	3.41 (+)	i	SMA
	-52	-24	24	3.61 (*)	c	Inferior parietal gyrus
	-4	-20	72	3.17 (§)	c	Paracentral lobule
	-16	8	24	3.22 (+)	c	Caudate
	-28	-2	14	3.58 (*)	c	Posterior putamen
FP > rest	-4	50	16	3.62 (§)	c	Superior frontal gyrus
	18	-16	24	3.70 (§)	i	Caudate
	52	-60	40	3.30 (§)	i	Angular gyrus
	26	20	38	3.27 (§)	i	Middle frontal gyrus
P > rest	-12	-36	60	3.10 (+)	c	M1
	12	-34	60	3.56 (*)	i	M1
	-12	-40	62	3.27 (+)	c	S1
	22	-38	62	3.55 (*)	i	Postcentral gyrus
	-14	-38	62	3.28 (+)	c	Postcentral gyrus
	14	-20	46	3.90 (§)	i	Median cingulate gyrus
Main effect FES	60	-26	40	3.58 (*)	i	SII
	-34	28	46	3.36 (*)	c	Middle frontal gyrus
	-42	-64	52	3.97 (*)	c	Angular gyrus
	30	-74	42	3.97 (§)	i	Superior occipital gyrus
	60	-26	40	3.58 (§)	i	Supramarginal gyrus
	10	34	18	3.63 (§)	i	Anterior cingulate gyrus
	12	46	23	3.50 (§)	i	Superior frontal gyrus
	30	-68	50	3.39 (§)	i	Superior parietal gyrus
Main effect VOL	-28	46	0	3.12 (§)	c	Superior frontal gyrus
	-24	-30	72	3.03 (+)	c	Postcentral gyrus
Interaction	-44	-66	42	4.14 (*)	c	Angular gyrus
	-64	-20	28	3.95 (§)	c	Postcentral gyrus

§ = $p<0.001$ uncorrected all brain; + = trends ($p<0.1$ FWE corrected within the ROI); * = $p<0.05$ FWE corrected within the ROI; c = contralateral; i = ipsilateral. FV = FES and voluntary effort; FP = FES induced movement; V = voluntary movement; P=passive movement; Main FES = main effect of FES. i.e. (FV-V)+(FP-P); main VOL = main effect of voluntary effort, i.e. (FV-FP)+(V-P); inter. = interaction between the factors, i.e. (FV-V)-(FP-P).

(ii) Comparison between patients and controls groups

The conjunction analysis revealed a very clean pattern of activation in bilateral sensorimotor cortex, confirming that the motor task employed was valid (Table 13). Statistical comparison of patients and controls revealed that patients activated more than controls in several areas for different conditions, especially in the passive ones (i.e. P, FP) and in the interaction contrast. Also there were few regions that were more activated in controls than in patients for the main effect of voluntary effort contrast (i.e. superior frontal gyrus, Caudate, angular gyrus, Supramarginal gyrus) and in the Rolandic opeculum for FP condition (Table 13).

Table 13 - Comparison between patients and controls

	MNI coordinates			Z	Side	Region
	x	y	Z			
Conjunction analysis						
V > rest	4	-22	64	3.80 (§)	i	M1
	-4	-20	68	3.47 (§)	c	M1
FV > rest	8	-18	64	4.44 (°)	i	M1
	-20	-32	68	4.21 (§)	c	S1
	-6	-14	68	3.80 (§)	c	M1
	-60	-20	32	3.66 (§)	c	SII
	66	-20	24	3.36 (§)	i	SII
FP > rest	-4	-20	68	2.90 (#)	c	M1
P > rest	-2	-34	56	3.80 (§)	c	S1
	-4	-22	68	3.14 (§)	c	M1
Main effect FES	-42	-62	50	3.51 (§)	c	Angular gyrus
	-14	50	20	3.25 (§)	c	Superior frontal gyrus
	30	34	22	3.14 (§)	i	Middle frontal gyrus
Patients > Controls						
A	-20	8	22	3.17 (*)	c	Caudate
FA	28	36	32	3.65 (*)	i	Middle frontal gyrus
	8	-26	12	3.11 (+)	i	Thalamus
	-20	10	24	3.74 (*)	c	Caudate
FP	26	58	12	3.60 (*)	i	Superior frontal gyrus
	26	36	34	4.60 (*)	i	Middle frontal gyrus
	8	-26	12	3.59 (*)	i	Thalamus
	-14	-8	12	2.70 (*)	c	Thalamus
	-20	16	22	3.10 (+)	c	Caudate
	36	-64	44	3.59 (*)	i	Angular gyrus
	-40	-52	46	3.98 (*)	c	Angular gyrus
	54	-54	34	4.04 (*)	i	Supramarginal gyrus
	-42	-50	44	3.80 (*)	c	Supramarginal gyrus
P	24	60	8	3.38 (*)	i	Superior frontal gyrus
	28	36	32	3.29 (*)	i	Middle frontal gyrus

	16	-18	46	2.99 (+)	i	Middle cingulate gyrus
	-40	-22	28	3.11 (+)	c	Inferior parietal gyrus
	-22	4	18	3.19 (*)	c	Posterior putamen
	8	16	20	3.72 (*)	i	Caudate
	-14	20	22	4.32 (*)	c	Caudate
	-46	-64	42	3.63 (*)	c	Angular gyrus
	46	-46	24	3.18 (*)	i	Supramarginal gyrus
	-46	-58	40	3.46 (*)	c	Supramarginal gyrus
interaction	-64	-18	26	2.81 (+)	c	SII
	26	28	42	3.43 (+)	i	Middle frontal gyrus
	-26	28	42	2.95 (+)	c	Middle frontal gyrus
	44	42	14	3.01 (+)	i	Inferior frontal gyrus
	-42	24	4	3.26 (*)	c	Inferior frontal gyrus
	-14	-4	40	2.70 (*)	c	Middle cingulate cortex
	-28	10	16	3.63 (+)	c	Posterior putamen
	-22	14	10	3.12 (*)	c	Caudate
	-44	-66	42	3.01 (+)	c	Angular gyrus
Main VOL	-24	-32	70	2.86 (+)	c	Postcentral gyrus
Controls > Patients						
FP	46	4	10	3.46 (*)	i	Rolandic operculum
Main VOL	22	56	6	2.70 (+)	i	Superior frontal gyrus
	18	10	12	3.04 (*)	i	Caudate
	38	-68	46	3.21 (*)	i	Angular gyrus
	-40	-60	52	4.23 (*)	c	Angular gyrus
	-40	-52	44	3.19 (*)	c	Angular gyrus
	46	-50	26	4.35 (*)	i	Supramarginal gyrus
	54	-56	40	3.62 (*)	i	Supramarginal gyrus
	-42	-46	44	3.15 (*)	c	Supramarginal gyrus
	-46	-54	44	3.14 (*)	c	Supramarginal gyrus
	-40	-50	42	3.49 (*)	c	Supramarginal gyrus

° = p<0.05 FWE corrected in all brain; § = p<0.001 uncorrected all brain; # = trend (p<0.005 uncorrected – all brain analysis); + = trend (p<0.1 FWE corrected within the ROI); * = p<0.05 FWE corrected within the ROI; c = contralateral; i = ipsilateral. FV = FES and voluntary effort; FP = FES induced movement; V = voluntary movement; P=passive movement; Main FES = main effect of FES. i.e. (FV-V)+(FP-P); main VOL = main effect of voluntary effort, i.e. (FV-FP)+(V-P); inter. = interaction between the factors, i.e. (FV-V)-(FP-P).

(iii) Comparison of single patient with control group

In the comparison of the main effects of each condition for single stroke patient with the control group (i.e., V, FV, FP, P), the task-related activation patterns resulted to be very different across the patient's group (Table 14). The activated regions were often bilaterally distributed, involving all the predefined ROIs, encompassing a wide bilateral network including primary and secondary sensorimotor cortices, parietal and frontal regions. The activated network is differently distributed for all patients, regardless of their degree of impairment.

Table 14 - Task-related activity for single stroke patient compared with control group.

	V																																	
	SF		EM		SB		LL		RM		MF		PR		PP		AF		MT		FV															
	c	i	c	i	c	i	c	i	c	i	c	i	c	i	c	i	c	i	c	i	SF		EM		SB		LL		RM		MF		PR		PP		AF		MT	
																					c	i	c	i	c	i	c	i	c	i	c	i	c	i	c	i	c	i	c	i
M1			+	+	+	+	+		+		+				+		+		+						+	+	+		+				+		+		+	
S1			+		+		+		+						+													+					+			+	+
SII	+				+		+				+		+				+		+								+						+					
Postcentral g.			+		+		+	+	+		+				+														+				+					
SMA			+	+	+		+		+	+	+				+		+		+				+		+		+		+				+		+		+	
PM			+		+		+	+	+		+				+								+		+				+				+		+			
Sup. front g.			+						+		+								+									+	+							+	+	+
Middle front g.									+								+	+																			+		+	
Inferior front g.	+						+		+		+		+						+		+							+				+							
Rolandic operculum																	+											+											
Middle cing.			+	+	+				+								+							+	+			+				+	+						
Inf. parietal g.					+		+		+		+		+					+	+							+	+	+		+				+			+	+	
Precuneus			+		+			+	+						+											+	+	+						+			+	+	
Insula	+										+										+									+									
Thalamus	+			+	+		+	+	+		+		+	+				+			+			+	+	+	+	+	+	+		+		+		+	+	
Post.putamen	+								+												+						+		+									+		
Caudate	+	+	+		+				+		+		+					+	+		+	+	+						+	+	+		+					+	+	
Angular g.			+		+		+		+		+						+								+			+				+						+	
Supramarginal g.	+		+						+		+		+								+				+			+				+						+	
	FP																				P																			
	SF		EM		SB		LL		RM		MF		PR		PP		AF		MT		SF		EM		SB		LL		RM		MF		PR		PP		AF		MT	
	c	i	c	i	c	i	c	i	c	i	c	i	c	i	c	i	c	i	c	i	c	i	c	i	c	i	c	i	c	i	c	i	c	i	c	i	c	i	c	i
M1							+		+																		+		+						+			+	+	
S1																	+																					+	+	
SII		+															+	+	+																		+		+	+	
Postcentral g.																		+																						+	
SMA							+		+		+																+		+		+									
PM								+		+												+					+		+		+				+				+	
Sup. frontal g.		+					+		+								+		+								+								+					
Middle frontal g.								+						+				+		+								+										+		+	
Inferior frontal gyrus									+		+		+					+																				+		+	
Rolandic operculum											+						+																							
Middle cing.							+		+		+			+		+											+		+		+				+					
Inf. parietal g.							+		+		+							+		+							+		+								+		+	
Precuneus									+								+		+																				+		+	
Insula											+																													
Thalamus							+		+		+		+						+								+		+										+		+	
Post.putamen		+					+		+		+		+				+		+			+					+		+		+		+						+	
Caudate	+	+	+				+		+		+		+						+		+	+	+				+		+		+		+				+		+	
Angular g.	+																+					+		+					+		+								+		+	
Supramarginal g.	+						+		+				+				+		+			+		+			+		+		+								+		+	

(⟵) The table illustrates single patient activation with respect to control group. Each column shows the areas of increased task-related activation for an individual patient compared with controls. Patients (represented by patient initials; see Table 10) are ranked by outcome (from more impaired on the left to less impaired on the right). + = increased activation present in patient compared with control group (voxels significant at $p < 0.05$, corrected for multiple comparisons within the defined ROIs). M1 = primary motor cortex; S1 = primary somatosensory cortex; SII = secondary somatosensory cortex; g. = gyrus; front = frontal; c = contralateral; i = ipsilateral.

(iv) Correlation between recovery score and sensorimotor integration across stroke patients

A correlation analysis has been performed between the positive interaction contrast and the overall outcome score (i.e., sum of the first three principal component, accounting for 90.7% of the variance of all outcome scores). A significant negative linear correlation was found in the contralateral SII area (Figure 24, panel A), meaning that this area is more likely to be active during sensorimotor integration in patients that are more impaired. In addition, significant positive linear correlation was found in ipsilateral cingulate cortex, middle frontal gyrus and insula (Figure 24, panels B, C, and D respectively), meaning that those areas are increasingly more likely to be active in patients with less impairment.

Figure 24 - Correlation analysis

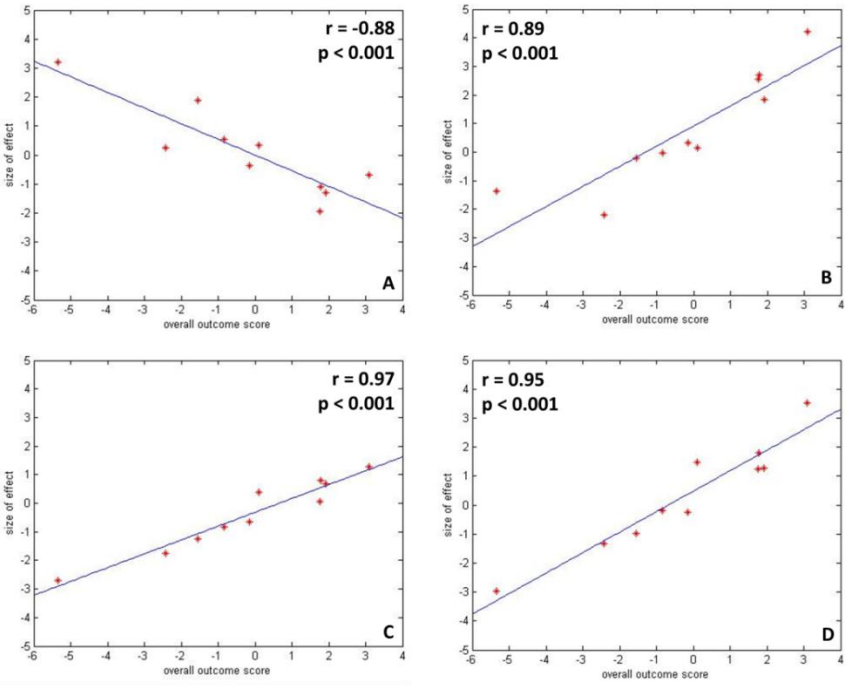

Plots of parameter estimates (size of effect) against relative overall outcome recovery score (normalized) for all stroke patients in different areas of the brain. Correlation coefficient and associated p-values for peak voxel in each region are indicated in each panel. A) contralateral SII ([-44 -44 38]); B) ipsilateral cingulate cortex ([2 36 26]); C) ipsilateral middle frontal gyrus ([40 4 36]); D) ipsilateral insula ([34 -2 10]).

2.4 Discussion

The aim of the present study was to explore FES-induced cortical correlates and sensorimotor integration at the cortical level during a simple motor task in post-stroke chronic patients. The focus point was in investigating how artificially augmented proprioceptive afferent information affects functional reorganisation after brain lesion and sensorimotor integration in the central nervous system during movement control. As far as it is known, for the first time the cortical correlates of FES induced movements in post-stroke patients are here reported.

Characterisation of group fMRI activations - The present study identified brain functional reorganisation associated with ankle dorsiflexion task in chronic post-stroke patients in all conditions, encompassing primary and secondary areas known to be involved in movement processing and control of ankle movement (Ciccarelli et al., 2006; Dobkin et al., 2004; Freund et al., 2011; Iftime-Nielsen et al., 2012; Sahyoun et al., 2004; Wegner et al., 2008). FES-induced ankle dorsiflexion concurrent with voluntary effort elicited a more widespread active network with respect to FES in the context of passive movement, in accord with what was found in healthy subjects (chapter 3, (Iftime-Nielsen et al., 2012; Joa et al., 2012). The differential effect of action of FES in the context of active and passive movement is confirmed by the cluster of activation revealed by the interaction contrast in the contralateral angular and postcentral gyrus. Postcentral gyrus has been found to be active in healthy controls while executing complex or novel tasks (Sahyoun et al., 2004; Filippi et al., 2004), and angular gyrus has been suggested to be recipient of proprioceptive information encoded specifically in the postcentral gyrus (Vesia and Crawford, 2012). Angular gyrus is quite a specific area, that has been shown to be an associative area (Geschwind, 1965). This same interaction contrast has been show in primary sensorimotor cortex for healthy humans (see chapter 3). Our results suggest that patients perform sensorimotor integration as a more complex task by using predominantly secondary cortices that are used in healthy controls only to perform novel or complex motor tasks, in order to compensate for the weakness induced by the lesion. Active and passive ankle dorsiflexion induced significant activation, particularly in sensorimotor cortices. In contrast to what has been shown by Ciccarelli and colleagues (Ciccarelli et al., 2006), passive related activation (i.e., FP, P conditions) are more widespread with respect to active ones (i.e. FV, V conditions). The same functional movement (i.e. ADF) recruits a larger network in the case of passive conditions suggesting that the volitional intention drives the brain effort only to a subgroup of the larger network activated in the passive case, as if there would be "more order" in the brain in terms of effort. Moreover, the patients enrolled in this study were chronic, and therefore it can speculated that they already have

established a novel pattern in the "voluntary control", having completed an exploratory phase of novel possible connection.

Comparison between patients and controls – The conjunction analysis revealed clear pattern of activation in primary somatosensory cortex that has been reported to be principally involved during the same motor task execution for healthy subjects (chapter 3). This result clearly shows that although patients use a quite widespread network in order to execute even a simple movement, they also share the principal regions devoted to motor control with healthy subjects. As in previous fMRI studies, significant differences in the fMRI response to active and passive movements between patients and controls have been found. Patients significantly activated more than controls in a highly distributed pattern, which include regions that are active when healthy controls perform complex motor tasks, included regions located in the prefrontal and frontal cortex (Ciccarelli et al., 2006; Katschnig et al., 2011). It has been suggested that this finding might be indicative of higher demand and increased effort in patients to ensure adequate motor function despite existing deficits (Katschnig et al., 2011). Again the passive conditions (i.e. FP, P) report a more significant difference with respect to active conditions (i.e., FV, V) when compared to controls. This confirms the hypothesis that the attempted volitional intention drives order in the brain activity, especially in chronic patients. It has been suggested that the increased activity with passive movements in regions that participate in sensorimotor integration reflects true functional reorganisation, since passive movements induce brain activation through sensory afferents only (Ciccarelli et al., 2006). The interaction contrast, i.e. sensorimotor integration, shows profound differences between patients and controls, located in frontal regions, SII, angular gyrus, caudate, posterior putamen. These activations might reflect the contribution of these regions in processing sensory and proprioceptive information for foot movements (Abbruzzese and Berardelli, 2003; Ciccarelli et al., 2006).

Comparison between single patient and controls – The comparison between a single patient and the control group has highlighted a widespread bilateral network of activation in all considered ROIs. It has been demonstrated that the amount of differences between single patients and control group should reflect the degree of impairment (Ward et al., 2003) during a handgrip motor task. However in our study the activated ROIs are independent from the overall outcome score defined. It is possible that our results reflect the different patterns of brain reorganisation used by each patient to support functional movements following a lesion. It is possible that each subject is implementing his/her strategy exploiting different mechanisms and that this might be dependent on other anatomical constraints (such as the exact topography of the damage) that have not been fully characterised here.

fMRI activity correlation with outcome measures – Whether there was any variability in sensorimotor integration across the patient group was further investigated through a correlation analysis. Here sensorimotor integration was quantified by the (voxel-wise) parameter estimates of the positive interaction contrast. In this work, contralateral SII has been shown to be more likely to be active in more impaired patients. It has been suggested a sensorimotor integration role for SII (Iftime-Nielsen et al., 2012) that could be exploited by patients when primary sensorimotor areas (i.e., M1 and S1) are unable to provide the needed processing of information. In addition, within the interaction contrast, significant positive linear correlation was found in ipsilateral cingulate cortex, middle frontal gyrus and insula, indicating distinct networks involved in sensorimotor integration processing.

This work highlights for the first time a clear network of activation related to FES-induced motor task in the context both of voluntary effort or passive movement in post-stroke subjects. The angular and postcentral gyri exhibit an interaction between artificially enhanced sensory feedback and volitional movement. Moreover, contralateral SII has been shown to be more likely to be a sensorimotor integration centre for more impaired patients. A significant limitation of this study was the number of subjects acquired. Although the group analysis is globally significant, there are some activations that only represent a trend. To fully characterise the behaviour and to propose a complete sensorimotor integration model, some more patients have to be involved in the study. The presented results may be important for future studies in patients (e.g. stroke) during rehabilitation (for a comprehensive review see Sheffler and Chae 2007), by correlating changes in FES and interaction cortical correlates in a longitudinal design. Indeed the brain correlates that has been shown to have a correlation between sensorimotor integration (i.e. interaction contrast) and the degree of impairment might be important in the investigation of the carryover effect brain signature.

Chapter 5 – Conclusions and visions for future

The channel humans have to get in touch with the world is movement, that is the result of the interplay between the intention to perform an action and its physical execution. We get a sense of our action in the world through sensation that realises and shapes the movement we are performing. This PhD thesis went deep into this challenge to investigate the localisation and mechanism of action of sensorimotor integration in the human brain. Sensorimotor integration is a surprising mechanism in everyone, but most of all in neurological patients, where everything changed. It is great importance to understand how lesioned human brain reacts and implements sensorimotor integration, so as to design customized rehabilitation treatment exploiting brain plasticity. In this challenging context non-invasive investigations are needed. The role of the bioengineer is therefore important to propose experimental set-ups that make possible to acquire useful and good quality data and to propose methods to analyse those data so to convert acquired data into reliable and meaningful information.

This work represents a small but significant step forward in understanding sensorimotor control in humans first of all from a bioengineering prospective, but also from a general scientific and clinical point of view, thanks to the strict collaboration with radiologist and physicians at the Villa Beretta Rehabilitation Centre, and with neurologists and researchers at the Sobell Department of Motor Neuroscience, UCL Institute of Neurology.

Hence, during these three years my work contributed to:

(i) *Define and validate an experimental set-up that is suited to measure movement related cortical correlates during functional electrical stimulation, used a way to enhance proprioception during an active motor task.* The feasibility of the proposed multi-modal experimental set-up so as to functionally electrically stimulate subjects while undergoing fMRI scanner and simultaneously record the effectively executed movement was demonstrated. The kinematic measure of the executed movement under the scanner allows to record multi-segment movement without any constraint to the movement itself. Moreover, it allows to control for all movement parameters (e.g. timing, amplitude, frequency etc.) that cannot be kept for granted when patients are performing an experimental protocol. The reliability of the acquired images in the integrated set-up has been demonstrated, with particular attention to the detectability of the BOLD signal, marker of neural activity. The possibility to analyse FES-induced motor tasks is of great interest for the scientific and clinical community because it allows to investigate the central mechanisms of action of FES, as an enhanced proprioceptive afference, that are still unclear.

(ii) *Define an experimental protocol that is suited to study sensorimotor integration during an active motor task.* A 2x2 event-related fMRI protocol with voluntary effort [V: with the levels volitional and passive] and FES [F: with the levels present and absent] as factors was performed during ankle dorsiflexion (ADF). FES was introduced as a means of artificially supplementing proprioception during movement execution. The positive interaction defined as (FV-V)-(FP-P) identifies regions where the FES augmented proprioception in the context of volitional intent (i.e. FV-V) produced a higher activation than FES augmented proprioception in the absence of volitional movement (i.e. FP-P). The interaction contrast directly represents the sensorimotor integration during an active motor task, when in the brain there is the planning of the volitional movements coupled to augmented proprioceptive afferences.

(iii) *Investigate the functional anatomy of sensorimotor integration in the human brain.* Primary sensorimotor areas (i.e. M1 and S1) exhibit a profound interaction between artificially enhanced sensory feedback and volitional movement. In other words, the effect of augmented proprioception depends on the presence of concurrent motor signals in both M1 and S1. Using dynamic causal modelling (DCM), it has been shown that augmented proprioception preferentially increased the influence of M1 on S1, while attenuating the excitability of S1 (increasing self-inhibition), although only slightly increasing the importance of the proprioceptive input. Crucially, the fact that augmented proprioception selectively increased input to S1 from M1 suggests that effect of stimulation depends upon the presence of top-down volitional or intentional signals. This is because the primary determinant of M1 activity is an effect of volitional movement. In this context, one can regard the modulation of the M1 to S1 connection as mediating the interaction between augmented proprioception and volitional movement (as encoded by the activity of M1). Since the update of the proprioceptive prediction occurs via the modulation of the influence of M1 on S1, changes in coupling between these regions support an active inference model of motor control.

(iv) *Investigate how functional anatomy of sensorimotor integration is affected by a brain lesion (e.g. stroke).* Sensorimotor integration in chronic stroke patients has been investigated demonstrating the feasibility and the reliability of FES cortical correlates in patients, highlighting for the first time a clear network of activation related to FES-induced motor task in the context both of voluntary effort or passive movement in chronic stroke patients. Angular and postcentral gyri exhibit an interaction between artificially enhanced sensory feedback and volitional movement. Postcentral gyrus has been found to be active in healthy controls while executing complex or novel tasks (Filippi et al., 2004; Sahyoun et al., 2004), and angular gyrus has been suggested to be recipient of proprioceptive information encoded specifically in the postcentral gyrus (Vesia and Crawford, 2012). Moreover, contralateral SII is more likely to be sensorimotor integration centre

for more impaired patients as suggested by the correlation between the positive interaction contrast and an overall index representing patients' residual ability.

Indeed, the presented results may be important for disclose the central FES-induced mechanism that is yet not clear. The positive interaction between augmented proprioception (i.e. FES) and volitional intention revealed in primary sensorimotor cortices might represent the preferential site of action of FES stimulus during volitional movements, to induce cortical modifications. However, other areas might be important for sensorimotor integration such as angular gyrus, postcentral gyrus or contralateral SII, as shown in chronic post-stroke patients. It might be possible that sensorimotor integration mechanism depends on the level of residual ability of the patient, and that its cortical correlates might speak about carryover prediction. 'Carryover effect' is introduced in literature to define the FES-induced outlasting effect (Ambrosini et al., 2011; Merletti et al., 1979; Waters et al., 1985). It is scientifically and clinically relevant to investigate and to be able to predict the carryover effect through cortical correlates, since peripheral evaluation are insufficient. Carryover prediction would lead to the possibility to customise the treatment depending on patients chances to succeed. Indeed, the brain correlates that has been shown to have a correlation between sensorimotor integration (i.e. interaction contrast) and the degree of impairment might be important in the investigation of the carryover effect brain signature. Indeed, thanks to the positive results obtained within this work, a trial has been designed so as to longitudinally explore sensorimotor integration cortical correlates in relation to the outcome of an FES-based treatment. Data acquisition are already on-going with the collaboration of Villa Beretta Rehabilitation centre.

From another prospective, the mechanism of action of sensorimotor integration proposed in this work could add a brick in the understanding of the motor control underlying model. The presented mechanism suggests an active inference view of the motor system, that is a quite new framework. Active inference suggests that M1 is part of a hierarchical generative model that sends predictions of the sensory consequences of a movement to the periphery (Friston et al., 2009). Moreover, the presented results may also have important implications for the mechanisms that underlie sensory attenuation; i.e. the decreased intensity of perceived stimulus attributes when they are the consequences of self-generated behaviour. Under active inference, sensory attenuation corresponds to the attenuation of the precision of (ascending) sensory information that allows top-down predictions to produce a movement through classical reflex arcs (Brown et al. – submitted).

These examples represent of course only possible studies that could contribute to infer pieces of the fascinating puzzle of neuromotor control, just like the work done in these here has tried to do.

References

Adams RA, Shipp S, Friston Karl J. Predictions not commands: active inference in the motor system. Brain Structure and Function 2012 [Epub ahead of print].

Alkadhi H, Crelier GR, Boendermaker SH, Golay X, Hepp-Reymond M-C, Kollias SS. Reproducibility of primary motor cortex somatotopic under controlled conditions. American Journal of neuroradiology 2002; 23: 1524–1532.

Alon G, Conroy VM, Donner TW. Intensive training of subjects with chronic hemiparesis on a motorized cycle combined with functional electrical stimulation (FES): a feasibility and safety study. Physiotherapy research international 2011; 16: 81–91.

Ambrosini E, Ferrante S, Ferrigno G, Molteni F, Pedrocchi A. Cycling induced by electrical stimulation improves muscle activation and symmetry during pedaling in hemiparetic patients. IEEE Transactions on neural systems and rehabilitation 2012; 20: 320–330.

Ambrosini E, Ferrante S, Pedrocchi A, Ferrigno G, Molteni F. Cycling induced by electrical stimulation improves motor recovery in postacute hemiparetic patients: a randomized controlled trial. Stroke 2011; 42: 1068–1073.

Andersson JL, Hutton C, Ashburner J, Turner R, Friston K. Modeling geometric deformations in EPI time series. NeuroImage 2001; 13: 903–919.

Asanuma H, Keller A. Neuronal Mechanisms of Motor Learning in Mammals. Neuroreport 1991; 2: 217–224.

Ashworth B. Preliminary trial of Carisoprol in multiple sclerosis. Practitioner 1964; 192: 540–542.

Balasubramanian CK, Bowden MG, Neptune RR, Kautz SA. Relationship between step length asymmetry and walking performance in subjects with chronic hemiparesis. Archives of Physical Medicine and Rehabilitation 2007; 88: 43–49.

Baroni G, Pedrocchi A, Ferrigno G, Massion J, Pedotti A. Motor coordination in weightless conditions revealed by long-term microgravity adaptation. Acta Astronautica 2001; 49: 199–213.

Barsi GI, Popovic DB, Tarkka IM, Sinkjaer T, Grey MJ. Cortical excitability changes following grasping exercise augmented with electrical stimulation. Experimental Brain Research 2008 ; 191: 57–66.

Bergquist AJ, Clair JM, Lagerquist O, Mang CS, Okuma Y, Collins DF. Neuromuscular electrical stimulation: implications of the electrically evoked sensory volley. European Journal of Applied Physiology 2011; 111: 2409–2426.

Bigland-Ritchie B, Jones DA, Woods JJ. Excitation frequency and muscle fatigue: electrical responses during human voluntary and stimulated contractions. Experimental Neurology 1979; 64:414-27.

Binkofski F, Buccino G, Posse S, Seitz RJ, Rizzolatti G, Freund H. A fronto-parietal circuit for object manipulation in man: evidence from an fMRI-study. The European Journal of neuroscience 1999; 11: 3276–3286.

Blakemore SJ, Frith CD, Wolpert D M. The cerebellum is involved in predicting the sensory consequences of action. Neuroreport 2001; 12: 1879–1884.

Blickenstorfer A, Kleiser R, Keller T, Keisker B, Meyer M, Riener R, et al. Cortical and subcortical correlates of functional electrical stimulation of wrist extensor and flexor muscles revealed by fMRI. Human Brain Mapping 2009; 30: 963–975.

Bliss T, Lømo T. Long-lasting potentiation of synaptic transmission in the dentate area of the anaesthetized rabbit following stimulation of the perforant path. Journal of Physiology 1973; 232: 331–356.

Bogataj U, Gros M, Kljajic M, Acimovic R, Malezic M. The Rehabilitation of Gait in Patients with Hemiplegia - a Comparison Between Conventional Therapy and Multichannel Functional Electrical-Stimulation Therapy. Physical Therapy 1995; 75: 490–502.

Bolognini N, Pascual-Leone A, Fregni F. Using non-invasive brain stimulation to augment motor training-induced plasticity. Journal of Neuroengineering and Rehabilitation 2009; 6: 8.

Bonakdarpour B, Parrish T B, Thompson CK. Hemodynamic response function in patients with stroke-induced aphasia: implications for fMRI data analysis. NeuroImage 2007; 36: 9322–331.

Borghese NA, Ferrigno G. An algorithm for 3-D automatic movement detection by means of standard TV cameras. IEEE Transactions on Biomedical Engineering 1990; 37: 1221–1225.

Boudrias M-H, Gonçalves CS, Penny Will D, Park C-H, Rossiter HE, Talelli P, et al. Age-related changes in causal interactions between cortical motor regions during hand grip. NeuroImage 2012; 59: 3398–3405.

Burke RE, Levine DN, Tsairis P, Zajac FE 3rd. Physiological types and histochemical profiles in motor units of the cat gastrocnemius. J. Physiol. (Lond.) 1973; 234: 723–748.

Burke D, Gandevia SC, McKeon B. The afferent volleys responsible for spinal proprioceptive reflexes in man. J Physiol 1983; 339:535–552.

Calautti C, Naccarato M, Jones PS, Sharma N, Day DD, Carpenter AT, et al. The relationship between motor deficit and hemisphere activation balance after stroke: A 3T fMRI study. NeuroImage 2007; 34: 322–331.

Casellato C, Ferrante S, Gandolla M, Volonterio N, Ferrigno Giancarlo, Baselli G, et al. Simultaneous measurements of kinematics and fMRI: compatibility assessment and case report on recovery evaluation of one stroke patient. Journal of neuroengineering and rehabilitation 2010; 7:49.

Chapman CE, Ageranioti-Bélanger SA. Discharge properties of neurones in the hand area of primary somatosensory cortex in monkeys in relation to the performance of an active tactile discrimination task. I. Areas 3b and 1. Experimental Brain Research 1991; 87: 319–339.

Chaudhary UJ, Kokkinos V, Carmichael DW, Rodionov R, Gasston D, Duncan JS, et al. Implementation and evaluation of simultaneous video-electroencephalography and functional magnetic resonance imaging. Magnetic Resonance Imaging 2010; 28: 1192–1199.

Chen TL, Babiloni C, Ferretti A, Perrucci MG, Romani GL, Rossini Paolo Maria, et al. Human secondary somatosensory cortex is involved in the processing of somatosensory rare stimuli: an fMRI study. NeuroImage 2008; 40: 1765–1771.

Chen TL, Babiloni C, Ferretti A, Perrucci MG, Romani GL, Rossini Paolo Maria, et al. Effects of somatosensory stimulation and attention on human somatosensory cortex: an fMRI study. NeuroImage 2010; 53: 181–188.

Cheng EJ, Brown IE, Loeb GE. Virtual muscle: a computational approach to understanding the effects of muscle properties on motor control. Journal of Neuroscience Methods 2000; 101: 117–130.

Christensen MS, Lundbye-Jensen J, Geertsen SS, Petersen TH, Paulson OB, Nielsen JB. Premotor cortex modulates somatosensory cortex during voluntary movements without proprioceptive feedback. Nature Neuroscience 2007; 10: 417–419.

Ciccarelli O, Toosy AT, Marsden JF, Wheeler-Kingshott CM, Miller DH, Matthews P M, et al. Functional response to active and passive ankle movements with clinical correlations in patients with primary progressive multiple sclerosis. Journal of neurology 2006; 253: 882–891.

Ciccarelli O, Toosy AT, Marsden JF, Wheeler-Kingshott CM, Sahyoun C, Matthews P M, et al. Identifying brain regions for integrative sensorimotor processing with ankle movements. Experimental Brain Research 2005; 166: 31–42.

Cohen DA, Prud'homme MJ, Kalaska JF. Tactile activity in primate primary somatosensory cortex during active arm movements: correlation with receptive field properties. Journal of neurophysiology 1994; 71: 161–172.

Cramer SC, Nelles G, Benson RR, Kaplan JD, Parker RA, Kwong KK, et al. A functional MRI study of subjects recovered from hemiparetic stroke. Stroke 1997; 28: 2518–2527.

Dai TH, Liu JZ, Sahgal V, Brown RW, Yue GH. Relationship between muscle output and functional MRI-measured brain activation. Experimental Brain Research 2001; 140: 290–300.

Darian-Smith C, Darian-Smith I, Burman K, Ratcliffe N. Ipsilateral cortical projections to areas 3a, 3b, and 4 in the macaque monkey. The Journal of comparative neurology 1993; 335: 200–213.

Davis GM, Hamzaid NA, Fornusek C. Cardiorespiratory, metabolic, and biomechanical responses during functional electrical stimulation leg exercise: Health and fitness benefits. Artificial Organs 2008; 32: 625–629.

Davis R, Ounpuu S, Tyburski D, Gage J. A Gait Analysis Data-Collection and Reduction Technique. Human Movement Science 1991; 10: 575–587.

Diciotti S, Gavazzi C, Della Nave R, Boni E, Ginestroni A, Paoli L, et al. Self-paced frequency of a simple motor task and brain activation. An fMRI study in healthy subjects using an on-line monitor device. NeuroImage 2007; 38: 402–412.

Dingwell JB, Mah CD, Mussa-Ivaldi FA. Experimentally confirmed mathematical model for human control of a non-rigid object. Journal of Neurophysiology 2004; 91: 1158–1170.

Di Piero V, Chollet FM, Maccarthy P, Lenzi G, Frackowiak R. Motor Recovery After Acute Ischemic Stroke - a Metabolic Study. Journal of Neurology Neurosurgery & Psychiatry 1992; 55: 990–996.

Disbrow E, Litinas E, Recanzone GH, Padberg J, Krubitzer L. Cortical connections of the second somatosensory area and the parietal ventral area in macaque monkeys. The Journal of comparative neurology 2003; 462: 382–399.

Dobkin BH, Firestine A, West M, Saremi K, Woods Roger. Ankle dorsiflexion as an fMRI paradigm to assay motor control for walking during rehabilitation. NeuroImage 2004; 23: 370–381.

Donoghue JP, Parham C. Afferent connections of the lateral agranular field of the rat motor cortex. The Journal of comparative neurology 1983; 217: 390–404.

Van Duinen H, Renken R, Maurits NM, Zijdewind I. Relation between muscle and brain activity during isometric contractions of the first dorsal interosseus muscle. Human Brain Mapping 2008; 29: 281–299.

Van Duinen H, Zijdewind I, Hoogduin H, Maurits N. Surface EMG measurements during fMRI at 3T: accurate EMG recordings after artifact correction. NeuroImage 2005; 27: 240–246.

Ehrsson HH, Fagergren A, Forssberg H. Differential fronto-parietal activation depending on force used in a precision grip task: An fMRI study. Journal of Neurophysiology 2001; 85: 2613–2623.

Enzinger Christian, Johansen-Berg Heidi, Dawes H, Bogdanovic M, Collett J, Guy C, et al. Functional MRI correlates of lower limb function in stroke victims with gait impairment. Stroke; a journal of cerebral circulation 2008; 39: 1507–1513.

Everaert DG, Thompson AK, Chong SL, Stein RB. Does functional electrical stimulation for foot drop strengthen corticospinal connections? Neurorehabilitation and neural repair 2010; 24: 168–177.

Ferrante S, Pedrocchi A, Ferrigno G, Molteni F. Cycling induced by functional electrical stimulation improves the muscular strength and the motor control of individuals with post-acute stroke. European journal of physical and rehabilitation medicine 2008; 44: 159–167.

Ferretti A, Del Gratta C, Babiloni C, Caulo M, Arienzo D, Tartaro A, et al. Functional topography of the secondary somatosensory cortex for nonpainful and painful stimulation of median and tibial nerve: an fMRI study. 2004: 1217–1225.

Filippi M, Rocca MA, Mezzapesa DM, Falini A, Colombo B, Scotti G, et al. A functional MRI study of cortical activations associated with object manipulation in patients with MS. NeuroImage 2004; 21: 1147–1154.

Francis S, Lin X, Aboushoushah S, White TP, Phillips M, Bowtell R, et al. fMRI analysis of active, passive and electrically stimulated ankle dorsiflexion. NeuroImage 2009; 44: 469–479.

Freund P, Weiskopf N, Ward Nick S, Hutton Chloe, Gall A, Ciccarelli O, et al. Disability, atrophy and cortical reorganization following spinal cord injury. Brain: a journal of neurology 2011; 134: 1610–1622.

Friston K J, Fletcher P, Josephs O, Holmes A, Rugg MD, Turner R. Event-related fMRI: characterizing differential responses. NeuroImage 1998; 7: 30–40.

Friston K J, Harrison L, Penny W. Dynamic causal modelling. NeuroImage 2003; 19: 1273–1302.

Friston K J, Holmes AP, Worsley KJ. How many subjects constitute a study? NeuroImage 1999; 10: 1–5.

Friston K J, Williams S, Howard R, Frackowiak RS, Turner R. Movement-related effects in fMRI time-series. Magnetic resonance in medicine 1996; 35: 346–355.

Friston K J., Ashburner J, Frith CD, Poline JB, Heather JD, Frackowiak RSJ. Spatial registration and normalization of images. Human Brain Mapping 1995; 3: 165–189.

Friston K J, Daunizeau J, Kiebel SJ. Reinforcement learning or active inference? PLoS ONE 2009; 4: e6421.

Friston K J. The free-energy principle: a unified brain theory? Nature reviews Neuroscience 2010; 11: 127–138.

Friston K J. What is optimal about motor control? Neuron 2011; 72: 488–498.

Gandolla M, Ferrante S, Casellato C, Ferrigno G, Molteni F, Martegani A, et al. fMRI brain mapping during motion capture and FES induced motor tasks: signal to noise ratio assessment. Medical Engineering & Physics 2011; 33: 1027–1032.

Ganesh G, Franklin DW, Gassert R, Imamizu H, Kawato M. Accurate real-time feedback of surface EMG during fMRI. Journal of Neurophysiology 2007; 97: 912–920.

Glover GH, Law CS. Spiral-in/out BOLD fMRI for increased SNR and reduced susceptibility artifacts. Magnetic Resonance in Medicine 2001; 46: 515–522.

Gordon AM, Huxley AF, Julian FJ. The variation in isometric tension with sarcomere length in vertebrate muscle fibres. Journal of Physiology 1966; 184: 170–192.

Graham KM, Scott Stephen H. Morphometry of Macaca mulatta forelimb. III. Moment arm of shoulder and elbow muscles. Journal of Morphology 2003; 255: 301–314.

Gresham GE, Alexander D, Bishop DS, Giuliani C, Goldberg G, Holland A, et al. American Heart Association Prevention Conference. IV. Prevention and Rehabilitation of Stroke. Rehabilitation. Stroke 1997; 28: 1522–1526.

Han BS, Jang SH, Chang Y, Byun WM, Lim SK, Kang DS. Functional magnetic resonance image finding of cortical activation by neuromuscular electrical stimulation on wrist extensor muscles. American journal of physical medicine & rehabilitation 2003; 82: 17–20.

Hanakawa T, Immisch I, Toma K, Dimyan MA, Van Gelderen Peter, Hallett Mark. Functional properties of brain areas associated with motor execution and imagery. Journal of neurophysiology 2003; 89: 989–1002.

Hauptmann B, Sosnik R, Smikt O, Okon E, Manor D, Kushnir T, et al. A new method to record and control for 2D-movement kinematics during functional magnetic resonance imaging (fMRI). Cortex 2009; 45: 407–417.

Heiland S. From A as in Aliasing to Z as in Zipper: artefacts in MRI. Clinical neuroradiology 2008; 18: 25–36.

Henneman E, Olson CB. Relations Between Structure and Function in the Design of Skeletal Muscles. Journal of neurophysiology 1965; 28:581-598.

Hinkley LB, Krubitzer LA, Nagarajan SS, Disbrow EA. Sensorimotor integration in S2, PV, and parietal rostroventral areas of the human sylvian fissure. Journal of neurophysiology 2007; 97: 1288–1297.

Ho CL, Holt KG, Saltzman E, Wagenaar RC. Functional electrical stimulation changes dynamic resources in children with spastic cerebral palsy. Physical Therapy 2006; 86: 987–1000.

Holmes JW. Teaching from classic papers: Hill's model of muscle contraction. Advances in Physiology Education 2006; 30: 67–72.

Horenstein C, Lowe MJ, Koenig KA, Phillips MD. Comparison of unilateral and bilateral complex finger tapping-related activation in premotor and primary motor cortex. Human Brain Mapping 2009; 30: 1397–1412.

Hummelsheim H, MaierLoth ML, Eickhof C. The functional value of electrical muscle stimulation for the rehabilitation of the hand in stroke patients. Scandinavian Journal of Rehabilitation Medicine 1997; 29: 3–10.

Iftime-Nielsen SD, Christensen MS, Vingborg RJ, Sinkjaer T, Roepstorff A, Grey MJ. Interaction of electrical stimulation and voluntary hand movement in SII and the cerebellum during simulated therapeutic functional electrical stimulation in healthy adults. Human Brain Mapping 2012; 33: 40–49.

Jacobs K, Donoghue J. Reshaping the Cortical Motor Map by Unmasking Latent Intracortical Connections. Science 1991; 251: 944–947.

Jenkins I, Fernandez W, Playford E, Lees A, Frackowiak R, Passingham R, et al. Impaired Activation of the Supplementary Motor Area in Parkinsons-Disease Is Reversed When Akinesia Is Treated with Apomorphine. Annals of Neurology 1992; 32: 749–757.

Joa K-L, Han Y-H, Mun C-W, Son B-K, Lee C-H, Shin Y-B, et al. Evaluation of the brain activation induced by functional electrical stimulation and voluntary contraction using functional magnetic resonance imaging. Journal of Neuroengineering and Rehabilitation 2012; 9: 48.

Johnstone T, Ores Walsh KS, Greischar LL, Alexander AL, Fox AS, Davidson RJ, et al. Motion correction and the use of motion covariates in multiple-subject fMRI analysis. Human Brain Mapping 2006; 27: 779–788.

Jones EG, Coulter JD, Hendry SH. Intracortical connectivity of architectonic fields in the somatic sensory, motor and parietal cortex of monkeys. The Journal of comparative neurology 1978; 181: 291–347.

Katschnig P, Schwingenschuh P, Jehna M, Svehlik M, Petrovic K, Ropele S., et al. Altered functional organization of the motor system related to ankle movements in Parkinson's disease - Insights from functional MRI. Movement Disorders 2011; 26: S245–S245.

Kaufman L, Kramer DM, Crooks LE, Ortendahl DA. Measuring signal-to-noise ratios in MR imaging. Radiology 1989; 173: 265–267.

Kesar TM, Binder-Macleod SA, Hicks GE, Reisman DS. Minimal detectable change for gait variables collected during treadmill walking in individuals post-stroke. Gait Posture 2011; 33: 314–317.

Khaslavskaia S, Ladouceur M, Sinkjaer T. Increase in tibialis anterior motor cortex excitability following repetitive electrical stimulation of the common peroneal nerve. Experimental Brain Research 2002; 145: 309–315.

Khaslavskaia S, Sinkjaer T. Motor cortex excitability following repetitive electrical stimulation of the common peroneal nerve depends on the voluntary drive. Experimental Brain Research 2005; 162: 497–502.

Kim JH, Jang SH, Kim CS, Jumg JH, You JH. Use of Virtual Reality to Enhance Balance and Ambulation in Chronic Stroke: A Double-Blind, Randomized Controlled Study. American Journal of Physical Medicine and Rehabilitation 2009; 88: 693-701.

Kimberley TJ, Lewis SM, Auerbach EJ, Dorsey LL, Lojovich JM, Carey JR. Electrical stimulation driving functional improvements and cortical changes in subjects with stroke. Experimental Brain Research 2004; 154: 450–460.

Knaflitz M, Merletti R. Suppression of simulation artifacts from myoelectric-evoked potential recordings. IEEE Transactions on Biomedical Engineering1988; 35: 758–763.

Knash ME, Kido A, Gorassini M, Chan KM, Stein RB. Electrical stimulation of the human common peroneal nerve elicits lasting facilitation of cortical motor-evoked potentials. Experimental Brain Research 2003; 153: 366–377.

Kottink AIR, Oostendorp LJM, Buurke JH, Nene AV, Hermens HJ, IJzerman MJ. The orthotic effect of functional electrical stimulation on the improvement of walking in stroke patients with a dropped foot: a systematic review. Artificial Organs 2004; 28: 577–586.

Kraft GH, Fitts SS, Hammond MC. Techniques to improve function of the arm and hand in chronic hemiplegia. Archives of Physical Medicine and Rehabilitation 1992; 73:220-227.

Krainak DM, Parrish Todd B, Dewald JPA. A method to capture six-degrees-of-freedom mechanical measurements of isometric shoulder and elbow torques during event-related fMRI. Journal of neuroscience methods 2007; 161: 314–322.

Krakow K, Allen PJ, Symms MR, Lemieux L, Josephs O, Fish DR. EEG recording during fMRI experiments: image quality. Human Brain Mapping 2000; 10: 10–15.

Lancaster JL, Rainey LH, Summerlin JL, Freitas CS, Fox PT, Evans AC, et al. Automated labeling of the human brain: a preliminary report on the development and evaluation of a forward-transform method. Human brain mapping 1997; 5: 238–242.

Lazeyras F, Zimine I, Blanke O, Perrig SH, Seeck M. Functional MRI with simultaneous EEG recording: feasibility and application to motor and visual activation. Journal of magnetic resonance imaging 2001; 13: 943–948.

Liberson WT, Holmquest HJ, Scot D, Dow M. Functional electrotherapy: stimulation of the peroneal nerve synchronized with the swing phase of the gait of hemiplegic patients. Archives of physical medicine and rehabilitation 1961; 42: 101-105.

Liu JZ, Dai TH, Elster TH, Sahgal V, Brown RW, Yue GH. Simultaneous measurement of human joint force, surface electromyograms, and functional MRI-measured brain activation. Journal of neuroscience methods 2000; 101: 49–57.

Lloyd-Jones. Heart Disease and Stroke Statistics-2009 Update: A Report From the American Heart Association Statistics Committee and Stroke Statistics Subcommittee (vol 119, pg e21, 2009). Circulation 2010; 122: E424–E424.

Lømo T. Frequency potentiation of excitatory synaptic activity in the dentate area of the hippocampal formation. Acta Physiologica Scandinavica 68 (Suppl. 277), 128.

Lømo T. The discovery of long-term potentiation. Phylosofical Transactions of the Royal Society B 2003; 358:617-620.

Lotze M, Erb M, Flor H, Huelsmann E, Godde B, Grodd W. fMRI evaluation of somatotopic representation in human primary motor cortex. NeuroImage 2000; 11: 473–481.

Luft AR, Forrester L, Macko RF, McCombe-Waller S, Whitall J, Villagra F, et al. Brain activation of lower extremity movement in chronically impaired stroke survivors. NeuroImage 2005; 26: 184–194.

Lum PS, Burgar CG, Shor PC, Majmundar M, Van der Loos M. Robot-Assisted Movement Training Compared With Conventional Therapy Techniques for the Rehabilitation of Upper-Limb Motor Function After Stroke. Archives of Physical Medicine and Rehabilitation 2002; 83: 952-959.

Lutz K, Koeneke S, Wüstenberg T, Jäncke L. Asymmetry of cortical activation during maximum and convenient tapping speed. Neuroscience Letters 2005; 373: 61–66.

Machado S, Cunha M, Velasques B, Minc D, Teixeira S, Domingues CA, Silva JG, Bastos VH, Budde H, Cagy M, Basile L, Piedade R, Ribeiro P. Sensorimotor integration: basic concepts, abnormalities related to movement disorders and sensorimotor training-induced cortical reorganization. Rev Neurol 2010; 51: 427-436.

MacIntosh BJ, Baker S Nicole, Mraz R, Ives JR, Martel AL, McIlroy WE, et al. Improving functional magnetic resonance imaging motor studies through simultaneous electromyography recordings. Human brain mapping 2007; 28: 835–845.

MacIntosh BJ, Mraz R, Baker N, Tam F, Staines WR, Graham SJ. Optimizing the experimental design for ankle dorsiflexion fMRI. NeuroImage 2004; 22: 1619–1627.

Mazziotta J, Toga A, Evans A, Fox P, Lancaster J, Zilles K, et al. A probabilistic atlas and reference system for the human brain: International Consortium for Brain Mapping (ICBM). Philosophical transactions of the Royal Society of London. Series B, Biological sciences 2001; 356: 1293–1322.

Merletti R, Andina A, Galante M, Furlan I. Clinical experience of electronic peroneal stimulators in 50 hemiparetic patients. Scandinavian journal of rehabilitation medicine 1979; 11: 111-121.

Muellbacher W, Richards C, Ziemann U, Wittenberg G, Weltz D, Boroojerdi B, et al. Improving hand function in chronic stroke. Archives of Neurology 2002; 59: 1278–1282.

Mullinger K, Debener S, Coxon R, Bowtell R. Effects of simultaneous EEG recording on MRI data quality at 1.5, 3 and 7 tesla. International journal of psychophysiology 2008; 67: 178–188.

Nudo RJ, Milliken GW. Reorganization of movement representations in primary motor cortex following focal ischemic infarcts in adult squirrel monkeys. Journal of Neurophysiology 1996; 75: 2144–2149.

Oostra K, VanLaere M, Scheirlinck B. Use of electrical stimulation in brain-injured patients: a case report. Brain Injury 1997; 11: 761–764.

Ostry DJ, Darainy M, Mattar AAG, Wong J, Gribble PL. Somatosensory plasticity and motor learning. Journal of Neuroscience 2010; 30: 5384–5393.

Otten E. Concepts and models of functional architecture in skeletal muscle. Exercise and sport sciences reviews 1988; 16: 89–137.

Padberg J, Disbrow E, Krubitzer L. The organization and connections of anterior and posterior parietal cortex in titi monkeys: Do new world monkeys have an area 2? Cerebral Cortex 2005; 15: 1938–1963.

Page SJ, Levine P. Modified constraint-induced therapy increases affected limb use and function in subacute stroke. Stroke 2004; 35: 286–286.

Parrish T B, Gitelman DR, LaBar KS, Mesulam MM. Impact of signal-to-noise on functional MRI. Magnetic resonance in medicine 2000; 44: 925–932.

Pavlides C, Miyashita E, Asanuma H. Projection from the sensory to the motor cortex is important in learning motor skills in the monkey. Journal of Neurophysiology 1993; 70: 733–741.

Peckham PH, Keith MW, Kilgore KL, Grill JH, Wuolle KS, Thrope GB, et al. Efficacy of an implanted neuroprosthesis for restoring hand grasp in tetraplegia: A multicenter study. Archives of Physical Medicine and Rehabilitation 2001; 82: 1380–1388.

Penny WD, Stephan KE, Mechelli A, Friston KJ. Comparing dynamic causal models. NeuroImage 2004; 22: 1157–1172.

Penny WD, Stephan KE, Daunizeau J, Rosa MJ, Friston KJ, Schofield TM, et al. Comparing families of dynamic causal models. PLoS computational biology 2010; 6: e1000709.

Perry J, Garrett M, Gronley J, Mulroy S. Classification of Walking Handicap in the Stroke Population. Stroke 1995; 26: 982–989.

Plautz EJ, Milliken GW, Nudo RJ. Effects of repetitive motor training on movement representations in adult squirrel monkeys: Role of use versus learning. Neurobiology of Learning Memory 2000; 74: 27–55.

Pomeroy VM, King L, Pollock A, Baily-Hallam A, Langhorne P. Electrostimulation for promoting recovery of movement or functional ability after stroke. Cochrane database of systematic reviews 2006; 2: CD003241.

Radlinska B, Ghinani S, Leppert IR, Minuk J, Pike GB, Thiel A. Diffusion tensor imaging, permanent pyramidal tract damage, and outcome in subcortical stroke. Neurology 2010; 75: 1048–1054.

Rao RP, Ballard DH. Predictive coding in the visual cortex: a functional interpretation of some extra-classical receptive-field effects. Nature Neuroscience 1999; 2: 79–87.

Rushworth MF, Nixon PD, Renowden S, Wade DT, and Passingham RE. The left parietal cortex and motor attention. Neuropsychologia 1997; 35:1261-1273.

Rijntjes M, Dettmers C, Büchel C, Kiebel S, Frackowiak RS, Weiller C. A blueprint for movement: functional and anatomical representations in the human motor system. Journal of Neuroscience 1999; 19: 8043–8048.

Robbins SM, Houghton PE, Woodbury MG, Brown JL. The therapeutic effect of functional and transcutaneous electric stimulation on improving gait speed in stroke patients: a meta-analysis. Archives of Physical Medicine and Rehabilitation 2006; 87: 853–859.

Van Rootselaar A-F, Renken R, De Jong BM, Hoogduin JM, Tijssen MAJ, Maurits NM. fMRI analysis for motor paradigms using EMG-based designs: a validation study. Human Brain Mapping 2007; 28: 1117–1127.

Rorden C, Brett M. Stereotaxic display of brain lesions. Behavioural neurology 2000; 12: 191–200.

Rosenkranz K, Rothwell JC. Modulation of proprioceptive integration in the motor cortex shapes human motor learning. Journal of Neuroscience 2012; 32: 9000–9006.

Rowe JB, Siebner HR. The motor system and its disorders. NeuroImage 2012; 61: 464–477.

Royet J-P, Plailly J, Delon-Martin C, Kareken DA, Segebarth C. fMRI of emotional responses to odors: influence of hedonic valence and judgment, handedness, and gender. NeuroImage 2003; 20: 713–728.

Rushton DN. Functional electrical stimulation and rehabilitation--an hypothesis. Medical engineering & physics 2003; 25: 75–78.

Sabut SK, Sikdar C, Mondal R, Kumar R, Mahadevappa M. Restoration of gait and motor recovery by functional electrical stimulation therapy in persons with stroke. Disability and rehabilitation 2010; 32: 1594–1603.

Sadato N, Ibañez V, Campbell G, Deiber MP, Le Bihan D, Hallett M. Frequency-dependent changes of regional cerebral blood flow during finger movements: functional MRI compared to PET. Journal of cerebral blood flow and metabolism 1997; 17: 670–679.

Sahyoun C, Floyer-Lea A, Johansen-Berg H, Matthews P M. Towards an understanding of gait control: brain activation during the anticipation, preparation and execution of foot movements. NeuroImage 2004; 21: 568–575.

Scarff CJ, Reynolds A, Goodyear BG, Ponton CW, Dort JC, Eggermont JJ. Simultaneous 3-T fMRI and high-density recording of human auditory evoked potentials. NeuroImage 2004; 23: 1129–1142.

Schieber M, Hibbard L. How Somatotopic Is the Motor Cortex Hand Area. Science 1993; 261: 489–492.

Schwarz DW, Deecke L, Fredrickson JM. Cortical projection of group I muscle afferents to areas 2, 3a, and the vestibular field in the rhesus monkey. 1973: 516–526.

Scott SH, Brown IE, Loeb GE. Mechanics of feline soleus: I. Effect of fascicle length and velocity on force output. Journal of Muscle Research and Cell Motility 1996; 17: 207–219.

Scott SH. Role of motor cortex in coordinating multi-joint movements: is it time for a new paradigm? Canadian Journal of Physiology and Pharmacology 2000; 78: 923–933.

Scott SH. Optimal feedback control and the neural basis of volitional motor control. Nature Reviews Neuroscience 2004; 5: 532–546.

Shadmehr R, Smith MA, Krakauer JW. Error Correction, Sensory Prediction, and Adaptation in Motor Control. Annual Review of Neuroscience 2010; 33: 89–108.

Sheffler LR, Chae J. Neuromuscular electrical stimulation in neurorehabilitation. Muscle Nerve 2007; 35: 562–590.

Singh K, Melis EH, Richmond FJR, Scott Stephen H. Morphometry of Macaca mulatta forelimb. II. Fiber-type composition in shoulder and elbow muscles. Journal of Morphology 2002; 251: 323–332.

Small DM, Voss J, Mak YE, Simmons KB, Parrish T, Gitelman D. Experience-dependent neural integration of taste and smell in the human brain. Journal of neurophysiology 2004; 92: 1892–1903.

Smith GV, Alon G, Roys SR, Gullapalli RP. Functional MRI determination of a dose-response relationship to lower extremity neuromuscular electrical stimulation in healthy subjects. Experimental Brain Research 2003; 150: 33–39.

Stephan KE, Roebroeck A. A short history of causal modeling of fMRI data. NeuroImage 2012; 62: 856–863.

Stinear JW, Hornby TG. Stimulation-induced changes in lower limb corticomotor excitability during treadmill walking in humans. Journal of Physiology-London 2005; 567: 701–711.

Tang AM, Kacher DF, Lam EY, Wong KK, Jolesz FA, Yang ES. Simultaneous ultrasound and MRI system for breast biopsy: compatibility assessment and demonstration in a dual modality phantom. IEEE transactions on medical imaging 2008; 27: 247–254.

Taylor PN, Burridge JH, Dunkerley AL, Lamb A, Wood DE, Norton JA, et al. Patients' perceptions of the Odstock Dropped Foot Stimulator (ODFS). Clinical Rehabilitation 1999; 13: 439–446.

Todorov E, Jordan Michael I. Optimal feedback control as a theory of motor coordination. Nature Neuroscience 2002; 5: 1226–1235.

Todorov E. Optimality principles in sensorimotor control. Nature Neuroscience 2004; 7: 907–915.

Thompson AK, Stein RB. Short-term effects of functional electrical stimulation on motor-evoked potentials in ankle flexor and extensor muscles. Experimental Brain Research 2004; 159: 491-500.

Vesia M, Crawford JD. Specialization of reach function in human posterior parietal cortex. Experimental Brain Research 2012; 221: 1–18.

Vonschroeder H, Coutts R, Lyden P, Billings E, Nickel V. Gait Parameters Following Stroke - a Practical Assessment. Journal of Rehabilitation Research and Development 1995; 32: 25–31.

Waldvogel D, Van Gelderen P, Ishii K, Hallett M. The effect of movement amplitude on activation in functional magnetic resonance imaging studies. Journal of cerebral blood flow and metabolism 1999; 19: 1209–1212.

Ward NS, Brown MM, Thompson A J, Frackowiak RSJ. Neural correlates of outcome after stroke: a cross-sectional fMRI study. Brain 2003; 126: 1430–1448.

Ward NS. Future perspectives in functional neuroimaging in stroke recovery. Europa medicophysica 2007; 43: 285-294.

Ward NS, Cohen LG. Mechanisms underlying recovery of motor function after stroke. Archives of Neurology 2004; 61: 1844–1848.

Ward NS, Swayne OBC, Newton JM. Age-dependent changes in the neural correlates of force modulation: an fMRI study. Neurobiology of aging 2008; 29: 1434–1446.

Waters RL, McNeal DR, Faloon W, Clifford B. Functional electrical stimulation of the peroneal nerve for hemiplegia. Long-term clinical follow-up. Journal of Bone and Joint Surgery-American 1985; 67: 792–793.

Wegner C, Filippi M, Korteweg T, Beckmann C, Ciccarelli O., De Stefano N., et al. Relating functional changes during hand movement to clinical parameters in patients with multiple sclerosis in a multi-centre fMRI study. European Journal Neurology 2008; 15: 113–122.

Weiller C, Juptner M, Fellows S, Rijntjes M, Leonhardt G, Kiebel S, et al. Brain representation of active and passive movements. Neuroimage 1996; 4: 105–110.

Williams LM, Kemp AH, Felmingham K, Barton M, Olivieri G, Peduto A, et al. Trauma modulates amygdala and medial prefrontal responses to consciously attended fear. NeuroImage 2006; 29: 347–357.

Witham CL, Wang M, Baker Stuart N. Corticomuscular coherence between motor cortex, somatosensory areas and forearm muscles in the monkey. Frontiers in systems neuroscience 2010; 4.

Wittenberg GF, Bastian AJ, Dromerick AW, Thach WT, Powers WJ. Mirror movements complicate interpretation of cerebral activation changes during recovery from subcortical infarction. Neurorehabilitation and neural repair 2000; 14: 213–221.

Wolf SL, Winstein CJ, Miller JP, Taub E, Uswatte G, Morris D, et al. Effect of constraint-induced movement therapy on upper extremity function 3 to 9 months after stroke: the EXCITE randomized clinical trial. Journal of the American Medical 2006: 2095–2104.

Wolpert D M, Ghahramani Z, Jordan M I. An internal model for sensorimotor integration. Science 1995; 269: 1880–1882.

Wolpert D M, Kawato M. Multiple paired forward and inverse models for motor control. Neural Networks 1998; 11: 1317–1329.

Wong JD, Wilson ET, Gribble PL. Spatially selective enhancement of proprioceptive acuity following motor learning. Journal of Neurophysiology 2011; 105: 2512–2521.

Wynne MM, Burns JM, Eland DC, Conatser RR, Howell JN. Effect of Counterstrain on Stretch Reflexes, Hoffmann Reflexes, and Clinical Outcomes in Subjects With Plantar Fasciitis. JAOA 2006; 106: 547-556.

Yan TB, Hui-Chan CWY, Li LSW. Functional electrical stimulation improves motor recovery of the lower extremity and walking ability of subjects with first acute stroke - A randomized placebo-controlled trial. Stroke 2005; 36: 80–85.

Yetkin FZ, Mueller WM, Hammeke TA, Morris GL 3rd, Haughton VM. Functional magnetic resonance imaging mapping of the sensorimotor cortex with tactile stimulation. Neurosurgery 1995; 36: 921–925.

Zajac FE, Faden JS. Relationship among recruitment order, axonal conduction velocity, and muscle-unit properties of type-identified motor units in cat plantaris muscle. Journal of Neurophysiology 1985; 53: 1303–1322.

Zajac FE. Muscle and tendon: properties, models, scaling, and application to biomechanics and motor control. Critical Reviews in Biomedical Engineering 1989; 17: 359–411.